Nonperturbative QCD simulations with 2+1 flavors of improved staggered quarks

A. Bazavov and D. Toussaint

Department of Physics, University of Arizona, Tucson, Arizona 85721, USA

C. Bernard and J. Laiho

Department of Physics, Washington University, St. Louis, Missouri 63130, USA

C. DeTar, L. Levkova, and M. B. Oktay

Physics Department, University of Utah, Salt Lake City, Utah 84112, USA

Steven Gottlieb

Department of Physics, Indiana University, Bloomington, Indiana 47405, USA

U. M. Heller

American Physical Society, One Research Road, Ridge, New York 11961, USA

J. E. Hetrick

Physics Department, University of the Pacific, Stockton, California 95211, USA

P. B. Mackenzie

Theoretical Physics Department, MS 106, Fermilab, P.O. Box 500, Batavia, Illinois 60510-0500, USA

R. Sugar

Department of Physics, University of California, Santa Barbara, California 93106, USA

R. S. Van de Water

Department of Physics, Brookhaven National Laboratory, Upton, New York 11973, USA

(Published 6 May 2010)

Dramatic progress has been made over the last decade in the numerical study of quantum chromodynamics (QCD) through the use of improved formulations of QCD on the lattice (improved actions), the development of new algorithms, and the rapid increase in computing power available to lattice gauge theorists. In this article simulations of full QCD are described using the improved staggered quark formalism, "asqtad" fermions. These simulations were carried out with two degenerate flavors of light quarks (up and down) and with one heavier flavor, the strange quark. Several light quark masses, down to about three times the physical light quark mass, and six lattice spacings have been used. These enable controlled continuum and chiral extrapolations of many low energy QCD observables. The improved staggered formalism is reviewed, emphasizing both advantages and drawbacks. In particular, the procedure for removing unwanted staggered species in the continuum limit is reviewed. Then the asqtad lattice ensembles created by the MILC Collaboration are described. All MILC lattice ensembles are publicly available, and they have been used extensively by a number of lattice gauge theory groups. The physics results obtained with them are reviewed, and the impact of these results on phenomenology is discussed. Topics include the heavy quark potential, spectrum of light hadrons, quark masses, decay constants of light and heavy-light pseudoscalar mesons, semileptonic form factors, nucleon structure, scattering lengths, and more.

DOI: 10.1103/RevModPhys.82.1349 PACS number(s): 12.38.Gc, 11.15.Ha

CONTENTS

I. INTRODUCTION

The standard model of high-energy physics encompasses our current knowledge of the fundamental interactions of subatomic physics. It consists of two quantum field theories: the Weinberg-Salam theory of electromagnetic and weak interactions, and quantum chromodynamics (QCD), the theory of the strong interactions. The standard model has been enormously successful in explaining a wealth of data produced in accelerator and cosmic ray experiments over the past 30 years. Our knowledge of it is incomplete, however, because it has been difficult to extract many of the most interesting predictions of QCD: those that depend on the strong coupling regime of the theory and therefore require nonperturbative calculations.

At present, the only means of carrying out nonperturbative QCD calculations from first principles and with controlled errors is through large-scale numerical simulations within the framework of lattice gauge theory. These simulations are needed to obtain a quantitative understanding of the physical phenomena controlled by the strong interactions, such as the masses, widths, and scattering lengths of the light hadrons, and to make possible the determination of the weak interaction Cabibbo-Kobayashi-Maskawa (CKM) matrix elements from experiment. A central objective of the experimental program in high-energy physics, and of lattice QCD simulations, is to determine the range of validity of the standard model, and to search for new physics beyond it. Thus, QCD simulations play an important role in efforts to obtain a deeper understanding of the fundamental laws of physics.

Major progress has been made in the numerical study of QCD over the last decade through the use of improved formulations of QCD on the lattice, the development of new algorithms, and the increase in computing power available to lattice gauge theorists. The lattice formulation of QCD is not merely a numerical approximation to the continuum formulation. The lattice regularization is every bit as valid as any of the popular continuum regularizations, and has the distinct advantage of being nonperturbative. The lattice spacing a establishes a momentum cutoff π/a that removes ultraviolet divergences. Standard renormalization methods apply, and in the perturbative regime they allow a straightforward conversion of lattice results to any of the standard continuum regularization schemes.

There are several formulations of the lattice QCD Lagrangian in current widespread use. The gauge field action can be constructed with varying degrees of improvement that are designed to reduce cutoff effects at nonzero lattice spacing. The quark action can be formulated using Wilson's original method (Wilson, 1974) with modern improvements (Sheikholeslami and Wohlert,

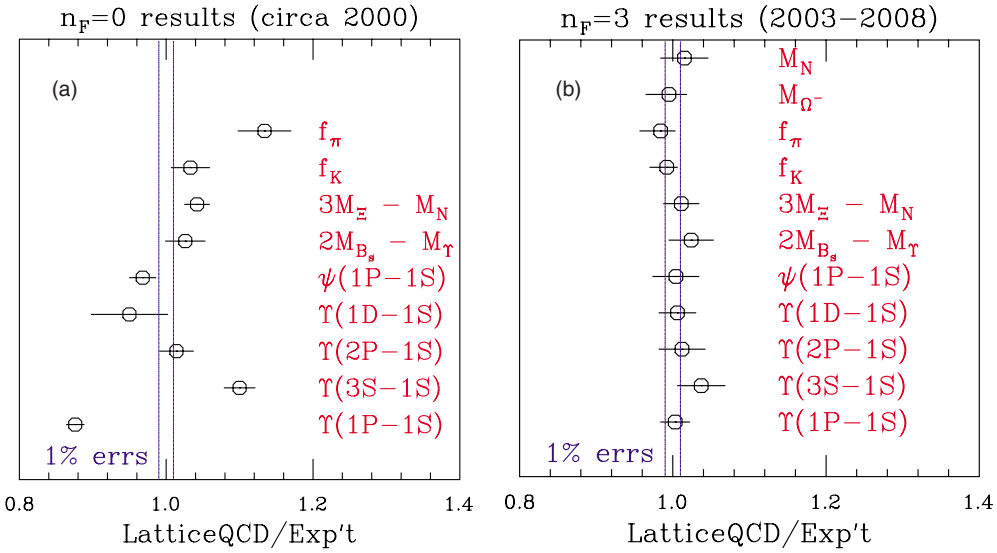

FIG. 1. (Color online) Comparison of the ratio of lattice QCD and experimental values for several observables, where the lattice QCD calculations are done in the quenched approximation (left) and with 2+1 flavors of asqtad sea quarks (right). Adapted from Davies *et al.*, 2004.

1985) or with the twisted mass (Frezzotti *et al.*, 2000, 2001; Frezzotti and Rossi, 2004) or other variants (Zanotti *et al.*, 2002; Morningstar and Peardon, 2004), with the Kogut-Susskind or staggered fermion formulation (Kogut and Susskind, 1975; Banks *et al.*, 1976, 1977; Susskind, 1977) with improvements, and with the more recently implemented chiral methods that include domain-wall fermions (Kaplan, 1992; Shamir, 1993; Furman and Shamir, 1995) and overlap fermions (Narayanan and Neuberger, 1995; Neuberger, 1998b). Other improvements also in production use are Wilson quarks with hypercubic (HYP) smearing to reduce lattice artifacts (Hasenfratz *et al.*, 2007; Schaefer *et al.*, 2007), or to approximate good chiral behavior (Gattringer, 2001).

In this article, we review a ten-year research program founded on a particular improvement of staggered fermions called "asqtad" (Blum *et al.*, 1997; Lepage, 1998; Lagae and Sinclair, 1999; Orginos and Toussaint, 1999; Orginos *et al.*, 1999; Bernard *et al.*, 2000b) [named for its $\mathcal{O}(a^2)$ level of improvement and its inclusion of a "tadpole" renormalization]. Over this time, the MILC Collaboration has created a significant library of gauge field configuration ensembles with the full complement of the light sea quarks u, d, and s. The masses of the u and d quarks have been taken to be equal, which has a negligible effect ($<1\%$) on isospin-averaged quantities. In planning the parameters of these ensembles, an attempt has been made to address the three primary sources of systematic errors in lattice QCD calculations: the chiral and continuum extrapolations, and finite size effects. It is straightforward to perform simulations with the mass of the s quark close to its physical value, and in most of the ensembles that has been done. However, up to now it has been too computationally expensive to perform simulations at the physical mass of the u and d quarks. Instead, ensembles have been generated with a range of light quark masses in order to perform extrapolations to the chiral (physical value of the u and d quark mass) limit guided by chiral perturbation theory. Simulations have been performed with six values of the lattice spacing in order to enable controlled extrapolations to the continuum (zero lattice spacing) limit, and in almost all cases the physical size of the box in which the simulations have been carried out has been taken to be more than four times the Compton wavelength of the pion in order to minimize finite size effects. Finally, because SU(3) chiral perturbation theory converges rather slowly for the s quark mass close to its physical value, a number of ensembles have been generated with lighter than physical s quark masses to improve the chiral extrapolation. These ensembles are publicly available, and have been used by a number of research groups to calculate a variety of hadronic quantities ranging from chiral properties of light mesons to hadronic parton distributions to semileptonic decays of mesons with a charm or bottom quark to the spectroscopy of heavy quarkonium.

The asqtad improved staggered fermion approach has enjoyed considerable success. Its comparatively high degree of improvement and its relatively low computational cost enabled a broad set of full QCD phenomenological calculations earlier than was possible with other fermion methods. In Fig. 1 we show the effects of including sea quarks in a variety of physical quantities (Davies *et al.*, 2004). Computations with asqtad sea quarks are able to account for a variety of known decay constants, some hadronic masses, and several quarkonium mass splittings to a precision of a few percent (Davies *et al.*, 2004). Their predictions for a few heavy-light leptonic (Aubin *et al.*, 2005a) and semileptonic decays (Aubin *et al.*, 2005b) have been experimentally confirmed. They provide values for the strong fine structure constant α_s (Davies *et al.*, 2008), the charm quark mass (Davies *et al.*, 2009), the CKM matrix elements $|V_{us}|$ (Bernard *et al.*,

2007b), $|V_{cb}|$ (Bernard *et al.*, 2009a), and $|V_{ub}|$ (Bailey *et al.*, 2009), and the D^+ and D_s leptonic decay constants (Follana *et al.*, 2008) that are competitive with the most accurate determinations to date.

In Sec. II, we begin with a review of lattice gauge theory, discussing gauge field and fermion field formulations and numerical simulation methods. We end Sec. II with an overview of the asqtad and the more recent highly improved staggered quark (HISQ) fermion formulations.

Section III first discusses the inclusion of staggered discretization errors in chiral perturbation theory, resulting in "staggered chiral perturbation theory" (SχPT). The application to the light pseudoscalar meson sector is described in detail; applications to heavy-light mesons and to a mixed-action theory (with chiral valence quarks and staggered sea quarks) are treated more briefly. We then turn attention to the procedure used to deal with the extra species that occur for staggered fermions. Each staggered field (each flavor of quark) normally gives rise to four species in the continuum limit. The additional degree of freedom is called "taste." To obtain the correct counting of sea quarks it is necessary to take the fourth-root of the fermion determinant. This rooting procedure has been shown to produce a theory that is nonlocal on the lattice, leading to the legitimate question of whether the nonlocality persists as the lattice spacing goes to zero. Such nonlocality would spoil the continuum limit, giving a theory inequivalent to QCD. Recently, however, there has been much work on this issue, and there is now a substantial body of theoretical and computational evidence that the fourth root methodology is indeed correct. We discuss some of that work in Sec. III, and also explain how to take rooting into account properly in the chiral effective theory.

In Sec. IV, we list the ensembles of publicly available asqtad gauge configurations, and describe tests of their intended properties, including the determination of the lattice scale and the topological susceptibility. In the following sections, we review physics results obtained with them. In Sec. V, we review the spectroscopy of light hadrons other than the pseudoscalar mesons, including vector and scalar mesons and baryons. Section VI is devoted to properties of the pseudoscalar mesons, including masses, decay constants, and Gasser-Leutwyler low energy constants. We turn in Secs. VII and VIII to the masses and decays of mesons containing one heavy (charm or bottom) quark and one light antiquark. Section VII treats masses and leptonic decays; Sec. VIII, semileptonic decays.

In Sec. IX, we review a variety of other calculations, including the determination of the strong coupling α_s, quarkonium spectroscopy, the spectroscopy of baryons containing one or two heavy quarks, K_0-$\bar{K}_0$ and B_0-$\bar{B}_0$ mixing, the muon anomalous magnetic moment, and quark and gluon propagators.

Finally, in Sec. X, we discuss further improvements under way or under consideration, including the incorporation of electromagnetic effects and the implementation of the HISQ action, and briefly comment on future prospects for the field.

We do not review applications of the asqtad formulation to QCD thermodynamics. A recent article by DeTar and Heller (2009) contains a review of high temperature and nonzero density results, including those obtained using the asqtad fermion action.

II. FERMIONS ON THE LATTICE: IMPROVED STAGGERED FORMALISM

A. Brief introduction to lattice gauge theory

1. Basic setup

Euclidean, i.e., imaginary time, field theories can be regulated by formulating them on a space-time lattice, with the lattice points, called sites, separated by the lattice spacing a. This introduces an ultraviolet cutoff π/a on any momentum component. Matter fields then reside only on the lattice sites, while the gauge fields are associated with the links joining neighboring sites. The gauge fields are represented by gauge group elements $U_\mu(x)$ on the links, which represent parallel transporters from site x to the neighboring site $x+a\hat{\mu}$, where $\hat{\mu}$ is the unit vector in the direction μ, with $\mu=1,\ldots,d$ for a d-dimensional lattice,

$$\begin{aligned} U_\mu(x) &= \mathcal{P}\exp\left\{ ig\int_x^{x+a\hat{\mu}} dy_\nu A_\nu(y)\right\} \\ &= \exp\left\{ iga\left[A_\mu(x+a\hat{\mu}/2) \right.\right. \\ &\quad \left.\left. + \frac{a^2}{24}\partial_\mu^2 A_\mu(x+a\hat{\mu}/2) + \cdots \right]\right\} \\ &= 1 + iagA_\mu(x+a\hat{\mu}/2) + \cdots . \end{aligned} \tag{1}$$

Under gauge transformations $V(x)$, restricted to the sites of the lattice, the gauge links transform as

$$U_\mu(x) \to V(x)U_\mu(x)V^\dagger(x+a\hat{\mu}). \tag{2}$$

The traces of products of gauge links around closed loops on the lattice, so-called Wilson loops, are then gauge invariant. The gauge action can be built from the sum over the lattice of combinations of small Wilson loops with coefficients adjusted such that in the continuum limit, $a\to 0$, it reduces to $\int d^dx \frac{1}{2}\,\mathrm{Tr}\,F_{\mu\nu}^2$ up to terms of $\mathcal{O}(a^2)$. The simplest gauge action, the original action introduced by Wilson (1974), consists of a sum over plaquettes (1×1 Wilson loops)

$$S_G = \frac{\beta}{N}\sum_{pl} \mathrm{Re}\,\mathrm{Tr}\,(1-U_{pl}), \tag{3}$$

where $\beta=2N/g^2$, for gauge group SU(N), with g^2 the bare coupling constant.

Fermions, in Euclidean space, are represented by Grassmann fields ψ_x and $\bar{\psi}_x$, which in the lattice formulation reside on the sites of the lattice. A generic fermion action can be written as

$$S_F = \sum_{x,y} \bar{\psi}_x M_{F;x,y} \psi_y, \tag{4}$$

where the fermion matrix $M_{F;x,y}$ is some lattice discretization of the continuum Dirac operator $D+m$. Details of lattice fermion actions are described below.

The lattice gauge theory partition function is then given by

$$Z(\beta) = \int \prod_{x,\mu} dU_\mu(x) \prod_x [d\bar{\psi}_x d\psi_x] \exp\{-S_G - a^4 S_F\}, \tag{5}$$

where $dU_\mu(x)$ is the invariant SU(N) Haar measure and $d\bar{\psi}_x d\psi_x$ indicate integration over the Grassmann fields.

Since S_F is quadratic in the fermion fields, the integration over the Grassmann fields can be carried out, leading to (up to a trivial overall factor)

$$\begin{aligned} Z(\beta) &= \int \prod_{x,\mu} dU_\mu(x) \det M_F \exp\{-S_G\} \\ &= \int \prod_{x,\mu} dU_\mu(x) \exp\{-S_{\text{eff}}\}, \end{aligned} \tag{6}$$

with $S_{\text{eff}} = S_G - \text{Tr} \ln M_F$.

The expectation value of some observable O is given by

$$\begin{aligned} \langle O \rangle &= \frac{1}{Z(\beta)} \int \prod_{x,\mu} dU_\mu(x) \\ &\quad \times \prod_x [d\bar{\psi}_x d\psi_x] O \exp\{-S_G - a^4 S_F\} \\ &= \frac{1}{Z(\beta)} \int \prod_{x,\mu} dU_\mu(x) O \det M_F \exp\{-S_G\} \\ &= \frac{1}{Z(\beta)} \int \prod_{x,\mu} dU_\mu(x) O \exp\{-S_{\text{eff}}\}. \end{aligned} \tag{7}$$

If the observable O involves fermion fields ψ_x and $\bar{\psi}_y$ then, in the third line of Eq. (7) each pair is replaced by $M^{-1}_{F;x,y}$ in all possible combinations with the appropriate minus signs for Wick contractions of fermion fields.

2. Improved action

As mentioned before Eq. (3), the typical gauge action on the lattice reduces to the continuum action up to terms of $\mathcal{O}(a^2)$. These terms lead to $\mathcal{O}(a^2)$ deviations from the continuum result of physical observables computed at finite lattice spacing. These $\mathcal{O}(a^2)$ effects can be reduced by using an improved gauge action (together with improved operators, where necessary) in an improvement program initiated by Symanzik (1980, 1983).

For the gauge action, the improvement can be achieved by adding 2×1 (planar) rectangle (labeled "rt") and generalized three-dimensional $1\times1\times1$ parallelogram (labeled "pg") Wilson loop terms (see Fig. 2) to the

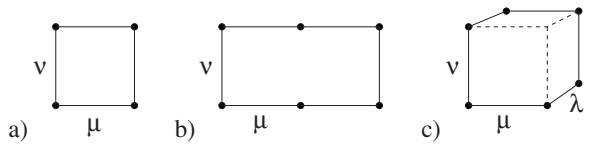

FIG. 2. Lüscher-Weisz action Wilson loops: (a) standard plaquette, (b) 2×1 rectangle, and (c) $1\times1\times1$ parallelogram.

Wilson action, Eq. (3), with coefficients computed, at one-loop order in perturbation theory, by Lüscher and Weisz (1985a, 1985b),

$$\begin{aligned} S_{LW} = \frac{\beta}{N} \Bigg\{ &\sum_{pl} c_{pl} \,\text{Re Tr}(1 - U_{pl}) + \sum_{rt} c_{rt} \,\text{Re Tr}(1 - U_{rt}) \\ &+ \sum_{pg} c_{pg} \,\text{Re Tr}(1 - U_{pg}) \Bigg\}. \end{aligned} \tag{8}$$

The coefficients $c_i = c_i^{(0)} + 4\pi\alpha_0 c_i^{(1)}$ at one loop can be found in Table I of Lüscher and Weisz (1985a).

Bare lattice perturbation theory results generally converge slowly but can be improved by using tadpole-improved perturbation theory (Lepage and Mackenzie, 1993). This starts with using a more continuumlike gauge link $U_\mu \to \tilde{U}_\mu = u_0^{-1} U_\mu$. The so-called tadpole factor u_0 is determined in numerical simulations either as the expectation value of U_μ in Landau gauge or, more commonly, from the expectation value of the average plaquette

$$u_0 = \langle N^{-1} \,\text{Re Tr}\, U_{pl} \rangle^{1/4}. \tag{9}$$

The Lüscher-Weisz action can now be tadpole improved by explicitly pulling a u_0^{-1} factor out of each link and replacing α_0 in the one-loop perturbative coefficients c_i with a nonperturbatively renormalized coupling α_s defined, for gauge group SU(3), in terms of the measured lattice value of u_0 by

$$\alpha_s \equiv -1.303615 \ln u_0, \tag{10}$$

where the proportionality factor is determined by the one-loop expression for $\ln u_0$. Defining $\beta_{LW} \equiv u_0^{-4} \beta c_{pl}$, since U_{pl} involves the product of four links, the improved action can be written as (Alford *et al.*, 1995)

$$\begin{aligned} S_{LW} = \frac{\beta_{LW}}{3} \Bigg\{ &\sum_{pl} \,\text{Re Tr}(1 - U_{pl}) \\ &- \sum_{rt} \frac{[1 + 0.4805\alpha_s]}{20u_0^2} \,\text{Re Tr}(1 - U_{rt}) \\ &- \sum_{pg} \frac{0.03325\alpha_s}{u_0^2} \,\text{Re Tr}(1 - U_{pg}) \Bigg\}. \end{aligned} \tag{11}$$

Since higher perturbative orders in the coefficients are neglected, the one-loop improved Lüscher-Weisz action, Eq. (11), leads to remaining lattice artifacts of $\mathcal{O}(\alpha_s^2 a^2)$. Sometimes, only a tree-level improved action without the terms proportional to α_s in Eq. (11) is used, leading to lattice artifacts of $\mathcal{O}(\alpha_s a^2)$. Since the parallelogram terms are then absent such simulations are somewhat faster. It should be noted that Eq. (11) does not include

the one-loop contributions from dynamical fermions, which were unknown at the time the MILC Collaboration started the (2+1)-flavor simulations reviewed in this article. Therefore, for those simulations, the leading lattice artifacts in the gauge sector are $\mathcal{O}(\alpha_s a^2)$ as in the fermion sector, described later. The one-loop fermion contribution has recently been computed by Hao, von Hippel, Horgan, Mason, and Trottier (2007).

B. Fermions on the lattice

1. The doubling problem

Putting fermions on a lattice, one replaces the covariant derivative in the continuum fermion action with a covariant (central) difference

$$S_{\text{naive}} = \sum_x \bar{\psi}(x)\left\{\sum_\mu \gamma_\mu \nabla_\mu \psi(x) + m\psi(x)\right\}, \tag{12}$$

where

$$\nabla_\mu \psi(x) = \frac{1}{2a}[U_\mu(x)\psi(x+a\hat{\mu}) - U_\mu^\dagger(x-a\hat{\mu})\psi(x-a\hat{\mu})]. \tag{13}$$

The inverse propagator in momentum space derived from the action Eq. (12) in the free case, with all link fields $U_\mu = 1$, is

$$aS^{-1}(ap) = i\sum_\mu \gamma_\mu \sin(ap_\mu) + am. \tag{14}$$

In the massless case, this inverse propagator not only vanishes when $p=0$, but also when $p_\mu = 0$ or $p_\mu = \pi/a$ for each $\mu = 1,\ldots,4$, i.e., on all 16 corners of the Brillouin zone in $d=4$ dimensions. Thus, when we try to put one fermion on the lattice we actually get 16 in the continuum limit. This is the infamous doubling problem of lattice fermions.

2. Wilson fermions

This doubling problem was recognized by Wilson when he first formulated lattice gauge theories. He also proposed a solution: adding an irrelevant term—a term that vanishes in the continuum limit, $a \to 0$ (Wilson, 1975),

$$S_W = S_{\text{naive}} - \frac{ar}{2}\sum_x \bar{\psi}(x)\sum_\mu \Delta_\mu \psi(x) = \bar{\psi} D_W(m)\psi, \tag{15}$$

where r is a free parameter, usually set to $r=1$, and the Laplacian is

$$\Delta_\mu \psi(x) = \frac{1}{a^2}[U_\mu(x)\psi(x+a\hat{\mu}) + U_\mu^\dagger(x-a\hat{\mu})\psi(x-a\hat{\mu}) - 2\psi(x)]. \tag{16}$$

The free inverse propagator now is

$$aS^{-1}(ap) = i\sum_\mu \gamma_\mu \sin(ap_\mu) + am - r\sum_\mu [\cos(ap_\mu) - 1]. \tag{17}$$

The doublers, with n momentum components $p_\mu = \pi/a$, now attain masses $m + 2nr/a$, and only one fermion, with $p \approx 0$, remains light.

We note that the Wilson Dirac operator is γ_5 Hermitian,

$$D_W^\dagger(m) = \gamma_5 D_W(m)\gamma_5. \tag{18}$$

Thus $\det D_W^\dagger(m) = \det D_W(m)$, implying that two flavors—and by extension any even number of flavors of Wilson fermions—lead to a manifestly positive (semi) definite fermion determinant, $\det[D_W^\dagger(m) D_W(m)]$.

The price for eliminating the doubling problem in this Wilson fermion approach is that the action Eq. (15) violates the chiral symmetry $\delta\psi = i\alpha\gamma_5\psi$, $\delta\bar{\psi} = i\alpha\bar{\psi}\gamma_5$ of massless fermions (with α an infinitesimal parameter). As a consequence, the massless limit of fermions is no longer protected—the mass gets an additive renormalization; to get massless quarks requires a fine tuning of the bare mass parameter.

According to the usual, renormalization group based universality arguments, the chiral symmetry, broken at finite lattice spacing only by an irrelevant dimension-five operator, will be recovered in the continuum limit after fine tuning of the bare mass parameter. But the explicit violation of chiral symmetry allows the generation of other contributions to dimension-five operators, which are suppressed by only one power of the lattice spacing a. The lattice artifacts for Wilson fermions are therefore of $\mathcal{O}(a)$, rather than $\mathcal{O}(a^2)$ as in the pure gauge sector.

Besides $\bar{\psi}(x)\Delta\psi(x)$, with $\Delta = \Sigma_\mu \Delta_\mu$, there is a second dimension-five (chiral symmetry breaking) operator

$$S_{SW} = \frac{iag}{4} c_{SW} \sum_x \bar{\psi}(x)\sigma_{\mu\nu}\mathcal{F}_{\mu\nu}(x)\psi(x), \tag{19}$$

where $\mathcal{F}_{\mu\nu}(x)$ is a lattice representation of the field strength tensor $F_{\mu\nu}(x)$, and $\sigma_{\mu\nu} = \frac{i}{2}[\gamma_\mu, \gamma_\nu]$. Inclusion of Eq. (19) into the fermion action, with properly adjusted coefficient c_{SW}, was proposed by Sheikholeslami and Wohlert (1985) to eliminate the $\mathcal{O}(a)$ effects of the Wilson fermion action. Since $\mathcal{F}_{\mu\nu}(x)$ on the lattice is usually represented by a "clover leaf" pattern of open plaquettes, the action including the term Eq. (19) is commonly referred to as the clover action.

The appropriate coefficient c_{SW} of the clover term, Eq. (19), can be computed in perturbation theory (Wohlert, 1987; Lüscher and Weisz, 1996), or even better nonperturbatively (Lüscher *et al.*, 1996, 1997)—truly reducing the remaining lattice effects from $\mathcal{O}(a)$ to $\mathcal{O}(a^2)$.

Another problem with Wilson fermions is that because of the additive mass renormalization the fermion determinant $\det D_W(m)$ is not positive definite even for putative positive quark mass. Configurations with $\det D_W(m) \approx 0$ can occur, called exceptional configurations, which can slow down numerical simulations con-

siderably. A formulation that removes such exceptional configurations, introduced by Frezzotti *et al.* (Frezzotti *et al.*, 2000, 2001; Frezzotti and Rossi, 2004) is called "twisted-mass QCD." For two flavors one considers the Dirac operator

$$D_{\text{twist}} = D + m + i\mu\gamma_5\tau_3, \tag{20}$$

where the isospin generator τ_3 acts in flavor space. In the continuum, the twisted-mass Dirac operator is equivalent to a usual Dirac operator with mass $\sqrt{m^2+\mu^2}$. On the lattice, however, with D replaced by the (massless) Wilson Dirac operator $D_W(0)$ of Eq. (15), the twisted-mass term ensures a positive-definite two-flavor determinant, $\det[D_W^\dagger(m)D_W(m)+\mu^2]>0$. An added benefit of the twisted-mass (Wilson) fermion formulation is, that at maximal twist $\tan\alpha=\mu/m$, the twisted-mass Wilson Dirac operator is automatically $\mathcal{O}(a^2)$ improved (Frezzotti and Rossi, 2004). Unfortunately, the real part of the mass m still receives an additive renormalization so that achieving maximal twist requires a fine tuning. Furthermore, at finite lattice spacing, isospin symmetry is broken, making the π^0 mass different from the mass of the $\pi^\pm$.

3. Staggered fermions

Another way of dealing with the doubling problem, alleviating though not eliminating it, is the staggered fermion formalism (Kogut and Susskind, 1975; Banks *et al.*, 1976, 1977; Susskind, 1977). One introduces a new fermion field by

$$\psi(x) = \Gamma_x\chi(x), \quad \bar{\psi}(x) = \bar{\chi}(x)\Gamma_x^\dagger, \tag{21}$$

with

$$\Gamma_x = \gamma_1^{(x_1/a)}\gamma_2^{(x_2/a)}\gamma_3^{(x_3/a)}\gamma_4^{(x_4/a)}. \tag{22}$$

Using $\Gamma_x^\dagger\Gamma_x=1$ and

$$\Gamma_x^\dagger\gamma_\mu\Gamma_{x+a\mu} = (-1)^{(x_1+\cdots+x_{\mu-1})/a} \equiv \eta_\mu(x), \tag{23}$$

the naive fermion action, Eq. (12), can be written as

$$\begin{aligned} S_{KS} &= \sum_x \bar{\chi}(x)\left\{\sum_\mu \eta_\mu(x)\nabla_\mu\chi(x) + m\chi(x)\right\} \\ &\equiv \bar{\chi}(D_{KS}+m)\chi, \end{aligned} \tag{24}$$

where matrix multiplication is implied in the final expression. Here, the four Dirac components decouple from each other, and the fermion field $\chi(x)$ can be restricted to a single component, thereby reducing the doubling by a factor of 4, from 16 to 4. It is, in principle, possible to interpret these four remaining degrees of freedom as physical flavor (u,d,s,c), but, in order to give different masses to the flavors, one must introduce general mass terms coupling nearby sites (Göckeler, 1984; Golterman and Smit, 1984). That approach then leads to a variety of practical problems including complex determinants and the necessity of fine tuning.

Instead, we follow modern usage and refer to the quantum number labeling the four remaining fermion species as taste, which, unlike flavor, is an unwanted degree of freedom that must be removed. We describe how this removal is accomplished by the so-called "fourth-root procedure" at the end of this section, and discuss it in more detail in Sec. III.C. If more than one physical flavor is required, as is, of course, the case for simulations of QCD, one then needs to introduce a separate staggered field for each flavor. For example, for QCD with three light flavors, one employs three staggered fields χ_u, χ_d, and χ_s.[1] However, for simplicity, we consider only a single staggered field (one flavor) in the remainder of this section.

The one-component fermions with action Eq. (24) are referred to as (standard) staggered or Kogut-Susskind fermions. The "standard" distinguishes them from improved versions, described later on.

An important discrete symmetry of the staggered fermion action, Eq. (24), is shift symmetry (van den Doel and Smit, 1983; Golterman and Smit, 1984)

$$\begin{aligned} \chi(x) &\to \rho_\mu(x)\chi(x+a\hat{\mu}), \\ \bar{\chi}(x) &\to \rho_\mu(x)\bar{\chi}(x+a\hat{\mu}), \\ U_\nu(x) &\to U_\nu(x+a\hat{\mu}), \end{aligned} \tag{25}$$

with the phase $\rho_\mu(x)$ defined by $\rho_\mu(x)=(-1)^{(x_{\mu+1}+\cdots+x_4)/a}$. Additional discrete symmetries of the staggered action are 90° rotations, axis inversions, and charge conjugation. In the continuum limit, these symmetries are expected to enlarge to a direct product of the Euclidean Poincaré group and a vector $\mathrm{SU}(4)_V$ among the tastes (plus parity and charge conjugation) (Golterman and Smit, 1984).

For massless quarks, $m=0$, the staggered fermion action also has a continuous even-odd $\mathrm{U}(1)_e\times\mathrm{U}(1)_o$ chiral symmetry (Kawamoto and Smit, 1981; Kluberg-Stern *et al.*, 1981; Kluberg-Stern, Morel, and Petersson, 1983), a remnant of the usual chiral symmetry for massless fermions in the continuum. The $\mathrm{U}(1)_e\times\mathrm{U}(1)_o$ symmetry is

$$\begin{aligned} &\chi(x) \to \exp\{i\alpha_e\}\chi(x), \quad \bar{\chi}(x) \to \bar{\chi}(x)\exp\{-i\alpha_o\} \\ &\qquad \text{for } x = \text{even}, \\ &\chi(x) \to \exp\{i\alpha_o\}\chi(x), \quad \bar{\chi}(x) \to \bar{\chi}(x)\exp\{-i\alpha_e\} \\ &\qquad \text{for } x = \text{odd}, \end{aligned} \tag{26}$$

where α_e and α_o are the symmetry parameters, and a site x is called even or odd if $\Sigma_\mu(x_\mu/a)$ is even or odd. The "axial part" of this symmetry, $\alpha_e=-\alpha_o\equiv\alpha_\varepsilon$, is known as $\mathrm{U}(1)_\varepsilon$ symmetry (Kawamoto and Smit, 1981) and takes the form

[1] In practice, since one usually takes $m_u=m_d\neq m_s$, the u and d fields can be simulated together, and one can use only two staggered fields. For clarity, we ignore this technical detail.

$$\chi(x) \to \exp\{i\alpha_\varepsilon \varepsilon(x)\}\chi(x), \quad \bar{\chi}(x) \to \bar{\chi}(x)\exp\{i\alpha_\varepsilon \varepsilon(x)\}$$
$$\text{with } \varepsilon(x) \equiv (-1)^{\Sigma_\mu (x_\mu/a)}. \tag{27}$$

The chiral symmetry, Eq. (26) or (27), protects the mass term in Eq. (24) from additive renormalization, while the discrete symmetries (especially shift symmetry) are also needed to prevent other mass terms (coupling χ and $\bar{\chi}$ at nearby sites) from arising (Golterman and Smit, 1984). In particular, an alternative version of staggered quarks called the "Dirac-Kähler action" (Becher and Joos, 1982) does not have shift symmetry and therefore generates a mass term at one loop even when $m=0$ (Mitra and Weisz, 1983).

The even-odd symmetry is spontaneously broken to the diagonal vector $\mathrm{U}(1)_V$ (quark number) symmetry, $\alpha_e=\alpha_o$, with an ensuing Goldstone boson. In addition, the mass term breaks the $\mathrm{U}(1)_e \times \mathrm{U}(1)_o$ symmetry explicitly, giving mass to the Goldstone boson, $m_G^2 \propto m$.

The staggered Dirac operator D_{KS} in Eq. (24) obeys (Smit and Vink, 1987)

$$D_{KS}^\dagger = -D_{KS} = \varepsilon D_{KS} \varepsilon, \tag{28}$$

where ε is a diagonal matrix in position space with $\varepsilon(x)$ along the diagonal, and the second equality follows from the fact that D_{KS} connects only even and odd sites. The fact that D_{KS} is antihermitian implies that its eigenvalues are purely imaginary; the ε relation in Eq. (28) then tells us that the nonzero eigenvalues come in complex-conjugate pairs. For $m>0$, which is the case of interest here, this ensures that the staggered determinant $\det(D_{KS}+m)$ is strictly positive.[2] Note that the continuum Euclidean Dirac operator D_{cont} is also anti-Hermitian and obeys a corresponding equation

$$D_{\mathrm{cont}}^\dagger = -D_{\mathrm{cont}} = \gamma_5 D_{\mathrm{cont}} \gamma_5, \tag{29}$$

which similarly results in a positive determinant for positive quark mass.

The one-component staggered fermion fields $\chi(x)$ can be assembled into Dirac fields $q(y)$, living on 2^4 hypercubes of the original lattice, labeled by y, with corners $x=2y+aA$, where $A_\mu=0,1$ (Duncan *et al.*, 1982; Gliozzi, 1982; Kluberg-Stern, Morel, Napoly, and Petersson, 1983). One has

$$q(y)_{\alpha i} = \frac{1}{8}\sum_A (\Gamma_A)_{\alpha i} U_A(y) \chi(2y+aA), \tag{30}$$

$$\bar{q}(y)_{i\alpha} = \frac{1}{8}\sum_A \bar{\chi}(2y+aA) U_A^\dagger(y) (\Gamma_A)_{i\alpha}^\dagger,$$

where α, i label the Dirac and taste indices, respectively, and $U_A(y)$ is a product of the gauge links over some fixed path from $2y$ to $2y+aA$. Bilinear quark operators, with spin structure $\gamma_s=\Gamma_s$ and taste structure $\xi_t=\Gamma_t^*$ are defined by (Sharpe and Patel, 1994)

$$\mathcal{O}_{st} = \bar{q}(y)(\gamma_s \otimes \xi_t) q(y)$$
$$= \frac{1}{16}\sum_{A,B} \bar{\chi}(2y+aA) U_A^\dagger(y) U_B(y)$$
$$\times \chi(2y+aB) \frac{1}{4}\mathrm{Tr}(\Gamma_A^\dagger \Gamma_s \Gamma_B \Gamma_t^\dagger). \tag{31}$$

In the free case [all $U_\mu(x)=1$], the quark action in Eq. (24) can be expressed in terms of the fields $q(y)$ as (Kluberg-Stern, Morel, Napoly, and Petersson, 1983)

$$S_{KS} = 16\sum_y \bar{q}(y)\Big\{ m(I\otimes I) + \sum_\mu [(\gamma_\mu \otimes I)\nabla_\mu$$
$$+ a(\gamma_5 \otimes \xi_\mu \xi_5)\Delta_\mu]\Big\} q(y), \tag{32}$$

where I is the identity matrix, the factor of 16 arises from the fact that there are $1/16$ as many y points as x points, and ∇_μ and Δ_μ are the free-field versions of Eqs. (13) and (16), but acting on the doubled (y) lattice

$$\nabla_\mu f(y) = \frac{1}{4a}[f(y+2a\hat{\mu}) - f(y-2a\hat{\mu})],$$

$$\Delta_\mu f(y) = \frac{1}{4a^2}[f(y+2a\hat{\mu}) - 2f(y) + f(y-2a\hat{\mu})]. \tag{33}$$

These derivatives go to $\partial_\mu f(y)$ and $\partial_\mu^2 f(y)$, respectively, in the continuum limit. In the interacting case there is another dimension-five, $\mathcal{O}(a)$, term, involving the field-strength tensor $\mathcal{F}_{\mu\nu}$, in addition to the Δ_μ term in Eq. (32). There are also higher contributions of $\mathcal{O}(a^2)$ starting at dimension six (Kluberg-Stern, Morel, Napoly, and Petersson, 1983).

In the ∇_μ (first derivative) kinetic energy term of Eq. (32), the even-odd $\mathrm{U}(1)_e \times \mathrm{U}(1)_o$ symmetry is enlarged to a full continuous chiral symmetry, $\mathrm{U}(4)_L \times \mathrm{U}(4)_R$, acting on the taste indices of the right and left fields, $q_R(y)=\frac{1}{2}(1+\gamma_5)q(y)$ and $q_L(y)=\frac{1}{2}(1-\gamma_5)q(y)$. The mass term breaks this down to an $\mathrm{SU}(4)_V$ vector taste symmetry [plus the $\mathrm{U}(1)_V$ of quark number]. On the other hand, because of the explicit taste matrices, the second derivative term in Eq. (32) breaks the full chiral symmetry to the $\mathrm{U}(1)_e \times \mathrm{U}(1)_o$ symmetry (plus the discrete staggered symmetries). Because these are all symmetries of the original staggered action, they remain symmetries in the taste basis, even when the additional terms that appear in Eq. (32) in the interacting case are taken into account.

[2]We do not expect any exact zero modes on generic configurations, even those with net topological charge. Such configurations will in general have only some near-zero [$\mathcal{O}(a)$ or smaller] eigenvalues. So, in fact, the determinant should be positive even for $m<0$. This is different from the case of chiral fermions discussed in Sec. II.B.4.

The key point is that, in the interacting theory, one can split the staggered Dirac operator in the taste basis as

$$D_{KS} = D \otimes I + a\Delta, \tag{34}$$

where I is the 4×4 identity matrix in taste space and Δ is the taste-violating (traceless) part, with minimum dimension five. One expects the $SU(4)_V$ vector taste symmetry to be restored in the continuum limit because Δ should be irrelevant in the renormalization-group sense.

In the free case, the shift symmetry, Eq. (25), takes the form for the Dirac fields $q(y)$ (Luo, 1997)

$$q(y) \to \tfrac{1}{2}[(I \otimes \xi_\mu + \gamma_5\gamma_\mu \otimes \xi_5)q(y) + (I \otimes \xi_\mu - \gamma_5\gamma_\mu \otimes \xi_5)q(y + 2a\hat{\mu})], \tag{35}$$

$$\bar{q}(y) \to \tfrac{1}{2}[\bar{q}(y)(I \otimes \xi_\mu - \gamma_5\gamma_\mu \otimes \xi_5) + \bar{q}(y + 2a\hat{\mu})(I \otimes \xi_\mu + \gamma_5\gamma_\mu \otimes \xi_5)]. \tag{36}$$

As the continuum limit is approached, shifts become simply multiplication by the taste matrix ξ_μ, plus higher-dimension terms involving derivatives. Thus shifts are basically discrete vector taste transformations, coupled with translations.

In the taste basis, the axial $U(1)_\varepsilon$ symmetry is

$$q(y) \to \exp\{i\alpha_\varepsilon(\gamma_5 \otimes \xi_5)\}q(y), \qquad \bar{q}(y) \to \bar{q}(y)\exp\{i\alpha_\varepsilon(\gamma_5 \otimes \xi_5)\}. \tag{37}$$

Because of the ξ_5, this is clearly a taste nonsinglet axial symmetry, and hence is nonanomalous. The anomalous axial symmetry $U(1)_A$ must be a taste singlet,

$$q(y) \to \exp\{i\alpha_A(\gamma_5 \otimes I)\}q(y), \qquad \bar{q}(y) \to \bar{q}(y)\exp\{i\alpha_A(\gamma_5 \otimes I)\}. \tag{38}$$

Indeed, this symmetry is not an invariance of the staggered lattice action in the massless limit, and the symmetry violations generate, through the triangle graph, the correct axial anomaly in the continuum limit (Sharatchandra *et al.*, 1981).

The bilinear quark operators in Eq. (31) can create (or annihilate) mesons. Therefore, for staggered quarks, each meson kind with given spin (Dirac) structure Γ_s (e.g., $\Gamma_s=\gamma_5$ for the pion, $\Gamma_s=\gamma_k$ for the rho, etc.) comes in 16 varieties, labeled by the taste index t. In the continuum limit all nonsinglet mesons of a given spin are degenerate[3]—$SU(4)_V$ taste symmetry connects them. But at nonzero lattice spacing, there is only the staggered symmetry group, the group of the discrete symmetries of the staggered action (shifts, 90° rotations, axis inversions, and charge conjugation) plus the $U(1)_V$ of quark number, which are remnants of the continuum Poincaré, taste $SU(4)_V$, quark number, and discrete symmetries. Meson states may be classified under the subgroup of the staggered symmetry group, the "staggered rest frame symmetry group," which is the symmetry group of the transfer matrix (Golterman, 1986a, 1986b). The 16 tastes of a meson with given spin structure are not degenerate at finite lattice spacing, but are split according to irreducible representations of the rest frame group. In particular, only the pion with pseudoscalar taste structure $\xi_t=\gamma_5^*$ is a Goldstone boson, denoted by π_P (P stands for pseudoscalar taste), whose mass vanishes for massless quarks, $m=0$. To leading order in the chiral expansion (see Sec. III.A) the other tastes have masses

$$m_{\pi_t}^2 = m_{\pi_P}^2 + a^2\delta_t = 2Bm + a^2\delta_t, \tag{39}$$

with B a low-energy constant and δ_t a taste-dependent splitting that is independent of a (up to logarithms) for small a. The non-Goldstone pions become degenerate with the Goldstone pion only in the continuum limit. The taste violations in the pion system are found to be larger than those for other hadrons (Ishizuka *et al.*, 1994).

Since staggered fermions have only one (spin) component per lattice site, and since they have a remnant chiral symmetry that insures positivity of the fermion determinant at positive quark mass, they are one of the cheapest fermion formulations to simulate numerically. The main drawback is the need to eliminate the unwanted extra tastes, using the so-called "fourth-root procedure." Each continuum fermion species gives a factor of $\det M_F$ in the partition function, Eq. (6). Therefore, to reduce the contribution from four tastes to a single one, we take the fourth root of the determinant, $(\det M_{KS})^{1/4}$, where $M_{KS}=D_{KS}+m\otimes I$, with D_{KS} given in Eq. (34). The procedure was first introduced in the two-dimensional version of staggered fermions (where it is a "square-root procedure" because there are only two tastes) by Marinari *et al.* (1981b). The point is that the Dirac operator D_{KS} (and hence M_{KS}) should become block diagonal in taste space in the continuum limit because Δ is an irrelevant operator. The fourth-root procedure then becomes equivalent to replacing the D_{KS} by its restriction to a single taste. Conversely, the nontriviality of the prescription arises because taste symmetry is broken at nonzero lattice spacing. In Sec. III.C, we discuss the status of this procedure and the evidence that it accomplishes the goal of producing, in the continuum limit, a single quark species with a local action.

4. Chirally invariant fermions

None of the ways of dealing with the fermion doubling problem outlined so far are entirely satisfactory. Wilson-type fermions explicitly break chiral symmetry, and staggered fermions have a remaining doubling prob-

[3]Mesons that are singlets under taste and any additional flavor symmetries need not be degenerate with the nonsinglet mesons, since they can have physically distinct disconnected contributions to their propagators. An important example is η', which will get a contribution from the anomaly and have a mass in the continuum limit different from that of all other pseudoscalars.

lem, requiring the fourth-root procedure, that continues to be somewhat controversial because of the broken taste symmetry at finite lattice spacing.

Indeed, the chiral anomaly implies that no lattice action can have an exact flavor-singlet chiral symmetry (Karsten and Smit, 1981). There is even a no-go theorem (Nielsen and Ninomiya, 1981) that states that the doubling cannot be avoided with an ultralocal[4] and unitary fermion action. However, actions with a modified form of chiral symmetry on the lattice can avoid doubling while retaining most of the desirable features of chiral symmetry. Such actions couple arbitrarily distant points on the lattice but with exponentially suppressed couplings, $\exp\{-r/r_d\}$, where r_d should be of the order the lattice spacing to ensure a local action in the continuum limit. There are three known ways of achieving this.

The first goes under the name of "domain-wall fermions" and was developed by Kaplan (1992), Shamir (1993), and Furman and Shamir (1995). The construction of Furman and Shamir is usually used nowadays. One introduces an additional, fifth dimension of length L_s and considers five-dimensional Wilson fermions with no gauge links in the fifth direction, and the four-dimensional (4D) gauge links independent of the fifth coordinate s,

$$S_{DW} = \sum_{s=0}^{L_s-1} \sum_x \bar{\psi}(x,s)\Bigg\{ \sum_\mu \left(\gamma_\mu \nabla_\mu - \frac{1}{2}\Delta_\mu\right)\psi(x,s) - M\psi(x,s) - P_-\psi(x,s+1) - P_+\psi(x,s-1)\Bigg\}, \tag{40}$$

where $P_\pm = \frac{1}{2}(1 \pm \gamma_5)$ are chiral projectors and we have set $r=a=1$. M, introduced here with a sign opposite that of the mass term for Wilson fermions, Eq. (15), is often referred to as the domain-wall height and needs to be chosen such that $0<M<2$. For free fermions, $M=1$ is the optimal choice, while in the interacting case M should be somewhat larger. The fermion fields satisfy the boundary condition in the fifth direction,

$$P_-\psi(x,L_s) = -m_f P_-\psi(x,0), \qquad P_+\psi(x,-1) = -m_f P_+\psi(x,L_s-1), \tag{41}$$

where m_f is a bare quark mass.

For $m_f=0$, the domain-wall action, Eq. (40), has 4D chiral modes bound exponentially to the boundaries at $s=0$ and $s=L_s-1$, which are identified with the chiral modes of 4D fermions as

$$q^R(x) = P_+\psi(x,L_s-1), \quad q^L(x) = P_-\psi(x,0), \qquad \bar{q}^R(x) = \bar{\psi}(x,L_s-1)P_-, \quad \bar{q}^L(x) = \bar{\psi}(x,0)P_+. \tag{42}$$

When $L_s\to\infty$ the chiral modes become exact zero modes, the left- and right-handed modes q^L and q^R do not interact for $m_f=0$, and the domain-wall action has a chiral symmetry. At finite L_s the chiral symmetry is slightly broken. Often $L_s=\mathcal{O}(10-20)$ is large enough to keep the chiral symmetry breaking negligibly small. The computational cost of domain-wall fermions is roughly a factor of L_s larger than that for Wilson-type fermions.

Related to these domain-wall fermions are the so-called overlap fermions developed by Narayanan and Neuberger (1995) and Neuberger (1998b). The overlap Dirac operator for massless fermions can be written as (Neuberger, 1998b)

$$aD_{ov} = M[1 + \gamma_5\Theta(\gamma_5 D_W(-M))], \tag{43}$$

where $D_W(-M)$ is the usual Wilson Dirac operator with negative mass $m=-M$, and again $0<M<2$ should be used. $\Theta(X)$ is the matrix sign function, for a Hermitian matrix X, that can be defined as

$$\Theta(X) = X/\sqrt{X^2}. \tag{44}$$

Using the fact that $\Theta^2(X)=1$, it is easy to see that the Neuberger Dirac operator satisfies the so-called Ginsparg-Wilson relation (Ginsparg and Wilson, 1982)

$$\{\gamma_5, D_{ov}\} = aD_{ov}\gamma_5 R D_{ov}, \tag{45}$$

with $R=1/M$, or equivalently, when the inverse of D_{ov} is well defined,

$$\{\gamma_5, D_{ov}^{-1}\} = a\gamma_5 R. \tag{46}$$

In the continuum, chiral symmetry implies that the massless fermion propagator anticommutes with γ_5. The massless overlap propagator violates this only by a local term that vanishes in the continuum limit. Ginsparg and Wilson argued that this is the mildest violation of the continuum chiral symmetry on the lattice possible. In fact, any Dirac operator satisfying the Ginsparg-Wilson relation (45) has a modified chiral symmetry at finite lattice spacing (Lüscher, 1998),

$$\delta\psi = i\alpha\gamma_5(1 - aD/2M)\psi, \quad \delta\bar{\psi} = i\alpha\bar{\psi}(1 - aD/2M)\gamma_5, \tag{47}$$

or

$$\delta\psi = i\alpha\gamma_5(1 - aD/M)\psi = i\alpha\hat{\gamma}_5\psi, \quad \delta\bar{\psi} = i\alpha\bar{\psi}\gamma_5, \tag{48}$$

with $\hat{\gamma}_5 = \gamma_5(1-aD/M)$ satisfying $\hat{\gamma}_5^\dagger = \hat{\gamma}_5$ and, using the Ginsparg-Wilson relation, Eq. (45), $\hat{\gamma}_5^2 = 1$.

The close connection between domain-wall and overlap fermions can be made more explicit by integrating out the "bulk fermions," which have masses of the order of the cutoff $1/a$, from the domain-wall action, Eq. (40) [see Neuberger (1998c), Kikukawa and Noguchi (1999), Borici (2000), and Edwards and Heller (2001)]. In the limit $L_s\to\infty$, one ends up with the overlap Dirac opera-

[4]We denote by "ultralocal" an action that couples only sites a finite number of lattice spacings apart. A "local" action is either ultralocal, or the coupling falls off exponentially with distance with a range of the order of a few lattice spacings, so that the action becomes local in the continuum limit. Such local actions are believed not to change the universality class in the renormalization group sense. Any other action is called nonlocal.

tor, but with the Hermitian Wilson kernel $H_W=\gamma_5 D_W$ in Eq. (43) replaced by a more complicated Hermitian kernel,

$$H_T=\frac{1}{1+2a_5H_w\gamma_5}H_W=H_W\frac{1}{1+2a_5H_w\gamma_5}. \tag{49}$$

Here we denote the lattice spacing in the fifth direction by a_5. It is usually chosen to be the same as the 4D lattice spacing, $a_5=a$, which, in turn, is usually set to 1. From Eq. (49) we see that domain-wall fermions in the limit $L_s\to\infty$, followed by the limit $a_5\to 0$ become identical to overlap fermions with the standard Neuberger Dirac operator.

The difficulty with numerical simulations using overlap fermions is the evaluation of the sign function $\Theta(H_W)$ of the Hermitian Wilson Dirac operator $H_W=\gamma_5 D_W$ in Eq. (43). This can be done with a Lanczos-type algorithm (Borici, 1999). Alternatively, $\Theta(H_W)$ can be represented as a polynomial, or, more efficiently, as a rational function that can be rewritten as a sum over poles (Neuberger, 1998a; Edwards *et al.*, 1999), with the optimal approximation, using a theorem of Zolotarev, first given in van den Eshof *et al.* (2002),

$$\Theta(H_W)=H_W\frac{\sum_j a_j H_W^{2j}}{\sum_j b_j H_W^{2j}}=H_W\left[c_0+\sum_{k=1}^{n}\frac{c_k}{H_W^2+d_k}\right]. \tag{50}$$

All d_k's are positive, and the necessary inversions with the sparse matrix H_W^2 are done using a multishift conjugate gradient inverter (Frommer *et al.*, 1995; Jegerlehner, 1996, 1998).

Finally, two versions of fermions that satisfy the Ginsparg-Wilson relation approximately have been considered. One, the so-called fixed point action (Hasenfratz, 1998), approximates the fixed point of a renormalization group transformation by truncating to a small range. Hasenfratz *et al.* (1998) showed that (untruncated) fixed point fermion actions satisfy the Ginsparg-Wilson relation. The second version (Gattringer, 2001) directly minimizes deviations from the Ginsparg-Wilson relation by adjusting the parameters in an arbitrary Dirac operator with a finite (small) number of terms.

C. Numerical simulations

After having chosen a gauge and fermion action one computes expectation values of interesting observables, Eq. (7), by numerical Monte Carlo simulations. For this one creates a sequence of gauge field configurations $\{U_\mu^{(i)}(x)\}$, $i=1,\ldots,N$, distributed with probability distribution

$$P(\{U_\mu^{(i)}(x)\})=\frac{1}{Z(\beta)}[\det M_F(U)]^\delta \exp\{-S_G(U)\}$$
$$=\frac{1}{Z(\beta)}\exp\{-S_{\text{eff}}(U)\}. \tag{51}$$

Here $\delta=n_f$, the number of flavors, for Wilson and chirally invariant fermions, and $\delta=n_f/4$ for (rooted) staggered fermions,[5] and now

$$S_{\text{eff}}(U)=S_G(U)-\delta\,\text{Tr}\ln M_F(U). \tag{52}$$

Expectation values $\langle O\rangle$ are then computed as an average over the ensemble of gauge field configurations,

$$\langle O\rangle=\frac{1}{N}\sum_{i=1}^{N}O^{(i)}, \tag{53}$$

where $O^{(i)}=O(U_\mu^{(i)})$ is the observable evaluated on the gauge field configuration i.

For pure gauge simulations, when no fermions are present, or in the quenched approximation, where the fermion determinant is set to one ($\det M_F=1$), the action is local (in the gauge fields) and the sequence of configurations can be generated with a local updating algorithm, such as the Metropolis algorithm (Metropolis *et al.*, 1953) or a heatbath algorithm (Creutz, 1980; Kennedy and Pendleton, 1985).

With the fermion determinant present, all gauge fields are coupled and the local updating algorithms become impractical. Molecular dynamics based algorithms (Callaway and Rahman, 1982, 1983) have become the standards for simulations with dynamical fermions. For a scalar lattice field theory with action $S(\phi_x)$ one introduces a fictitious momentum p_x on each lattice site, and considers the Hamiltonian

$$H(p,\phi)=\sum_x\frac{p_x^2}{2}+S(\phi). \tag{54}$$

This Hamiltonian defines a classical evolution in a fictitious time τ by

$$\dot\phi_x=p_x,\quad \dot p_x=-\partial S/\partial\phi_x, \tag{55}$$

where the dot denotes the derivative with respect to τ. Given some initial values $[p_x(0),\phi_x(0)]$ these equations of motion define a trajectory $[p_x(\tau),\phi_x(\tau)]$ through phase space. The classical partition function corresponding to the set of all such trajectories is

[5]The sketch here is somewhat schematic: each fermion with a different mass would get its own determinant factor. Furthermore, M_F should be Hermitian and positive semidefinite. For Wilson fermions one takes $M_F=D_W^\dagger D_W$ and uses $\delta=n_f/2$, while for staggered fermions one takes $M_F=[D_{KS}^\dagger D_{KS}]_{ee}$ where ee refers to the matrix restricted to the even sublattice. This is possible, since $D_{KS}^\dagger D_{KS}$ block diagonalizes to even and odd sublattices. Restricting to only one sublattice removes the doubling introduced by the "squaring."

$$Z = \int \prod_x [dp_x d\phi_x] \exp\{-H(p,\phi)\}$$
$$= \mathcal{N} \int \prod_x d\phi_x \exp\{-S(\phi)\}, \quad (56)$$

where in the second step the quadratic integration over the p_x has been carried out, and $\mathcal{N}$ is a normalization factor. The integration of Hamilton's equations, Eq. (55), conserves the Hamiltonian, Eq. (54), up to numerical errors. To get the correct distribution corresponding to the canonical partition function, Eq. (56), the fictitious momenta are "refreshed" periodically by replacement with new Gaussian random numbers (Duane and Kogut, 1985, 1986). This algorithm goes under the name of hybrid molecular dynamics (HMD).

Relying on the ergodicity hypothesis, the expectation value of observables can then be computed by averaging over many MD trajectories

$$\langle O \rangle = \frac{1}{T} \int_{\tau_0}^{T+\tau_0} d\tau O(\phi(\tau)). \quad (57)$$

Integration of the equations of motion, Eq. (55), is done numerically by introducing a finite step size $\Delta\tau$ and using a volume-preserving integration algorithm, such as leapfrog. Due to the finite step size, the Hamiltonian is not exactly conserved during the MD evolution, leading to finite step size errors in observables, including the Hamiltonian itself, of $O((\Delta\tau)^2)$ for the leapfrog integration algorithm. These step size errors can be eliminated—the algorithm made exact—by combining the refreshed MD evolution with a Metropolis accept-reject step at the end of each trajectory (Duane *et al.*, 1987), resulting in the so-called hybrid Monte Carlo (HMC) algorithm.

For a lattice gauge theory the equations of motion have to be set up such that the gauge fields remain group elements. This is ensured by writing

$$\dot{U}_\mu(x) = iH_\mu(x)U_\mu(x), \quad (58)$$

with $H_\mu(x) = \Sigma_a t^a h_\mu^a(x)$ a traceless Hermitian matrix and t^a the SU(N) generators, see, e.g., Gottlieb *et al.* (1987). The MD Hamiltonian is given by

$$H(H_\mu(x), U_\mu(x)) = \sum_{x,\mu} \frac{1}{2} \mathrm{Tr}\, H_\mu^2(x) + S_{\mathrm{eff}}(U_\mu(x)). \quad (59)$$

The equation of motion for $H_\mu(x)$ is then, somewhat schematically,

$$\dot{H}_\mu(x) = iU_\mu(x) \frac{\partial S_{\mathrm{eff}}(U)}{\partial U_\mu(x)}\bigg|_{TH}, \quad (60)$$

where TH denotes the traceless Hermitian part. The term on the right-hand side of Eq. (60) is usually referred to as the force term. With S_{eff} of Eq. (52) we have

$$\frac{\partial S_{\mathrm{eff}}(U)}{\partial U_\mu(x)} = \frac{\partial S_G(U)}{\partial U_\mu(x)} - \delta \mathrm{Tr}\left[\frac{\partial M_F(U)}{\partial U_\mu(x)} M_F^{-1}(U) \right]. \quad (61)$$

To evaluate Eq. (61) we need to know all matrix elements of $M_F^{-1}(U)$, a dense matrix, even though the fermion matrix $M_F(U)$ is sparse. This would be prohibitively expensive. Instead, one estimates the inverse stochastically. Let R be a Gaussian random field such that

$$\overline{R_A^*(x) R_B(y)} = \delta_{AB}\delta_{xy}, \quad (62)$$

where A, B denote color indices, and for Wilson-type fermions also Dirac indices. Then,

$$\mathrm{Tr}\left[\frac{\partial M_F(U)}{\partial U_\mu(x)} M_F^{-1}(U) \right] = \overline{R^\dagger \frac{\partial M_F(U)}{\partial U_\mu(x)} M_F^{-1}(U) R}, \quad (63)$$

and for each random vector R only a single inversion $M_F^{-1}(U)R$ is needed. Typically, for each time step in the MD evolution one uses just one Gaussian random vector, and hence one inversion. This algorithm goes under the name of HMD R algorithm (Gottlieb *et al.*, 1987).

Instead of doing molecular dynamics starting with S_{eff} of Eq. (52) one can first represent the fermion determinant by an integral over bosonic fields, called pseudofermions

$$\det M_F(U) = \int \prod_x [d\Phi^\dagger(x) d\Phi(x)] \times \exp\{-\Phi^\dagger M_F^{-1}(U)\Phi\}. \quad (64)$$

HMD using Eq. (64), referred to as the Φ algorithm (Gottlieb *et al.*, 1987), consists in creating, together with the momenta refreshments, a Φ-field distributed according to Eq. (64),[6] and then integrating the molecular dynamics equations for the effective action

$$S_{\mathrm{eff}}(U,\Phi) = S_G(U) + \Phi^\dagger M_F^{-1}(U)\Phi, \quad (65)$$

with the Φ field fixed. Now the force term becomes

$$\frac{\partial S_{\mathrm{eff}}(U,\Phi)}{\partial U_\mu(x)} = \frac{\partial S_G(U)}{\partial U_\mu(x)} - \Phi^\dagger M_F^{-1}(U) \frac{\partial M_F(U)}{\partial U_\mu(x)} M_F^{-1}(U)\Phi. \quad (66)$$

This again requires one inversion, $M_F^{-1}(U)\Phi$, in each step of the MD evolution. One major benefit of the Φ-algorithm formulation is that an accept-reject Metropolis step is easily implemented at the end of each trajectory resulting in an exact HMC algorithm.

The representation of the fermion determinant by an integral over pseudofermion fields, Eq. (64), can formally be extended to fractional powers $\delta = n_f/4$, as needed for rooted staggered fermions, and $\delta = n_f/2$, as needed for odd number of flavors for Wilson fermions,

[6] For $M_F = D^\dagger D$ this can be achieved by creating random Gaussian variables R and then setting $\Phi = D^\dagger R$.

$$[\det M_F(U)]^\delta = \int \prod_x [d\Phi^\dagger(x) d\Phi(x)] \times \exp\{-\Phi^\dagger M_F^{-\delta}(U)\Phi\}. \quad (67)$$

The problem then is how to deal with $M_F^{-\delta}$. In the HMD R algorithm this is handled by weighting the fermionic contribution to the force by a factor of δ and evaluating $M^{-1}R$ at a point in the integration time chosen so that the errors in observables remain order ε^2, where ε is the step size in the molecular dynamics integration (Gottlieb *et al.*, 1987). Clark and Kennedy proposed using a rational function approximation rewritten as a sum over poles (Clark and Kennedy, 2004, 2005),

$$M_F^{-\delta}(U) \approx r(M_F(U)) = a_0 + \sum_{k=1}^{n} \frac{a_k}{M_F(U) + b_k}, \quad (68)$$

with suitable constants a_k and b_k. A Φ algorithm can then easily be constructed, resulting in the so-called rational hybrid molecular dynamics (RHMD) algorithm, or, with inclusion of the Metropolis accept-reject step to eliminate errors from nonzero ε, the rational hybrid Monte Carlo (RHMC) algorithm. Elimination of the noisy estimator yields smaller errors than in the HMD R algorithm at a given integration step size.

Several improvements of the HMD-type algorithms over the last several years have made them substantially more efficient. These improvements include multiple time step integration schemes (Sexton and Weingarten, 1992), preconditioning of the fermion determinant by multiple pseudofermion fields (Hasenbusch, 2001; Hasenbusch and Jansen, 2003), and replacing the leapfrog integration scheme with more sophisticated "Omelyan integrators" (Sexton and Weingarten, 1992; Omelyan *et al.*, 2002a, 2002b, 2003; Takaishi and de Forcrand, 2006).

D. Asqtad improved staggered fermions

Staggered fermions, with only one component per lattice site, and the massless limit protected by a remnant even-odd $\mathrm{U}(1)_e \times \mathrm{U}(1)_o$ chiral symmetry, are numerically very fast to simulate. One of the major drawbacks is the violation of taste symmetry. At a lattice spacing a of order 0.1 fm, which until recently was typical of numerical simulations, the smallest pion taste splitting Eq. (39) for standard staggered fermions is of order $\Delta(m_P^2) = a^2\delta_P \sim (300\ \mathrm{MeV})^2$, i.e., more than twice the physical pion mass. Even when the lattice spacing is reduced to about 0.05 fm this smallest splitting is still the size of the physical pion mass. It is therefore important to reduce taste violations. Since the different taste components live on neighboring lattice sites and in momentum space have momentum components that differ by π/a, emission or absorption of gluons with (transverse) momentum components close to π/a can change the taste of a quark. Exchange of such ultraviolet gluons thus leads to taste violations.

Suppressing the coupling to such UV gluons thus should reduce the taste violations (Blum *et al.*, 1997; Lepage, 1998; Lagae and Sinclair, 1999; Orginos and Toussaint, 1999; Orginos *et al.*, 1999). This can be achieved by replacing the link field U_μ in the covariant difference operator ∇_μ [see Eq. (13)] by a smeared link built from three-link staples (fat3)

$$U_\mu(x) \to U_\mu^{f3}(x) \equiv \mathcal{F}^{f3} U_\mu(x) = U_\mu(x) + \omega a^2 \sum_{\nu \neq \mu} \Delta_\nu^\ell U_\mu(x), \quad (69)$$

where the superscript ℓ indicates that the Laplacian acts on a link field,

$$\Delta_\nu^\ell U_\mu(x) = \frac{1}{a^2}[U_\nu(x) U_\mu(x + a\hat{\nu}) U_\nu^\dagger(x + a\hat{\mu}) + U_\nu^\dagger(x - a\hat{\nu}) U_\mu(x - a\hat{\nu}) U_\nu(x - a\hat{\nu} + a\hat{\mu}) - 2U_\mu(x)]. \quad (70)$$

In momentum space, expanding to first order in g, Eq. (69) leads to

$$A_\mu(p) \to A_\mu(p) + \omega \sum_{\nu \neq \mu} \{2A_\mu(p)[\cos(ap_\nu) - 1] + 4 \sin(ap_\mu/2)\sin(ap_\nu/2) A_\nu(p)\}. \quad (71)$$

Choosing $\omega = 1/4$ eliminates the coupling to gluons $A_\mu(p)$ with a single momentum component $p_\nu = \pi/a$. Adding a five-link staple (fat5)

$$U_\mu(x) \to U_\mu^{f5}(x) \equiv \mathcal{F}^{f5} U_\mu(x) = U_\mu^{f3}(x) + \frac{a^4}{32} \sum_{\rho \neq \nu \neq \mu} \Delta_\rho^\ell \Delta_\nu^\ell U_\mu(x) \quad (72)$$

eliminates the coupling to gluons with two momentum components $p_\nu = \pi/a$ and adding a seven-link staple (fat7)

$$U_\mu(x) \to U_\mu^{f7}(x) \equiv \mathcal{F}^{f7} U_\mu(x) = U_\mu^{f5}(x) + \frac{a^6}{384} \sum_{\sigma \neq \rho \neq \nu \neq \mu} \Delta_\sigma^\ell \Delta_\rho^\ell \Delta_\nu^\ell U_\mu(x) \quad (73)$$

eliminates the coupling to gluons with all three transverse momentum components $p_\nu = \pi/a$.

For smooth gauge fields, with $p \approx 0$, the Laplacian, Eq. (70), becomes

$$\Delta_\nu^\ell U_\mu(x) = a D_\nu F_{\nu\mu} + \cdots, \quad (74)$$

where the ellipsis represents higher order terms in a. The change in Eq. (69) thus produces a change $\sim a^2 D_\nu F_{\nu\mu}$ to the gauge field A_μ. This is a new $\mathcal{O}(a^2)$ lattice artifact, and will occur when using fat3, fat5, or fat7 links. It, in turn, can be canceled by a straight five-link staple (Lepage, 1999)

$$\Delta_\nu^{2\ell} U_\mu(x) = \frac{1}{4a^2}[U_\nu(x)U_\nu(x+a\hat{\nu})U_\mu(x+2a\hat{\nu}) \times U_\nu^\dagger(x+a\hat{\nu}+a\hat{\mu})U_\nu^\dagger(x+a\hat{\mu}) + U_\nu^\dagger(x-a\hat{\nu}) \times U_\nu^\dagger(x-2a\hat{\nu})U_\mu(x-2a\hat{\nu})U_\nu(x-2a\hat{\nu}+a\hat{\mu}) \times U_\nu(x-a\hat{\nu}+a\hat{\mu}) - 2U_\mu(x)] = aD_\nu F_{\nu\mu} + \cdots, \quad (75)$$

referred to as the Lepage term. In momentum space, expanding to first order in g, this becomes

$$\frac{1}{2a}\{A_\mu(p)[\cos(2ap_\nu) - 1] + 2\sin(ap_\mu/2) \times [\sin(ap_\nu/2) + \sin(3ap_\nu/2)]A_\nu(p)\}, \quad (76)$$

and thus does not affect the coupling to gluons with momentum components at the corners of the Brillouin zone. Therefore, replacing

$$U_\mu(x) \to U_\mu^{f7L}(x) \equiv \mathcal{F}^{f7L}U_\mu(x) = U_\mu^{f7}(x) - \frac{a^2}{4}\sum_{\nu\neq\mu}\Delta_\nu^{2\ell}U_\mu(x) \quad (77)$$

eliminates, at tree level, the coupling to gluons with any of the transverse momentum components $p_\nu = \pi/a$ without introducing new lattice artifacts.

Finally, for a complete $\mathcal{O}(a^2)$ improvement we include a so-called Naik term (Naik, 1989) to improve the free propagator, and hence the free dispersion relation. To keep the structure of the couplings to the different tastes unchanged, this involves adding a three-hop term,

$$\nabla_\mu\chi(x) \to \nabla_\mu\chi(x) - \frac{a^2}{6}(\nabla_\mu)^3\chi(x) = \left(1+\frac{1}{8}\right)\nabla_\mu\chi(x) - \frac{1}{48a}[U_\mu(x)U_\mu(x+a\hat{\mu}) \times U_\mu(x+2a\hat{\mu})\chi(x+3a\hat{\mu}) - U_\mu^\dagger(x-a\hat{\mu}) \times U_\mu^\dagger(x-2a\hat{\mu})U_\mu^\dagger(x-3a\hat{\mu})\chi(x-3a\hat{\mu})]. \quad (78)$$

In the free inverse propagator this changes

$$a^{-1}\sin(ap_\mu) \to a^{-1}\sin(ap_\mu)[1 + \tfrac{1}{6}\sin^2(ap_\mu)] = p_\mu + \mathcal{O}(a^4). \quad (79)$$

The fermion action with only the improvement in Eq. (79) is referred to as the Naik action. This is also the free (noninteracting) limit of the asq and asqtad fermion actions, defined next.

We now have all ingredients for an improved staggered fermion action, called the asq action [$\mathcal{O}(a^2)$ improved action]: use the covariant derivative with the Naik term, Eq. (79), and in the one-link term replace the gauge links U_μ by the fat7 links with Lepage term U_μ^{f7L} of Eq. (77). Replacing the various coefficients in the asq action by tadpole improved coefficients finally gives the asqtad fermion action. The reduction of taste violations for pions with increasing amount of link fattening is shown in Fig. 3.

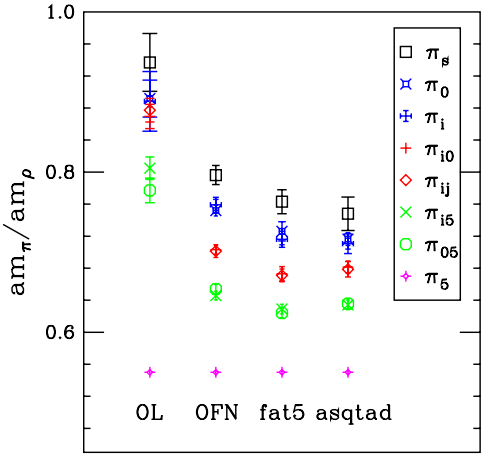

FIG. 3. (Color online) Illustration of taste violations for staggered fermion actions with various link fattenings. The valence quark masses were adjusted to give the same $m_{\pi_5}/m_\rho = 0.55$ for all fermion actions. The results are for quenched gauge field configurations with a Symanzik improved gauge action using $\beta = 7.30$. The staggered fermion actions are standard, or one-link (OL), fat3+Naik (OFN), fat5, and asqtad. The pions are labeled by the taste structure, with the taste singlet the heaviest, and the taste pseudoscalar (π_5), the pseudo-Goldstone boson, the lightest. For more comparisons see Orginos *et al.* (2000).

The Naik term, Eq. (79), reduces the lattice artifacts in the pressure for free fermions, and thus in the very high temperature limit of QCD as shown in Fig. 4, left panel, and in the "speed of light" determined from the pion dispersion relation, right panel, from Bernard *et al.* (1998)

In Fig. 4, left panel, p4 fermions are another variant of improved staggered fermions (Heller *et al.*, 1999) designed to improve the dispersion relation and high temperature behavior. The speed of light, shown in the right panel, is determined from pion energies $E_\pi(\vec{p})$ for various momenta as

$$c^2 = [E_\pi^2(\vec{p}) - E_\pi^2(\vec{0})]/\vec{p}^2. \quad (80)$$

The $\mathcal{O}(a^2)$ improvement of the asqtad action gives a staggered fermion formulation with good scaling properties, as shown in Fig. 5 for a quenched study (Bernard *et al.*, 2000b).

E. Highly improved staggered fermions

The largest contribution to the $O(a^2)$ error in the asqtad action originates from the taste-exchange interactions. This error can be completely eliminated at one-loop level by adding four-quark interactions (which are hard to implement in dynamical simulations) or reduced by additional smearings. Multiple smearings, for instance

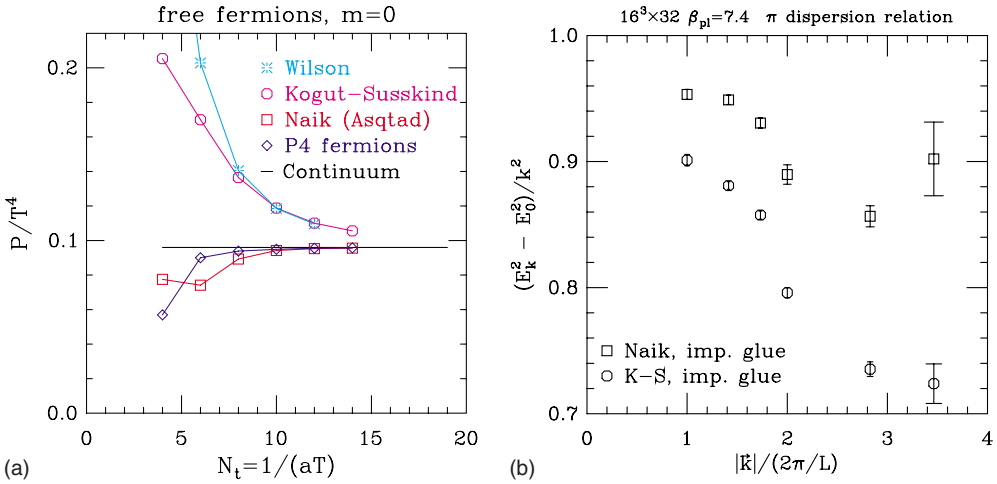

FIG. 4. (Color online) The pressure (left) per fermion degree of freedom for free Kogut-Susskind, Naik, Wilson, and p4 (Heller *et al.*, 1999) fermions as a function of $N_T=1/aT$. The continuum value is shown as the horizontal solid line. From Bernard *et al.*, 2005; an earlier version appeared in Bernard *et al.* (1998). The "speed of light squared" (right) calculated from the pion dispersion relation, for Naik and K-S pions. From Bernard *et al.*, 1998.

$$U_\mu(x) \to X_\mu(x) = \mathcal{F}^{fnL}\mathcal{F}^{fnL}U_\mu(x), \tag{81}$$

are found to further reduce mass splittings between pions of different taste. However, they increase the number of products of links in the sum for $X_\mu(x)$ links and effectively enhance the contribution of two-gluon vertices on quark lines [see Follana *et al.* (2007) for a detailed discussion]. Thus, an operation that bounds smeared links needs to be introduced,

$$U_\mu(x) \to X_\mu(x) = \mathcal{F}^{fnL}\mathcal{U}\mathcal{F}^{fnL}U_\mu(x), \tag{82}$$

where $\mathcal{U}$ is an operation that projects smeared links onto the U(3) or SU(3) group. Cancellation of the $O(a^2)$ artifacts introduced by fat7 smearing with the Lepage term can be achieved on the outermost level of smearing, and Eq. (82) can be simplified,

$$U_\mu(x) \to X_\mu(x) = \mathcal{F}^{fnL}\mathcal{U}\mathcal{F}^{fn}U_\mu(x) \equiv \mathcal{F}^{HISQ}U_\mu(x). \tag{83}$$

Introducing smeared and reunitarized links that arise after each operation in Eq. (83)

$$V_\mu(x) = \mathcal{F}^{fn}U_\mu(x), \tag{84}$$

$$W_\mu(x) = \mathcal{U}V_\mu(x) = \mathcal{U}\mathcal{F}^{fn}U_\mu(x), \tag{85}$$

$$X_\mu(x) = \mathcal{F}^{fnL}W_\mu(x) = \mathcal{F}^{HISQ}U_\mu(x), \tag{86}$$

we can write the covariant derivative that replaces the naive one,

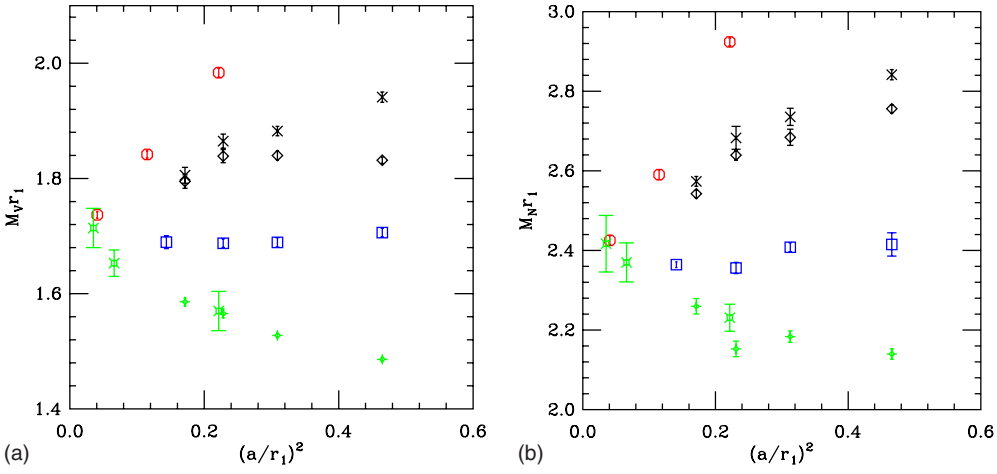

FIG. 5. (Color online) Rho masses (left) and nucleon masses (right) in units of $r_1 \approx 0.32$ fm. Octagons are unimproved staggered fermions with Wilson gauge action, diamonds are unimproved staggered fermions with Symanzik improved gauge action, crosses are Naik fermions, and squares are asqtad fermions, both with Symanzik improved gauge action. For comparison we also show tadpole clover improved Wilson fermions with Wilson gauge action (Bowler *et al.*, 2000) (fancy squares) and with Symanzik improved gauge action (Collins *et al.*, 1997) (fancy diamonds). Adapted from Bernard *et al.*, 2000b.

$$\nabla_\mu[U]\chi(x) \to \nabla_\mu(x)[X]\chi(x) - \frac{a^2}{6}(1+\varepsilon)(\nabla_\mu)^3[W]\chi(x). \tag{87}$$

Equation (87) is a recently proposed highly improved staggered quark (HISQ), discretization scheme (Follana *et al.*, 2007). In square brackets we indicate which links are used as gauge transporters in the derivatives. The second term is the Naik term evaluated using the reunitarized links $W_\mu(x)$. Its coefficient includes a correction ε introduced to compensate for the order $(am)^4$ and $\alpha_s(am)^2$ errors. This correction is negligible for light quarks, but may be relevant for charm physics if a level of accuracy better than 5–10 % is desired. The correction ε can be either tuned nonperturbatively or calculated in perturbation theory (Follana *et al.*, 2007).

The HISQ action suppresses the taste-exchange interactions by a factor of about 2.5 to 3 compared to the asqtad action, which makes it a good candidate for the next generation of simulations with 2+1 or 2+1+1 flavors of dynamical quarks, where in the latter case the last quark is the charm quark. We discuss preliminary studies of the HISQ action in more detail in Sec. X.

III. STAGGERED CHIRAL PERTURBATION THEORY AND "ROOTING"

A. Chiral effective theory for staggered quarks

Because simulation costs increase with decreasing quark mass, most QCD simulations are done with the masses of the two lightest quarks (up and down) larger than their physical values. The results, therefore, have to be extrapolated to the physical light quark masses. This is done using chiral perturbation theory, the effective field theory that describes the light quark limit of QCD (Weinberg, 1979; Gasser and Leutwyler, 1984, 1985).

Even with the asqtad improvement of staggered fermions, taste-symmetry violations are not negligible in current simulations. It is therefore important to include the effects of discretization errors in the chiral perturbation theory forms one uses to extrapolate lattice data to physical light quark masses and to infinite volume; in other words, one needs to use staggered chiral perturbation theory (SχPT). Indeed, it is not possible to fit the mass dependence of the staggered data to continuum chiral forms (Aubin *et al.*, 2004b). Once the discretization effects are included explicitly by making SχPT fits, one can gain good control of the errors from the continuum extrapolation. Furthermore, the effects of taking the fourth root of the staggered determinant can be included in SχPT. The resulting rooted staggered chiral perturbation theory (rSχPT) allows us to understand the nonlocal and nonunitary consequences of rooting on the lattice and to test that these sicknesses go to zero as $a \to 0$.

Lee and Sharpe (1999) first developed SχPT for a single staggered flavor (a single staggered field) at $\mathcal{O}(a^2)$; this was generalized to an arbitrary number of flavors by Aubin and Bernard (2003a, 2003b). Here we outline the theory with N_f flavors to this order; for the next order see Sharpe and Van de Water (2005).

To derive SχPT, one starts by determining, to the desired order in a^2, the Symanzik effective theory (SET) (Symanzik, 1983) for staggered quarks. The SET is an effective theory for physical momenta p small compared with the cutoff ($p \ll 1/a$); it parametrizes discretization effects by adding higher-dimensional operators to continuum QCD. In particular, taste violations appear to $\mathcal{O}(a^2)$ in the SET as four-quark (dimension six) operators. These operators arise from the exchange of gluons with net momenta $\sim \pi/a$ between two quark lines. Such gluons can change taste, spin, and color, but not flavor. Therefore, the operators generated have the form

$$O_{ss'tt'} = \bar{q}_i(\gamma_s \otimes \xi_t)q_i\bar{q}_j(\gamma_{s'} \otimes \xi_{t'})q_j, \tag{88}$$

where i and j are flavor indices, spin and taste matrices have the notation of Eq. (31), and color indices are omitted because they play no role in what follows. The SU(N_f) vector flavor symmetry guarantees that $O_{ss'tt'}$ is a flavor singlet, which means that i,j are (implicitly) summed over their N_f values in Eq. (88).

The possible choices of the spin and taste matrices in Eq. (88) are constrained by the staggered symmetries. First, we can use the separate U(1)$_\varepsilon$ for each flavor. This forces each of the bilinears making up $O_{ss'tt'}$, for example $\bar{q}_i(\gamma_s \otimes \xi_t)q_i$, to be U(1)$_\varepsilon$ invariant by itself for each i. From Eq. (37), we then have that $\{\gamma_5 \otimes \xi_5, \gamma_s \otimes \xi_t\}=0$, which gives 12 choices for γ_s and ξ_t: One of them must be a scalar, tensor, or pseudoscalar (S, T, or P) and the other must be a vector or axial vector (V or A). For example, we might have $A \otimes T$, that is, $\gamma_s \otimes \xi_t = \gamma_{\mu 5} \otimes \xi_{\nu\lambda}$, with the notation $\gamma_{\mu 5} \equiv \gamma_\mu\gamma_5$ (and similarly for tastes), and $\xi_{\nu\lambda} = \frac{1}{2}[\xi_\nu, \xi_\lambda]$ (and similarly for spins). Such operators are called "odd" because, in the original one-component form of Eq. (24), the fields χ and $\bar{\chi}$ are separated by an odd number of links (1 or 3) within an elementary hypercube. This is easily seen from the equivalence given in Eq. (31).

Shift symmetry gives the next constraint. As mentioned following Eq. (36), shift symmetries are a combination of discrete taste symmetries and translations. In the SET, however, where external momenta are always small compared with the cutoff, it is possible to redefine the fields $q(y)$ to make the action invariant under arbitrary translations, like in any continuum theory (Bernard, Goltermann, and Shamir, 2008). The shifts then have the form

$$q(y) \to (I \otimes \xi_\mu)q(y); \quad \bar{q}(y) \to \bar{q}(y)(I \otimes \xi_\mu). \tag{89}$$

Thus, for each of the 16 possibilities for ξ_t, the bilinear $\bar{q}_i(\gamma_s \otimes \xi_t)q_i$ undergoes a unique set of sign changes under shifts in the four directions $\hat{\mu}$. Since the only bilinears that are invariant under all shifts are those with $\xi_t = I$, this immediately shows why taste symmetry cannot be broken by bilinear operators. Moreover, it forces $\xi_t = \xi_{t'}$ in the four-quark operators of the SET, Eq. (88).

We now consider the implications of rotations and parity. Rotational symmetry requires that Lorentz (Euclidean) indices be repeated and summed over, but since the lattice action is invariant only under 90° rotations, an index can be repeated any even number of times before summing, not just twice. Further, with staggered quarks, the lattice rotational symmetry transforms the taste indices together with the space-time (and spin) indices (van den Doel and Smit, 1983; Golterman and Smit, 1984). Since, $\xi_t = \xi_{t'}$, the spin indices on $\gamma_{s'}$ must be the same as those on γ_s. Parity then forces γ_s and $\gamma_{s'}$ to be identical; combinations such as $\gamma_s = \gamma_\nu$, $\gamma_{s'} = \gamma_{\nu 5}$ are forbidden. There are now only two choices: either the spin indices and taste indices are separately summed over or there are some indices that are common to both the spin and taste matrices. Lee and Sharpe (1999) called the former class of operators type A, and the latter type B.

Because there are 12 choices for an odd bilinear, there are a total of 12 type-A operators. An example is

$$O_{[V\times P]} = a^2 \bar{q}_i (\gamma_\mu \otimes \xi_5) q_i \bar{q}_j (\gamma_\mu \otimes \xi_5) q_j, \tag{90}$$

with the repeated index μ summed over. The fields here have standard continuum dimensions, so we write explicit factors of a to give the operator dimension four. Note that type-A operators are invariant over the full Euclidean space-time rotation group, SO(4), as well as a corresponding SO(4) of taste, a subset of the complete $SU(4)_V$ of taste that appears in the continuum limit.

In order to have a sufficient number of indices to construct a type-B operator, either $\gamma_s = \gamma_{s'}$ or $\xi_t = \xi_{t'}$ must be a tensor (T); the other set is then either V or A. Thus there are four type-B operators. An example is

$$O_{[V_\mu \times T_\mu]} = a^2 [\bar{q}_i (\gamma_\mu \otimes \xi_{\mu\nu}) q_i \bar{q}_j (\gamma_\mu \otimes \xi_{\nu\mu}) q_j - \bar{q}_i (\gamma_\mu \otimes \xi_{\mu\nu}\xi_5) q_i \bar{q}_j (\gamma_\mu \otimes \xi_5 \xi_{\nu\mu}) q_j], \tag{91}$$

where the second term ensures that the operator has no separate spin- or taste-singlet piece. Since the index μ is repeated four times, one sees explicitly from Eq. (91) that type-B operators are invariant only under joint 90° rotations of spin and taste.

The SET to $\mathcal{O}(a^2)$ for N_f flavors of (unrooted) staggered fermions is then simply the continuum QCD Lagrangian for $4N_f$ species together with the above type-A and type-B operators.[7] Given this SET, the $\mathcal{O}(a^2)$ chiral Lagrangian is constructed by finding—with a "spurion" analysis, outlined below—the chiral operators that break the full $SU(4N_f)_L \times SU(4N_f)_R$ symmetry in the same way as the four-quark operators in the SET do. However, the symmetry is also broken by the quark mass terms in the SET. In order to arrive at a consistent expansion scheme (a consistent power counting) for the chiral theory, we must first decide how the breaking by a^2 terms compares with the breaking by mass terms.

The standard power counting, which we follow here, takes $a^2 \sim m$, where m is a generic quark mass. More precisely, we assume that [see Eq. (39)]

$$a^2 \delta \sim m_{\pi_P}^2 = 2Bm, \tag{92}$$

where $a^2\delta$ is a typical pion taste splitting. The taste splittings and squared Goldstone pion masses are indeed comparable in current MILC ensembles. Goldstone pion masses range from about 240 to 600 MeV; while, on the "coarse" ($a \approx 0.12$ fm) ensembles, the average taste splitting is about $(320\ \text{MeV})^2$. This splitting drops to about $(210\ \text{MeV})^2$ on the "fine" ($a \approx 0.09$ fm) ensembles and to about $(125\ \text{MeV})^2$ on the "superfine" ($a \approx 0.06$ fm) ensembles. It is clear that Eq. (92) is appropriate in the range of lattice spacings and masses we are working on. However, for future analysis of data that include still finer lattices and omit the coarse and possibly the fine ensembles, it might be reasonable to use a power counting where a^2 is taken to be smaller than m.

To derive the leading order (LO) chiral Lagrangian, we start with the Lagrangian in the continuum limit, i.e., in the absence of taste-breaking operators. In Euclidean space, we have

$$\mathcal{L}^{\text{cont}} = \frac{f^2}{8} \text{Tr}(\partial_\mu \Sigma \partial_\mu \Sigma^\dagger) - \frac{1}{4} B f^2 \text{Tr}(\mathcal{M}\Sigma + \mathcal{M}\Sigma^\dagger) + \frac{m_0^2}{24} [\text{Tr}(\Phi)]^2, \tag{93}$$

where the meson field Φ, $\Sigma = \exp(i\Phi/f)$, and the quark mass matrix $\mathcal{M}$ are $4N_f \times 4N_f$ matrices, and f is the pion decay constant at LO. The field Σ transforms under $SU(4N_f)_L \times SU(4N_f)_R$ as $\Sigma \to L\Sigma R^\dagger$. The field Φ is given by

$$\Phi = \begin{pmatrix} U & \pi^+ & K^+ & \cdots \\ \pi^- & D & K^0 & \cdots \\ K^- & \overline{K^0} & S & \cdots \\ \vdots & \vdots & \vdots & \ddots \end{pmatrix}, \tag{94}$$

where each entry is a 4×4 matrix in taste space, with, for example, $\pi^+ \equiv \Sigma_{a=1}^{16} \pi_a^+ T_a$. The 16 Hermitian taste generators T_a are $T_a = \{\xi_5, i\xi_{\mu 5}, i\xi_{\mu\nu}(\mu > \nu), \xi_\mu, I\}$. Since the normal staggered mass term is taste invariant [see Eq. (32)], the mass matrix has the form $\mathcal{M} = \text{diag}(m_u I, m_d I, m_s I, \ldots)$.

The quantity m_0 in Eq. (93) is the anomaly contribution to the mass of the taste- and flavor-singlet meson, the $\eta' \propto \text{Tr}(\Phi)$. As usual, the η' decouples in the limit $m_0 \to \infty$. However, one may postpone taking the limit and keep η' as a dynamical field (Sharpe and Shoresh, 2001) in order to avoid putting conditions on the diagonal elements of Φ. These diagonal fields, $U, D, \ldots$, are then simply the $u\bar{u}$, $d\bar{d}$ bound states, which makes it easy

[7] There are additional $\mathcal{O}(a^2)$ terms in the SET, for example, from the gluon sector, that we ignore here for simplicity. Such terms are taste invariant, and at leading order only produce "generic" effects in the chiral Lagrangian: $\mathcal{O}(a^2)$ changes in the physical low-energy constants.

to perform a "quark flow" analysis (Sharpe, 1990, 1992) by following the flow of flavor indices through diagrams.

Since a typical pion four-momentum p obeys $p^2 \sim m_\pi^2 \sim 2Bm$, both the kinetic energy term and the mass term in Eq. (93) are $\mathcal{O}(m)$. By our power counting scheme, Eq. (92), we need to add $\mathcal{O}(a^2)$ chiral operators to complete the LO Lagrangian. These are induced by the $\mathcal{O}(a^2)$ operators in the SET. We start with the type-A operator $O_{[V\times P]}$ of Eq. (90). Using $q_i = q_i^R + q_i^L$, with $q_i^{R,L} = [(1 \pm \gamma_5)/2]q_i$, and similarly for $\bar{q}_i$ with $\bar{q}_i^{R,L} = \bar{q}_i[(1 \mp \gamma_5)/2]$, we have

$$O_{[V\times P]} = a^2[\bar{q}_i^R(\gamma_\mu \otimes \xi_5)q_i^R + \bar{q}_i^L(\gamma_\mu \otimes \xi_5)q_i^L]^2 \equiv [\bar{q}^R(\gamma_\mu \otimes F_R)q^R + \bar{q}^L(\gamma_\mu \otimes F_L)q^L]^2, \quad (95)$$

where flavor indices are implicit in the last expression. The spurions F_R and F_L will eventually take the values

$$F_R = a\xi_5^{(N_f)} \equiv a\xi_5 \otimes I_{\text{flavor}}, \quad F_L = a\xi_5^{(N_f)} \equiv a\xi_5 \otimes I_{\text{flavor}}, \quad (96)$$

but for the moment are given spurious $\mathrm{SU}(4N_f)_L \times \mathrm{SU}(4N_f)_R$ transformation properties $F_R \to RF_RR^\dagger$ and $F_L \to LF_LL^\dagger$ in order to make $O_{[V\times P]}$ "invariant."

The corresponding $\mathcal{O}(a^2)$ operators in the chiral Lagrangian are then invariants constructed only from Σ, $\Sigma^\dagger$, and quadratic factors in F_R and/or F_L. We cannot use derivatives or factors of the mass matrix $\mathcal{M}$ because such terms would be higher order. It turns out that there is only one such operator,

$$C_1 \operatorname{Tr}(F_L\Sigma F_R\Sigma^\dagger) = C_1 a^2 \operatorname{Tr}(\xi_5^{(N_f)}\Sigma\xi_5^{(N_f)}\Sigma^\dagger), \quad (97)$$

where C_1 is a constant that can be determined in principle by fits to staggered lattice data.

The 11 other type-A operators can be treated in the same way, though of course different operators will have different spurions with different transformation properties. Some of the type-A operators give more than one chiral operator, but, because of repeats, a total of only eight chiral operators are generated.

The type-B operators couple space-time and taste indices, and are invariant only under 90° rotations. Their chiral representatives must therefore have derivatives to carry the space-time indices; an example is $\operatorname{Tr}(\Sigma\partial_\mu\Sigma^\dagger\xi_\mu^{(N_f)}\Sigma^\dagger\partial_\mu\Sigma\xi_\mu^{(N_f)})$ (Sharpe and Van de Water, 2005). Because of the derivatives, however, these operators are higher order and do not appear in the LO chiral Lagrangian. This was an important insight of Lee and Sharpe (1999). It means that at LO the physics has the "accidental" SO(4) taste symmetry of the type-A operators.

We can now write down the complete LO chiral Lagrangian,

$$\mathcal{L} = \frac{f^2}{8}\operatorname{Tr}(\partial_\mu\Sigma\partial_\mu\Sigma^\dagger) - \frac{1}{4}Bf^2\operatorname{Tr}(\mathcal{M}\Sigma + \mathcal{M}\Sigma^\dagger) + \frac{m_0^2}{24}[\operatorname{Tr}(\Phi)]^2 + a^2\mathcal{V}, \quad (98)$$

where the taste-violating potential $\mathcal{V}$ is given by

$$\begin{aligned}-\mathcal{V} = {} & C_1 \operatorname{Tr}(\xi_5^{(N_f)}\Sigma\xi_5^{(N_f)}\Sigma^\dagger) + \frac{C_3}{2}[\operatorname{Tr}(\xi_\nu^{(N_f)}\Sigma\xi_\nu^{(N_f)}\Sigma) + \text{H.c.}] + \frac{C_4}{2}[\operatorname{Tr}(\xi_{\nu 5}^{(N_f)}\Sigma\xi_{5\nu}^{(N_f)}\Sigma) + \text{H.c.}] \\ & + \frac{C_6}{2}\operatorname{Tr}(\xi_{\mu\nu}^{(N_f)}\Sigma\xi_{\nu\mu}^{(N_f)}\Sigma^\dagger) + \frac{C_{2V}}{4}[\operatorname{Tr}(\xi_\nu^{(N_f)}\Sigma)\operatorname{Tr}(\xi_\nu^{(N_f)}\Sigma) + \text{H.c.}] + \frac{C_{2A}}{4}[\operatorname{Tr}(\xi_{\nu 5}^{(N_f)}\Sigma)\operatorname{Tr}(\xi_{5\nu}^{(N_f)}\Sigma) + \text{H.c.}] \\ & + \frac{C_{5V}}{2}[\operatorname{Tr}(\xi_\nu^{(N_f)}\Sigma)\operatorname{Tr}(\xi_\nu^{(N_f)}\Sigma^\dagger)] + \frac{C_{5A}}{2}[\operatorname{Tr}(\xi_{\nu 5}^{(N_f)}\Sigma)\operatorname{Tr}(\xi_{5\nu}^{(N_f)}\Sigma^\dagger)], \end{aligned} \quad (99)$$

with implicit sums over repeated indices.

Expanding Eq. (98) to quadratic order in the meson field Φ, we find that pions with nonsinglet flavor fall into SO(4) taste multiplets, labeled by P, A, T, V, S. We show numerical evidence for this in Sec. III.C. The splittings δ_t of Eq. (39), with $t = P, A, T, V, S$, are given in terms of C_1, C_3, C_4, and C_6. The presence of two traces in the terms multiplied by C_{2V}, C_{2A}, C_{5V}, and C_{5A} means that they cannot contribute at this order to the masses of (flavor) charged mesons. Aubin and Bernard (2003a) showed that such terms do generate "taste hairpins," which mix the flavor-neutral mesons of taste V (and separately, taste A). In other words, there are terms of the form $\frac{a^2\delta_V'}{2}(U_\mu + D_\mu + S_\mu + \cdots)^2$ and $\frac{a^2\delta_A'}{2}(U_{\mu 5} + D_{\mu 5} + S_{\mu 5} + \cdots)^2$ in the expansion of Eq. (98), where δ_V' and δ_A' are functions of C_{2V}, C_{2A}, C_{5V}, and C_{5A}. These terms have been indirectly observed (Aubin *et al.*, 2004b) in fits to charged pion masses and decay constants to one-loop expressions derived from Eq. (98). Because of the practical difficulties in simulating disconnected diagrams, taste hairpins have not yet been studied directly in two-point functions of neutral mesons.

So far the entire discussion of SχPT has been in the context of unrooted staggered quarks. Bernard (2002) and Aubin and Bernard (2003a) proposed that rooting could be taken into account using quark flow to determine the presence of closed sea-quark loops in an SχPT diagram, and then multiplying the diagram by a factor of 1/4 for each such loop. This is a natural assumption, because it is exactly what happens in weak coupling perturbation theory (Bernard and Golterman, 1994). In the

chiral theory, however, the validity of the prescription is not obvious.

To study in more detail how rooting should be handled in SχPT, it is convenient to replace the quark-flow picture with a more systematic way to find and adjust the sea-quark loops. This is provided by a "replica rule," introduced for this problem by Aubin and Bernard (2004). Since rooting is defined as an operation on sea quarks, it is useful first to separate off the valence quarks by replacing the original theory with a partially quenched one: introduce new (valence) quarks along with ghost (bosonic) quarks to cancel the valence determinant. The adjustment to the SχPT theory, Eq. (98), is the standard one for a partially quenched theory (Bernard and Golterman, 1994): just add some additional quark flavors and corresponding bosonic flavors. The masses of the valence quarks may be equal to or different from the sea masses. The latter case is clearly unphysical, but is useful for getting more information out of a given set of sea-quark configurations.

We now replicate each sea-quark flavor n_r times, where n_r is a positive integer, so that there are a total of $n_r N_F$ flavors. We then calculate as usual with the replicated (and partially quenched) version of Eq. (98), going to some given order in chiral perturbation theory. The result will be a polynomial in n_r, where factors of n_r arise from summing over the indices in chiral loops. Finally, we put $n_r=1/4$ in the polynomial. We thus take into account the rooting by effectively counting each sea-quark flavor as $1/4$ of a flavor, which cancels the factor of 4 that arises from the taste degree of freedom. The chiral theory obtained by applying this replica rule to SχPT is called rSχPT.

Note that we have done nothing to the valence quarks. Since the number of tastes of the sea quarks has been reduced by a factor of 4, it is clear that there is a mismatch, even when the valence masses are taken equal to the sea masses. This is still true in the continuum limit, where the issue is particularly transparent. When taste symmetry is exact, rooting removes three of the four tastes from the quark sea for each physical flavor, but leaves the valence quarks unaffected. It is therefore possible to construct Green's functions, at either the quark or the chiral level, which are unphysical, in the sense that the external particles have no counterpart in the intermediate states. Sharpe has called this the "valence-rooting problem" (Sharpe, 2006b). The solution is, however, straightforward (Sharpe, 2006b; Bernard, Golterman, *et al.*, 2007, 2008b): the physical subspace can be obtained simply by choosing all external particles to have a single value of taste (taste 1, say). Using flavor and taste symmetries, other Green's functions may also be constructed that happen to equal these physical correlators in the continuum limit (Bernard, Golterman, *et al.*, 2007). Nevertheless, most Green's functions will be unphysical. This is not a cause for concern as long as there is a physical subspace. In fact such a situation has nothing, *per se*, to do with rooting: it will happen in continuum QCD, or in any lattice version thereof, if we introduce arbitrary numbers of valence quarks.

We emphasize that the replica rule tells us to take into account only the explicit factors of n_r from chiral loops. Putting $n_r=1/4$ in the polynomial resulting from the SχPT calculation is thus a well-defined procedure. We are not concerned with the fact that, if replication is done in the fundamental, QCD-level theory, the low-energy constants (LECs) such as f and B will be (implicit) functions of n_r. Such dependence is in general unknown and nonperturbative, and not amenable to analytic continuation in n_r. Instead, as is always the case in chiral perturbation theory, we treat the LECs as free parameters. After setting explicit factors of n_r to $1/4$ in our calculations, the LECs can be determined by fitting the lattice data to the resulting chiral forms. The unknown dependence of the LECs on n_r is however an obstacle in trying to show, directly from the fundamental theory, that rSχPT is the correct chiral theory. This is discussed further in Sec. III.C.

B. Extensions of staggered chiral perturbation theory

The purely staggered theory discussed thus far is often insufficient for calculations of many physical quantities. It would be very difficult, for example, to simulate heavy quarks with the asqtad action at currently available lattice spacings because of the large discretization errors that appear when $am\sim 1$. Thus, the determination of phenomenologically important properties of heavy-light mesons and baryons has usually been carried out by adding a heavy valence quark with the Fermilab (El-Khadra *et al.*, 1997) or NRQCD (Thacker and Lepage, 1991) action to asqtad simulations of the sea quarks and light valence quarks. Alternatively, HISQ valence quarks have been used on the asqtad sea configurations to get precise results for charmed mesons (Follana *et al.*, 2008). To the accuracy strived for in current calculations, the effects of heavy sea quarks can be neglected; that is, these quarks can be treated in the quenched approximation.

For several other quantities, the complicated effects of taste-symmetry violation make staggered quarks difficult to use. Since these effects often present the greatest obstacle in the valence sector, a very successful compromise, first introduced in Renner *et al.* (2005), has been to add domain-wall valence quarks on top of the MILC sea-quark ensembles. Such "mixed-action" simulations are being used to study scalar mesons (Aubin *et al.*, 2008), B_K and related quantities (Aubin *et al.*, 2007a, 2008, 2009), nucleon properties (Edwards *et al.*, 2006b; Renner *et al.*, 2007; Hägler *et al.*, 2008; Bratt *et al.*, 2009), hadron spectroscopy (Edwards *et al.*, 2006a; Walker-Loud *et al.*, 2009), meson scattering (Beane *et al.*, 2008b, 2008c), and nuclear-physics topics (Beane *et al.*, 2007, 2008a; Detmold *et al.*, 2008a, 2008b).

To take full advantage of simulations with heavy valence quarks or mixed actions, it is useful to have chiral effective theories that properly include the discretization

effects. We discuss such theories, starting with the mixed-action case of domain-wall valence quarks on a staggered sea. The basic ideas of mixed-action chiral perturbation theory were developed in Bär *et al.* (2003, 2004) and Golterman *et al.* (2005) for the case of Wilson fermions in the sea and chiral fermions in the valence sector. By chiral fermions we mean overlap or domain wall quarks, where we assume for domain wall quarks that L_s is large enough that the residual mass is negligible. The extension to chiral valence fermions on staggered sea quarks (Bär *et al.*, 2005) is then fairly straightforward. Features of mixed-action chiral theory that are universal, in the sense that they are independent of the sea-quark action, have been discussed by Chen *et al.* (2007, 2009).

Because the valence and sea quarks have different actions, a mixed-action theory lacks the symmetries that would normally rotate valence into sea quarks (or vice versa) in a standard theory. Since we assume that both the valence and sea sectors approach the expected continuum theories as $a \to 0$, these symmetries should be restored in the continuum limit. At the level of the Symanzik effective action, the violation of these symmetries first appears at $\mathcal{O}(a^2)$ in the existence of independent "mixed" four-quark operators: in our case, the product of a domain-wall (valence) bilinear and a staggered (sea) bilinear. We know, following the development in Sec. III.A, that each bilinear must be separately chirally invariant, and that any staggered bilinear must be taste invariant. It is then simple to see that only two mixed four-quark operators are possible,

$$O_V = a^2 \bar{\psi}_a \gamma_\mu \psi_a \bar{q}_i (\gamma_\mu \otimes I) q_i,$$
$$O_A = a^2 \bar{\psi}_a \gamma_\mu \gamma_5 \psi_a \bar{q}_i (\gamma_5 \gamma_\mu \otimes I) q_i, \tag{100}$$

where ψ_a is a domain-wall quark or ghost of valence flavor a, and q_i is a staggered quark of sea flavor i, and a and i are summed over. As in the pure staggered case, the color indices in these operators are irrelevant.

In addition to the operators in Eq. (100), there are the full complement of standard, purely staggered four-quark operators in the sea sector, and standard, purely domain-wall four-quark operators involving valence quarks and valence ghosts. In a normal theory, the relative coefficients of corresponding sea-sea, valence-valence, and valence-sea operators would be fixed by the symmetries. But in the mixed case, all such operators are independent and must be treated separately.

In the corresponding chiral effective theory, the purely sea-quark sector is the same as the sea-quark sector of a standard staggered theory. Similarly, the purely valence-quark sector is the same as the valence-quark sector of a standard domain-wall theory. Mixed valence-sea mesons are affected by various operators, including the operator corresponding to Eq. (100),

$$-a^2 C_{\mathrm{Mix}} \mathrm{Tr}(\tau_3 \Sigma \tau_3 \Sigma^\dagger), \tag{101}$$

where Σ is the complete chiral field involving both sea and valence (and ghost-valence) quarks, and τ_3 is a diagonal matrix that takes the value +1 in the sea sector and −1 in the valence sector. At LO one finds (Bär *et al.*, 2005; Chen, Golterman, *et al.*, 2009)

$$m^2_{\pi,ab} = B(m_a + m_b),$$
$$m^2_{\pi,ij,t} = B(m_i + m_j) + a^2 \delta_t, \tag{102}$$
$$m^2_{\pi,ia} = B(m_i + m_a) + a^2 \delta_{\mathrm{Mix}},$$

where a, b are domain-wall (valence) flavors, i, j are staggered (sea) flavors, t is the taste of a sea-sea meson, as in Eq. (39), and δ_{Mix} is a function of C_{Mix} and other low-energy constants. Aubin *et al.* (2008) and Orginos and Walker-Loud (2008) have determined δ_{Mix} numerically by measuring the masses of mixed mesons.

The mixed-action chiral Lagrangian thus developed can be used to calculate one-loop effects in pseudoscalar masses and decay constants (Bär *et al.*, 2005), in B_K (Aubin *et al.*, 2007b) and $I=2\pi-\pi$ scattering (Chen *et al.*, 2006).

Next, we consider the case of heavy-meson staggered chiral perturbation theory (HMSχPT), the relevant chiral theory for a heavy meson made out of a heavy valence quark and a light staggered valence quark, on the background of staggered sea quarks. HMSχPT is designed to parametrize the light quark chiral extrapolation and the light quark discretization effects. Discretization errors due to the heavy quark are not included; it is assumed that they can be estimated independently by using heavy-quark effective theory (HQET) (Isgur and Wise, 1992; Neubert, 1994) to describe the lattice heavy quark (Kronfeld, 2000, 2004).

At the level of the SET, the first nontrivial effect of combining the heavy quark with the staggered theory is again the generation of mixed four-quark operators (a heavy-quark bilinear times a light-quark one). As before, such operators do not break taste symmetry. Furthermore, unlike the mixed-action case, symmetry between heavy and light quarks is already strongly broken by the heavy-quark mass. So the mixed operators have no important effects in this case.

The power counting for heavy-light mesons in χPT makes the HMSχPT at LO rather simple (Aubin and Bernard, 2006). In the continuum, the chiral Lagrangian for heavy-light mesons (Manohar and Wise, 2000) starts at $\mathcal{O}(k)$, with k the residual momentum of the heavy quark. The light meson momentum p should also be $\mathcal{O}(k)$. In our staggered power counting, Eq. (92), we take $p^2 \sim m_\pi^2 \sim a^2$. This means that the LO heavy-light meson terms are lower order than the $\mathcal{O}(a^2)$ discretization errors in the light quark action. The LO heavy-light meson propagator and vertices are thus the same as in the continuum, as are the heavy-light currents that enter, e.g., in leptonic and semileptonic decays. The light-quark discretization errors in heavy-light meson quantities first appear at one loop (NLO), through the taste violations in the light meson propagators in the loop. These corrections have been calculated for heavy-light leptonic decay constants (Aubin and Bernard, 2006), for semilep-

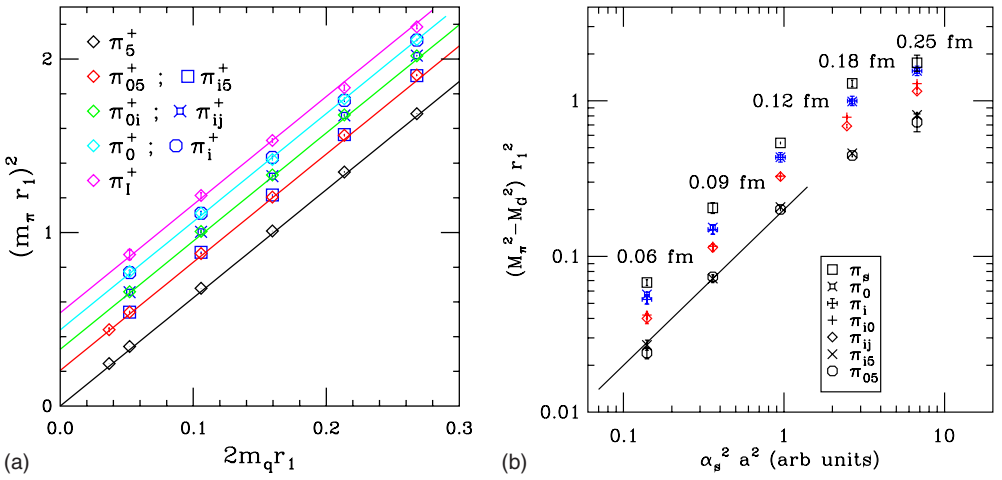

FIG. 6. (Color online) Squared charged pion masses, in units of r_1, as function of quark mass (left). From Bernard *et al.*, 2006c, 2007c. A previous version appeared in Bernard *et al.* (2001). The splittings appear to be independent of the quark mass. The taste splittings as function of a^2a^2 (right) in a log-log plot, showing the expected behavior, indicated by the diagonal straight line. Adapted from Bernard *et al.*, 2007a.

tonic heavy-to-light decays, e.g., $B \to \pi$ (Aubin and Bernard, 2007), and for semileptonic heavy-to-heavy decays, e.g., $B \to D$ and $B \to D^*$ (Laiho and Van de Water, 2006). There are also analytic NLO corrections to physical processes, coming both from light-quark mass corrections (as in the continuum) and from taste-violating corrections to the LO Lagrangian and currents. In practice, it is usually easy to guess these analytic NLO corrections from symmetry arguments, so it is not necessary to use the complicated NLO heavy-light Lagrangian (Aubin and Bernard, 2006).

C. The issue of rooting

The extra tastes are eliminated in staggered dynamical simulations by taking the fourth root of the fermion determinant—the fourth-root procedure. In the past few years there has been progress in understanding and validating this procedure, and we give a brief overview of this progress here. For more detailed discussions see Sharpe (2006b), Kronfeld (2007), and Golterman (2008).

The fourth-root procedure would be unproblematic if the action had full $\mathrm{SU}(4)_V$ taste symmetry, which would give a Dirac operator that was block diagonal in taste space. Indeed, this is the "cartoon version" of what we expect in the continuum limit. Assuming taste symmetry is restored, the positive fourth root of the positive staggered determinant would then become equal to the determinant of a single continuum species.

At nonzero lattice spacing a, taste symmetry is broken and the Dirac operator is not block-diagonal [see Eq. (32)]. From Eq. (34), one has

$$\ln \det(D_{KS} + m \otimes I) = 4 \ln \det(D + m) + \ln \det\{I + [(D + m)^{-1} \otimes I] a\Delta\}. \quad (103)$$

Since $(D+m)^{-1}$ is nonlocal, we should not expect the rooted theory to be local for $a \neq 0$. In fact it is possible to prove (Bernard, Golterman, and Shamir, 2006) that the fourth root of the determinant is not equivalent to the determinant of any local lattice Dirac operator.[8] The idea of the proof is simple: If there were such a local operator, then one could construct a theory with four degenerate quarks, each one with that local action. Calling this introduced degree of freedom taste, one now has a local theory with exact $\mathrm{SU}(4)_V$ taste symmetry by construction, and whose determinant is equivalent to that of the original staggered theory. This is a contradiction, because the taste symmetry of the constructed theory guarantees that it has 15 pseudo-Goldstone bosons (pions), whereas the staggered pions are known to split up into nondegenerate irreducible representations (Golterman, 1986b; Lee and Sharpe, 1999). Indeed, Fig. 6 shows our lattice measurements of the pion splittings as a function of quark mass (left) and lattice spacing (right). The left plot clearly shows the characteristic splitting of the charged pion (π^+) multiplet into the five nondegenerate submultiplets with tastes P, A, T, V, S. This is as predicted at $\mathcal{O}(a^2)$ in the chiral expansion, as discussed in Sec. III.A. Further splitting at higher order into a total of eight submultiplets is allowed by the lattice symmetries (Golterman, 1986b), but we see little evidence of that at the current level of statistics.

The same features of the rooted theory that imply nonlocality also imply nonunitarity on the lattice (Bernard, 2006; Prelovsek, 2006b; Bernard, DeTar, *et al.*, 2007; Bernard, Golterman, *et al.*, 2007). The issue is particularly sharp in the rooted one-flavor theory. The physical one-flavor theory should have no light pseudo-

[8] "Equivalent" here means equal up to a factor of the exponential of some local effective action of the gauge field. This is enough to guarantee that the two theories have the same physics at distances much larger than the lattice spacing (Adams, 2005; Shamir, 2005).

scalar mesons (pions) but only a heavy η'. In a rooted theory with exact taste symmetry (e.g., with four copies of rooted overlap quarks), this works automatically: the fourth power of the fourth root of a (positive) determinant is equal to the determinant itself. Alternatively, one can check directly in the rooted four-taste theory that, in physical correlators, the pion intermediate states cancel and only the η' remains (Bernard, Golterman, *et al.*, 2007). On the other hand, in the rooted one-flavor staggered theory, the pions have different masses at nonzero lattice spacing and cannot cancel, leaving light intermediate states with both positive and negative weights. This is a clear violation of unitarity.

In the continuum limit, we expect that all pions become degenerate. For the tree-level improved asqtad fermions, generic lattice artifacts are of order $\mathcal{O}(\alpha_s a^2)$. Taste violations, however, require exchange of at least two UV gluons, since the coupling of a quark to a single gluon with any momentum components equal to π/a vanishes. Therefore taste violations with the asqtad action should vanish as $\alpha_s^2 a^2$ as $a \to 0$. The lattice-spacing dependence of the pion splittings, shown in the right-hand plot of Fig. 6, agrees well with this expectation. Note that since we are looking here at flavor-nonsinglet pions, the taste singlet π_I^+ also becomes degenerate with the other 15 pions as the continuum limit is approached.

Thus, the rooted staggered theory is inherently nonlocal and nonunitary at nonzero lattice spacing, but should become local and unitarity in the continuum limit if taste symmetry is restored. This is because, in the limit of exact taste symmetry, rooting of the sea quarks is equivalent to restriction to a single taste, which is a local operation. Clearly, the numerical evidence for taste-symmetry restoration in the continuum is strong, and accords with the theoretical expectation coming from the fact that taste violation is due to an operator with dimension five. How, then, could rooting go wrong? The main problem is that the theoretical expectation is based on standard lore of the renormalization group (RG) that operators with dimension greater than four are irrelevant in the continuum limit. This standard lore for the scaling of operators assumes a local lattice action, which does not apply here. The numerical results indicate that the lore is not leading us astray, but of course numerical evidence does not constitute a proof.

There is a further problem in the formal argument we have made so far that rooting is equivalent in the continuum limit to restriction to a single taste. The argument seems to require that taste symmetry is restored for the Dirac operator D_{KS}, Eq. (34), itself. In Fig. 6, however, we are only testing the restoration of taste symmetry at physical scales, those much larger than the lattice spacing. At the scale of the cutoff, there is actually no reason to expect that taste symmetry is restored. Indeed, direct studies of the eigenvalues of D_{KS} on the lattice (Dürr *et al.*, 2004; Follana *et al.*, 2004) find only approximate quartets of eigenvalues (indicating approximate taste symmetry) for *low-lying* eigenvalues, those corresponding to long (physical) distance scales.

Shamir (2005, 2007) set up an RG framework for both unrooted and rooted staggered theories, and used it to address the potential problems of rooting. The renormalization group is clearly the natural framework to study the scaling of operators, and it also makes possible a more precise treatment of the continuum limit. As one blocks D_{KS} to longer distance scales, the eigenvalues at the scale of the cutoff are removed, and one may then expect that taste symmetry is truly restored.

Shamir's RG scheme starts with unrooted staggered quarks, and blocks them on the hypercubic lattice by a factor of 2 at each step, integrating out the finer quark fields. The gauge fields are also blocked, but the integration over them is postponed until the end, so that the quark action stays quadratic at every step. The starting "fine" lattice spacing a_f is blocked n times to a final "coarse" lattice spacing a_c. As n is increased, the coarse spacing is held fixed but small, with $a_c \ll 1/\Lambda_{QCD}$. The fine lattice spacing thus obeys $a_f = 2^{-n} a_c$, and the continuum limit is $n \to \infty$, which sends a_f to zero. In this unrooted theory, the scaling of Δ like a_f is guaranteed by the standard lore, since the action is local.

The rooted theory cannot be blocked in the same way because rooted quarks are not defined by a standard Lagrangian, but by a rule to replace the fermion determinant by its fourth root in the path integral. We can, however, apply the rule at every stage of the (unrooted) blocking, obtaining, at the nth step, the theory given by

$$Z_n^{\mathrm{KSroot}} = \int d\mathcal{A} \det{}^{1/4}(D_{KS,n} + m_n \otimes I), \tag{104}$$

where $D_{KS,n}$ is the blocked staggered Dirac operator, m_n is the (renormalized) mass on the blocked lattice, and $d\mathcal{A}$ is the full gauge measure (which includes integrals over gauge fields at each level of blocking, as well as Jacobian terms coming from integrating out the fermions on the coarse lattices). This defines a RG for the rooted theory. However, it is difficult to make progress directly from Eq. (104), because of the problem of nonlocality.

Shamir's key insight is that one may define, at each stage of blocking, an intermediate "reweighted theory," which becomes closer to the rooted staggered theory but retains locality. Define D_n to be the taste-singlet part of $D_{KS,n}$, and $a_f \Delta_n$ to be the remainder,

$$D_n = \tfrac{1}{4} \mathrm{Tr}_{ts}(D_{KS,n}), \quad D_{KS,n} = D_n \otimes I + a_f \Delta_n, \tag{105}$$

where Tr_{ts} is the trace over taste, and I is the identity in taste space. This parallels Eq. (34). We see below the explicit a_f in the second term of Eq. (105) does not mislead us about the scaling of $a_f \Delta$. The operator D_n is local because D_{KS} is. Further, $\det(D_n + m_n) = \det{}^{1/4}((D_n + m_n) \otimes I)$. The (rooted) reweighted theory is then defined by

$$Z_n^{\mathrm{reweighted}} = \int d\mathcal{A} \det(D_n + m_n). \tag{106}$$

Now, since the reweighted theory is QCD-like, *albeit* with a more complicated gauge integration than usual,

we expect it to be renormalizable and asymptotically free. The running of the operator $a_f\Delta_n$ from a_f to a_c can then be calculated perturbatively because in this range the lattice spacings are all $\ll 1/\Lambda_{QCD}$. Because the theory is local, the standard lore tells us that the perturbative running will be a reliable guide to the complete nonperturbative behavior. Thus we expect that the operator norm of $a_f\Delta_n$ will obey, in an ensemble-average sense,

$$\|a_f\Delta_n\| \lesssim a_f/a_c^2 = 2^{-n}/a_c, \tag{107}$$

where the $\lesssim$ sign implies that the scaling is true up to logarithms. For the same reasons, the mass m_n should run logarithmically, just as in QCD. From this and Eq. (105), we have

$$\begin{aligned}\det{}^{1/4}&(D_{KS,n}+m_n\otimes I)\\ &= \det(D_n+m_n)\\ &\quad\times\exp\left(\tfrac{1}{4}\mathrm{Tr}\,\ln\{I+[(D_n+m_n)^{-1}\otimes I]a_f\Delta_n\}\right)\\ &= \det(D_n+m_n)\left[1+\mathcal{O}\left(\frac{a_f}{a_c^2 m_n}\right)\right],\end{aligned} \tag{108}$$

where the quark mass provides a lower bound to the absolute value of the eigenvalues of D_n+m_n. Thus,

$$\lim_{n\to\infty} Z_n^{\mathrm{KSroot}} = \lim_{n\to\infty} Z_n^{\mathrm{reweighted}}. \tag{109}$$

In other words, the nonlocal rooted staggered theory coincides with a local one-taste theory in the continuum limit, as desired.

Note that Eq. (108) makes it clear that one must take the continuum ($a_f\to 0$) limit before the chiral ($m\to 0$) limit for rooting to work. This is not surprising, since it is already well known (Smit and Vink, 1987; Bernard, 2005; Dürr and Hoelbling, 2005; Bernard, Golterman, *et al.*, 2007) that the two limits do not commute for all physical quantities, and that taking the chiral limit first can give incorrect answers. This is true even for the unrooted staggered theory. As a trivial example, consider the low-energy constant B [see Eq. (39)] defined at a given lattice spacing a by $B(a)\equiv m_{\pi_t}^2/(2m)$ for some taste t. Unless $t=P$, giving the Goldstone pion, one has $\lim_{a\to 0}\lim_{m\to 0} B(a)=\infty$; while the desired result is $\lim_{m\to 0}\lim_{a\to 0} B(a)=B$.

One may worry that the argument thus far presumes too much about how perturbation theory works in the reweighted theory. After all, the perturbation theory involves multiple levels of gauge integrations, making it quite complicated. Indeed, no such perturbative calculations have been performed to date. Shamir (2007) pointed out, however, that we may avoid the details of perturbation theory in the reweighted theory by leaning a bit more on the standard lore and on perturbation theory in the *unrooted* staggered theory, which is fairly well understood; see Sharpe (2006b), and references therein. One starts by considering the unrooted staggered theory replicated n_r times, where n_r is an integer. In this theory the β function and the logarithmic anomalous dimension of $a_f\Delta_n$ will be the standard functions of the total number of fermion species, and $a_f\Delta_n$ will scale as expected as long as n_r is not so large that asymptotic freedom is lost.

Now, $a_f\Delta_n$ is just the difference between the (replicated) unrooted staggered theory and a (replicated) unrooted reweighted theory defined by the Dirac operator $(D_n+m_n)\otimes I$. Since $a_f\Delta_n$ gets small as $n\to\infty$ in one theory, it must get small in the other theory. Both theories are local, so the standard lore says that $a_f\Delta_n$ scales as expected in perturbation theory in the unrooted reweighted theory—however complicated such calculations would actually be in practice. The results of perturbation theory to any fixed order are polynomial in n_r, with the power of n_r just counting the number of closed quark loops. In this perturbation theory, we may put $n_r=1/4$ to obtain the perturbation theory for the rooted reweighted theory, Eq. (106). Thus we do not have to calculate explicitly in either the unrooted or rooted reweighted theories; we know that $a_f\Delta_n$ will scale to zero as expected in perturbation theory. Now the standard lore takes over for the local rooted reweighted theory, and says $a_f\Delta_n$ will scale to zero as $n\to\infty$ even nonperturbatively.

A numerical test of the scaling of $a_f\Delta_n$ was attempted by Bernard *et al.* (2006a). The results were encouraging but far from conclusive, due to quite large statistical errors.

Although the above arguments make it plausible that rooting works, they do not constitute a rigorous proof. As always in lattice QCD, one relies heavily on the standard lore about RG running of irrelevant operators, which is what "guarantees" universality. Further, we are unable to do justice here to all arguments and assumptions involved in the perturbative analysis. We have also ignored the nontrivial issues involving the Jacobian obtained by integrating out the fermions at each level of blocking. The Jacobian can be written as the exponential of an effective action for the gauge fields. The claim is that this effective action is local, basically because it comes from short-distance fluctuations of the fermions; see Shamir (2007), Sharpe (2006b), Kronfeld (2007), and Golterman (2008) for details and discussion.

We now consider the question of whether rSχPT is the correct chiral theory for rooted staggered QCD. This is important first because rSχPT allows us to fit lattice data and take the limits $a\to 0$ and $m\to 0$ in the correct order and with controlled errors. In addition, the validity of rSχPT, coupled with the strong numerical evidence for the restoration of taste symmetry for $a\to 0$ (see Fig. 6), guarantees that rooted staggered QCD produces the desired results for the pseudoscalar meson sector in the continuum limit. This is because rSχPT becomes continuum χPT when taste symmetry is restored.

Before discussing the arguments supporting rSχPT, we note that rSχPT has the main features desired for a chiral effective theory of the rooted theory. In particular rSχPT reproduces the nonunitarity and nonlocality of rooted staggered QCD at nonzero lattice spacing. This comes about because rSχPT, like the rooted staggered

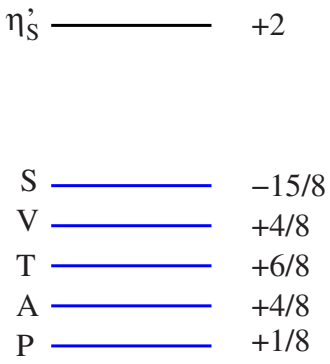

FIG. 7. (Color online) Relative weights (shown at the right of each line) of two-particle intermediate states in the scalar, taste-singlet correlator in the one-flavor case. The two-η'_S state (S indicates taste singlet) is shown at top; while the various two-pion states below are labeled by the pion taste (S, V, T, A, P). The height of each line represents, qualitatively, the relative mass of the state.

theory itself, is not an ordinary Lagrangian theory, but a Lagrangian theory *with a rule*. For rSχPT the rule is: calculate in the replicated theory for integer n_r number of replicas, and then set $n_r=1/4$. Setting $n_r=1/4$ gives "funny" relative weights for different diagrams, which can result ultimately in negative weights for some intermediate states in an ostensibly positive correlator. For example, Fig. 7 shows the weights of various two-meson intermediate states coming from a rSχPT calculation (Bernard, 2006; Bernard, DeTar, *et al.*, 2007) of the scalar taste-singlet correlator in a one-flavor rooted staggered theory. The physical theory should only have a two-η' intermediate state, but here we have various light pion states, with the taste-singlet pions[9] having a negative weight. In the continuum limit, however, the pions become degenerate, and they decouple since their weights add to zero.

The first argument for the validity of rSχPT was given by Bernard (2006). The starting point is the observation that the case of four degenerate flavors of rooted staggered quarks is particularly simple because it is the same as the case of one flavor of unrooted staggered quarks. Thus we know the chiral theory: it is exactly that obtained by Lee and Sharpe (1999) for one unrooted flavor. This chiral theory is equivalent to that of rSχPT for four degenerate flavors. The equivalence is manifest order by order in the chiral theory: Since the result for any physical quantity is polynomial in the number of degenerate flavors, taking $4n_R$ degenerate flavors and then putting $n_R=1/4$ gives the same chiral expansion as a one-flavor theory.

The case of four nondegenerate flavors may then be treated by expanding around the degenerate limit. The expansion is, however, somewhat subtle. Once we move away from the degenerate limit, nontrivial weighting factors of various diagrams, caused by the fourth root of the determinant of the sea quarks, come into play. This means that it is impossible to write all needed derivatives with respect to the quark masses as derivatives in the one-flavor unrooted theory of Lee and Sharpe. The solution is to keep the sea quarks degenerate, but to introduce arbitrary numbers of valence quarks. Bernard then showed that it is possible to rewrite all derivatives with respect to sea-quark masses as sums of various combinations of derivatives with respect to the valence quark masses. This approach allows us to remain in the degenerate sea-quark limit, where the chiral theory is known. It is however necessary to assume that partially quenched chiral perturbation theory (PQχPT) (Bernard and Golterman, 1994) is valid in the unrooted case. Since the unrooted case is local, this is very plausible. Further, there is a significant amount of numerical work that supports the validity of PQχPT for local theories, using other fermion discretizations, not just staggered quarks. It should be pointed out that partially quenched chiral theories rest on shakier ground than the standard chiral theory for QCD, as emphasized recently by Sharpe (2006a). For example, the argument by Weinberg (1979) for QCD invokes unitarity, which partially quenched theories do not have. On the other hand, the argument by Leutwyler (1994) emphasized cluster decomposition instead of unitarity and may be possible to apply to a partially quenched Euclidean theory. Work on putting PQχPT on a firmer foundation is in progress (Bernard and Golterman, 2009).

An additional, technical assumption for this approach is that the mass expansion does not encounter any singularities. This is reasonable because the expansion is about a *massive* theory, and one therefore does not expect infrared problems.

To reach the more interesting case of three light flavors, Bernard raised the mass of one of the four quarks (call it the charm quark, with mass m_c) to the cutoff, decoupling it from the theory. This requires an additional technical assumption, arising from the fact that there is a range of masses, which begins roughly at $m_c \sim 2m_s$ (with m_s the strange quark mass), where the charm quark has decoupled from the chiral theory, but not yet from the QCD-level theory. While the resulting three-flavor chiral theory has the same form as that of QCD when $a \to 0$, the assumption does leave open the possible "loophole" that the LECs have different numerical values from those of QCD.

The above argument takes place entirely within the framework of the chiral theory. It has the nice feature that the recovery of the correct QCD chiral expressions, and the vanishing of nonlocal and nonunitary effects, only requires taste violations to vanish in the continuum limit in the unrooted, and hence local, theories with integral n_r. The vanishing of these taste violations in the rooted chiral theory then follows. On the other hand, because the argument does not connect rSχPT to the QCD-level rooted staggered theory, the replica rule ends up emerging rather mysteriously. The chain of reasoning also depends on several technical assumptions.

[9]The taste-singlet pion is distinct from the η' here because it is a flavor nonsinglet arising at the arbitrary, integral n_r values at which the calculation is done.

An argument for the validity of rSχPT directly from the fundamental rooted staggered theory is therefore desirable. It has been developed by Bernard, Golterman, and Shamir (2008) by starting from the RG framework of Shamir. The basic idea is to generalize the fundamental (lattice-level) theory to one in which the dependence on the number of replicas n_r is polynomial to any given order in the fine lattice spacing a_f. Then we can find the chiral theory for each integer n_r in a standard way (because the theories are local), and apply the replica rule to get the rooted staggered theory at the fundamental level and rSχPT at the chiral level.

For simplicity we focus on a target theory with n_s degenerate quarks in the continuum limit. Unlike the previous argument, the extension here to quarks with nondegenerate masses is straightforward. Consider Eq. (104), the rooted staggered theory at the nth step of blocking, but with n_s degenerate staggered flavors

$$Z_n^{\mathrm{KSroot}}(n_s) = \int d\mathcal{A}\, \det{}^{n_s/4}(D_{KS,n} + m_n \otimes I). \tag{110}$$

Now generalize this, using the definitions of Eq. (105), to

$$Z_n^{\mathrm{gen}}(n_s,n_r) = \int d\mathcal{A}\, \det{}^{n_s}(D_n + m_n) \times \frac{\det{}^{n_r}[(D_n + m_n) \otimes I + t a_f \Delta_n]}{\det{}^{n_r}[(D_n + m_n) \otimes I]}, \tag{111}$$

where t is a convenient interpolating parameter. When $t=1$ and $n_r=n_s/4$, this reduces to Eq. (110) because the determinants of the reweighted fields [those involving D_n+m or $(D_n+m)\otimes I$ only] cancel, and the remaining determinant is just that of the rooted staggered theory. When $t=0$, on the other hand, Eq. (111) gives a local theory of n_s reweighted one-taste quarks.

Equation (111) has an important advantage over Eq. (110). While the dependence on n_s is unknown and nonperturbative in both cases, the dependence on n_r of $Z_n^{\mathrm{gen}}(n_s,n_r)$ is well controlled because it vanishes when the taste violations vanish ($a_f\Delta_n=0$ or $t=0$). This makes it possible to apply a replica rule on n_r at the fundamental QCD level. To see this, we first write

$$\frac{\det{}^{n_r}[(D_n + m_n) \otimes I + t a_f \Delta_n]}{\det{}^{n_r}[(D_n + m_n) \otimes I]} = \exp(n_r \mathrm{Tr}\, \ln\{1 + [(D_n + m_n)^{-1} \otimes I] t a_f \Delta_n\}). \tag{112}$$

We then expand in powers of the fine lattice spacing a_f. These can come from the explicit factor a_f in the taste-violating term or from the implicit dependence on a_f of the gluon action and the lattice operators D_n and Δ_n. The parameter t serves to keep track of the explicit dependence; the power of t must be less than or equal to the power of a_f to which we expand. From Eq. (112), the power of n_r must in turn be less than or equal to the power of t. Thus, to any fixed order in a_f, the dependence of the theory on n_r must be polynomial. This means that n_r is a valid replica parameter of the fundamental theory (again to any fixed order in a_f). We can in principle find the polynomial dependence of any correlation function by calculations for integer values of n_r only, and then determine the correlation function in the rooted staggered theory by simply setting $n_r=n_s/4$ (and $t=1$).

We now discuss the effective theories, the SET and the chiral theory. For convenience, we can work at $t=1$. For n_r and n_s (positive) integers, $Z_n^{\mathrm{gen}}(n_s,n_r)$ is a local, but partially quenched, theory that can be written directly as a path integral. It is partially quenched because the determinant in the denominator needs to be generated as an integral over ghost (bosonic) quarks. Finding the SET and the chiral effective theory for such local theories is standard, although the *caveats* about the foundations of PQχPT apply. All that we really need to know is that the effective theories exist for any integer n_r and n_s, and that their dependence on n_r is polynomial (because the dependence in the underlying theory is polynomial). In the chiral theory we can then set $n_r=n_s/4$. At the QCD level this just gives the rooted staggered theory for n_s flavors. At the chiral level, the reweighted parts of the theory again cancel order by order at $n_r=n_s/4$, because we have n_s flavors of one-taste quarks and n_r flavors of four-taste ghost quarks, with exact taste symmetry. We are then left with exactly the result we would have gotten from rSχPT.

This argument avoids the loophole and technical assumptions of the argument of Bernard (2006). It also makes clear how the replica rule arises from the fundamental theory. On the other hand, it inherits the assumptions of Shamir (2007), since it is based on that framework. Both arguments rely on the standard PQχPT for local theories. This is not surprising since rooted staggered QCD inherently shares some features of a partially quenched theory: Since rooting is done only on the sea quarks, there is an excess of valence quarks. As noted earlier, however, this valence-rooting issue is not a fundamental problem because there is a physical subspace.

A nice feature of the current argument is that, by coupling rSχPT directly to the RG framework it makes numerical tests of rSχPT into tests of the RG framework, and hence of the validity of rooting at the fundamental level. We discuss such tests in Sec. VI.

We now turn to the objections raised to rooted staggered quarks by Creutz (2006a, 2006b, 2007a, 2007b, 2007c, 2008a, 2008b). Since these objections have been refuted (Bernard, Golterman, *et al.*, 2007, 2008a, 2008b; Adams, 2008; Golterman, 2008)—see also Sharpe (2006b) and Kronfeld (2007)—we give only a very brief discussion here. The main point is that most of Creutz's claims apply equally well to the proposed continuum limit theory of rooted staggered quarks: a rooted four-taste theory with exact taste symmetry, which is called a rooted continuum theory (RCT) by Bernard, Golterman, *et al.* (2008b). Such a theory provides a tractable framework in which to examine Creutz's claims. Because, as emphasized before, $\det{}^{1/4}((D+m)\otimes I) = \det(D$

$+m$), the RCT is clearly equivalent to a well-behaved one-taste theory, and gives a counterexample to most of Creutz's objections. Alternatively, Adams (2008) found counterexamples to Creutz's claims in a simple lattice context, namely, a version of twisted Wilson quarks.

While the RCT is equivalent to a one-taste theory, it is not exactly the same in the following sense: In the RCT, with its four tastes, one can couple sources to various tastes and generate Green's functions that have no analog in the one-taste theory. Such unphysical Green's functions are at the basis of many of the "paradoxes" Creutz finds. For example, one can find 't Hooft vertices that are singular in the limit $m \to 0$. Nevertheless, these unpleasant effects exist purely in the unphysical sector of the RCT; in the physical sector all 't Hooft vertices are well behaved.

Finally, Creutz noticed that there is a subtlety involving rooted staggered quarks for negative quark mass, and this is in fact true. Independent of the sign of the quark mass, the staggered determinant is positive, as discussed following Eq. (28). The fourth root of the determinant generated by the dynamical algorithms, Sec. II.C, is then automatically positive for any sign of m. In other words, the rooted staggered theory is actually a function of $|m|$, not m. This means that rooted staggered fermions cannot be used straightforwardly to investigate the effects that are expected (Dashen, 1971; Witten, 1980) to occur for an odd number of negative quark masses.[10] A related problem occurs when one adds a chemical potential to the theory—the determinant becomes complex, and the fourth root, ambiguous (Golterman *et al.*, 2006). Nevertheless, these problems have no relevance to the validity of the rooted staggered theory in the usual case of positive quark mass and zero chemical potential. For more details, see Bernard, Golterman, *et al.* (2007).

IV. OVERVIEW OF THE MILC LATTICE ENSEMBLES

In this program of QCD simulations, ensembles of lattices were generated at several lattice spacings and several light quark masses. This allows extrapolations to zero lattice spacing (the "continuum extrapolation") and to the physical light quark mass (the "chiral extrapolation"). In all ensembles the masses of the up and down quarks are set equal, which has a negligible effect ($<1\%$) on isospin-averaged quantities. The original goals of the program were to simulate with three dynamical quark flavors, with a large enough physical volume to make finite size effects small, and to vary the quark masses to study the effects of "turning on" the dynamical quarks. It later became clear that more lattice spacings were needed to understand the continuum limit. Fortunately, computer power was increasing rapidly, which made the simulations with smaller a practical.

Currently, the lattice spacings of the ensembles fall into six sets, with lattice spacings $\approx$0.18, 0.15, 0.12, 0.09, 0.06, and 0.045 fm. In many places these are called extracoarse, medium coarse, coarse, fine, superfine, and ultrafine, respectively. The 0.12 fm lattices were the first to be generated. Over time, as computer power permitted, the lattice spacing was reduced progressively by $\approx 1/\sqrt{2}$ so that in each reduction the estimated leading finite lattice spacing artifacts were a factor of 2 smaller than in the previous set. The coarser lattices were added to support thermodynamics studies and to provide further leverage for continuum extrapolations. The medium coarse ensemble was added after coarse and fine and has a better tuned strange quark mass based on analysis of the other ensembles.

For comparison, at $a \approx 0.12$, 0.09, and 0.06 fm, quenched ensembles with the same gauge action were also generated. For each of these lattice spacings, the gauge coupling $\beta = 10/g^2$ was adjusted as the light quark mass was changed to keep the lattice spacing approximately fixed. However, the lattice spacing could only be determined accurately after the large ensembles were generated, so it is necessary to take into account the small differences in lattice spacing among the ensembles in the same set. In Sec. IV.B, we describe measurement of the lattice spacing on each ensemble, and a parametrized fit to smooth out statistical fluctuations.

The strange quark mass in lattice units am_s was estimated before simulations began, and was held fixed as the light quark mass and gauge coupling were varied. Later analysis, described in Sec. VI, determined the correct strange quark mass more accurately, and in fact the initial estimates turned out to be wrong by as much as 25%.

In the $a \approx 0.12$ fm set, several ensembles have a large dynamical quark mass—as large as 11 times the physical strange quark mass. This was done to investigate the physics of continuously turning on the quarks by lowering their masses from infinity. There are also a number of ensembles with a lighter-than-physical strange quark mass. These were generated to explicitly study dependence on the sea strange quark mass, and, since the lighter strange quark implies less sensitivity to higher orders in SU(3) chiral perturbation theory, enable improved determinations of the parameters in the chiral expansion, particularly of the low-energy constants (see Sec. VI).

The fields satisfy periodic boundary conditions in the space directions, while the boundary condition in the Euclidean time direction is periodic for the gauge fields and antiperiodic for the quark fields.

Table I shows the parameters of the asqtad ensembles (a few short "tuning" ensembles are not included). Here am_l is the dynamical light quark mass in lattice units and am_s is the strange quark mass. Figure 8 shows the quark masses and lattice spacings of these ensembles.

[10] In principle, the negative mass region can be simulated by adding a θ term to the action. Because of the sign problem, this would be extremely challenging in four dimensions. However, it has been shown to work well in the Schwinger model (Dürr and Hoelbling, 2006).

TABLE I. The asqtad ensembles. u_0 is the input tadpole factor, Eq. (9), rather than the value determined from the ensemble average of the plaquette. Lattice spacings are from the smoothed fit described in the text, except where indicated by a ∗. For these ensembles, r_1/a is from this ensemble alone, rather than the smoothed fit. To convert to physical units, use $r_1 \approx 0.31$ fm. A † indicates that the run is in progress. This list of ensembles and counts of archived lattices are as of December 2008.

$\beta=10/g^2$	am_l	am_s	$(L/a)^3\times(T/a)$	Lats.	u_0	r_1/a	$m_\pi L$
			$a\approx 0.18$ fm				
6.503	0.0492	0.0820	$16^3\times 48$	250	0.85636	1.778(8)	9.07
6.485	0.0328	0.0820	$16^3\times 48$	334	0.85585	1.785(7)	7.47
6.467	0.0164	0.0820	$16^3\times 48$	416	0.85492	1.801(8)	5.36
6.458	0.0082	0.0820	$16^3\times 48$	484	0.85489	1.813(8)	3.84
			$a\approx 0.15$ fm				
6.628	0.0484	0.0484	$16^3\times 48$	621	0.8623	2.124(6)	8.48
6.600	0.0290	0.0484	$16^3\times 48$	596	0.8614	2.129(5)	6.63
6.586	0.0194	0.0484	$16^3\times 48$	640	0.8609	2.138(4)	5.46
6.572	0.0097	0.0484	$16^3\times 48$	631	0.8604	2.152(5)	3.93
6.566	0.00484	0.0484	$20^3\times 48$	603	0.8602	2.162(5)	3.50
			$a\approx 0.12$ fm				
8.000	∞	∞	$20^3\times 64$	408	0.8879	2.663(6)∗	na
7.350	0.4000	0.4000	$20^3\times 64$	332	0.8822	2.661(7)∗	29.4
7.150	0.2000	0.2000	$20^3\times 64$	341	0.8787	2.703(7)∗	19.6
6.960	0.1000	0.1000	$20^3\times 64$	340	0.8739	2.687(0)∗	13.7
6.850	0.0500	0.0500	$20^3\times 64$	425	0.8707	2.686(8)	9.70
6.830	0.0400	0.0500	$20^3\times 64$	351	0.8702	2.664(5)	8.70
6.810	0.0300	0.0500	$20^3\times 64$	564	0.8696	2.650(4)	7.56
6.790	0.0200	0.0500	$20^3\times 64$	1758	0.8688	2.644(3)	6.22
6.760	0.0100	0.0500	$20^3\times 64$	2023	0.8677	2.618(3)	4.48
6.760	0.0100	0.0500	$28^3\times 64$	275	0.8677	2.618(3)	6.27
6.760	0.0070	0.0500	$20^3\times 64$	1852	0.8678	2.635(3)	3.78
6.760	0.0050	0.0500	$24^3\times 64$	1802	0.8678	2.647(3)	3.84
6.790	0.0300	0.0300	$20^3\times 64$	367	0.8689	2.650(7)	7.56
6.750	0.0100	0.0300	$20^3\times 64$	357	0.8675	2.658(3)	4.48
6.715	0.0050	0.0050	$32^3\times 64$	701	0.8671	2.697(5)	5.15
			$a\approx 0.09$ fm				
8.400	∞	∞	$28^3\times 96$	396	0.89741	3.730(7)∗	na
7.180	0.0310	0.0310	$28^3\times 96$	500	0.8808	3.822(10)	8.96
7.110	0.0124	0.0310	$28^3\times 96$	1996	0.8788	3.712(4)	5.78
7.100	0.0093	0.0310	$28^3\times 96$	1138	0.8785	3.705(3)	5.04
7.090	0.0062	0.0310	$28^3\times 96$	1946	0.8782	3.699(3)	4.14
7.085	0.00465	0.0310	$32^3\times 96$	540†	0.8781	3.697(3)	4.11
7.080	0.0031	0.0310	$40^3\times 96$	1012	0.8779	3.695(4)	4.21
7.075	0.00155	0.0310	$64^3\times 96$	530†	0.877805	3.691(4)	4.80
7.100	0.0062	0.0186	$28^3\times 96$	985	0.8785	3.801(4)	4.09
7.060	0.0031	0.0186	$40^3\times 96$	642	0.8774	3.697(4)	4.22
7.045	0.0031	0.0031	$40^3\times 96$	440†	0.8770	3.742(8)	4.20
			$a\approx 0.06$ fm				
7.480	0.0072	0.0180	$48^3\times 144$	625	0.8881	5.283(8)	6.33
7.475	0.0054	0.0180	$48^3\times 144$	617	0.88800	5.289(7)	5.48
7.470	0.0036	0.0180	$48^3\times 144$	771	0.88788	5.296(7)	4.49
7.465	0.0025	0.0180	$56^3\times 144$	800	0.88776	5.292(7)	4.39
7.460	0.0018	0.0180	$64^3\times 144$	826	0.88764	5.281(8)	4.27
7.460	0.0036	0.0108	$64^3\times 144$	483	0.88765	5.321(9)	5.96

TABLE I. (*Continued.*)

$\beta=10/g^2$	am_l	am_s	$(L/a)^3\times(T/a)$	Lats.	u_0	r_1/a	$m_\pi L$
			$a\approx 0.045$ fm				
7.810	0.0028	0.0140	$64^3\times 192$	861	0.89511	7.115(20)	4.56

A. Algorithms and algorithm tests

The earlier ensembles were generated using the *R* algorithm (Gottlieb *et al.*, 1987) described in Sec. II.C. The molecular dynamics step size was generally set at about two-thirds of the light quark mass in lattice units. Recent lattice generation has used rational function approximations for the fractional powers described in Sec. II.C. In those simulations, we have used the Omelyan second-order integration algorithm (Sexton and Weingarten, 1992; Omelyan *et al.*, 2002a, 2002b, 2003; Takaishi and de Forcrand, 2006). We used different step sizes for the fermion and gauge forces (Sexton and Weingarten, 1992), with the step size for the fermion force three times that of the gauge force. We used four sets of pseudofermion fields and corresponding rational functions (Hasenbusch, 2001; Hasenbusch and Jansen, 2003). The first set implements the ratio of the roots of the determinants for the physical light and strange quarks to the determinant for three heavy "regulator" quarks with mass $am_r=0.2$. That is, it corresponds to the weight $\det(M(m_l))^{1/2}\det(M(m_s))^{1/4}\det(M(m_r))^{-3/4}$. The remaining three pseudofermion fields each implement the force from one flavor of the regulator quark, or the fourth root of the corresponding determinant. These choices are known to be reasonably good, but could be optimized further.

For all but the largest lattices generated with rational function methods, we included the Metropolis accept-reject decision to eliminate step size errors, or the RHMC algorithm. Because the integration error is extensive, use of the RHMC algorithm for the largest lattices would have forced us to use very small step sizes and double precision in many parts of the integration. For these lattices it was much more efficient to run at a small enough step size that the integration error was less than other expected errors in the calculation (the RHMD algorithm).

Errors from the integration step size in the *R* algorithm were originally estimated from short runs with different step sizes, as described by Bernard *et al.* (2001) and Aubin *et al.* (2004a). In several cases, ensembles originally generated with the *R* algorithm were later extended with the RHMC algorithm. This allows an *ex post facto* test of the step size errors in the *R* algorithm, with much higher statistics than possible for a tuning run. Figure 9 shows the average plaquette for one $a\approx 0.12$ fm run as a function of step size squared, combining the early tuning runs with the *R* and RHMC algorithm production runs. Table II compares the expectation values of the plaquette and the light-quark condensate and, in some cases, the lattice spacing and pion mass, for the ensembles where both algorithms were used. The differences are small and in most cases are comparable to the statistical errors.

In one case, $a\approx 0.12$ fm and $am_q=0.01/0.05$, an ensemble with a larger spatial size (28^3) was generated to check for effects of the spatial size. In general, these effects were found to be small as expected, although the

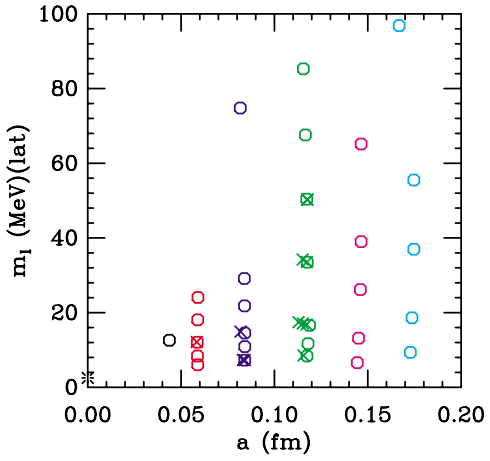

FIG. 8. (Color online) Lattice spacings and quark masses used. The octagons indicate ensembles with the strange quark near its physical value, while the crosses indicate those with an unphysically light strange quark. The burst at lower left shows the physical light quark mass. Here the quark masses are in units of MeV, but using the asqtad action lattice regularization.

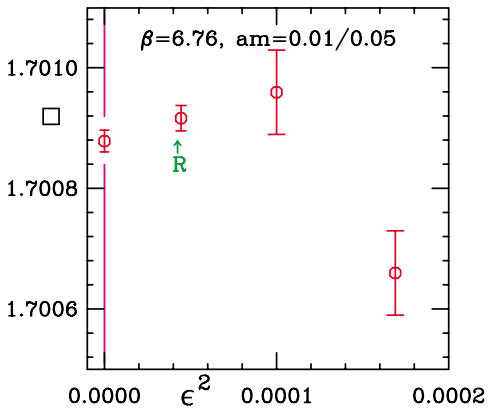

FIG. 9. (Color online) The plaquette as a function of integration step size squared for $20^3\times 64$ lattices with $\beta=6.76$ and $am_q=0.01/0.05$. The point at $\varepsilon^2=0$ is from the RHMC algorithm, and the point indicated by *R* is the value used in the *R* algorithm production runs. The remaining two points are from short test runs described by Aubin *et al.* (2004a).

TABLE II. Comparison of plaquette and light-quark condensate for ensembles run partly with the R algorithm and partly with the RHMC algorithm. For the $a \approx 0.09$ fm ensembles, we also show r_1/a and the pion mass.

β	am_l	am_s	ϵ	$\square(R)$	$\square(RHMC)$	difference	$\bar{\psi}\psi(R)$	$\bar{\psi}\psi(RHMC)$	difference
6.79	0.020	0.050	0.01333	1.709160(26)	1.708805(16)	−0.000355(30)	0.052553(61)	0.052306(28)	0.000251(67)
6.76	0.010	0.050	0.00667	1.700917(21)	1.700879(18)	−0.000038(28)	0.036875(43)	0.037174(36)	0.000300(56)
6.76	0.007	0.050	0.00500	1.701183(22)	1.701177(18)	−0.000006(29)	0.031388(54)	0.031306(38)	−0.000082(66)
6.76	0.005	0.050	0.00300	1.701181(17)	1.701211(11)	0.000030(20)	0.027551(50)	0.027597(25)	0.000045(56)
7.11	0.0124	0.031	0.00800	1.789213(19)	1.789075(7)	−0.000138(20)	0.024584(22)	0.024620(10)	0.000036(24)
7.09	0.0062	0.031	0.00400	1.784552(9)	1.784541(6)	−0.000011(11)	0.015622(17)	0.015608(14)	−0.000015(22)
7.08	0.0031	0.031	0.00200	1.782300(8)	1.782254(11)	−0.000046(11)	0.010664(18)	0.010860(19)	0.000196(26)
β	am_l	am_s	ϵ	$\frac{r_1}{a}(R)$	$\frac{r_1}{a}(RHMC)$	difference	$am_\pi(R)$	$am_\pi(RHMC)$	difference
7.11	0.0124	0.031	0.00800	3.708(13)	3.684(17)	−0.024(21)	0.20640(20)	0.20648(20)	0.00008(28)
7.09	0.0062	0.031	0.00400	3.684(12)	3.681(8)	−0.003(14)	0.14797(20)	0.14767(13)	−0.00030(24)
7.08	0.0031	0.031	0.00200	3.702(8)	3.682(7)	−0.020(11)	0.10528(9)	0.10545(9)	0.00017(13)

effects on f_π and f_K differ significantly from one-loop chiral perturbation theory estimates, as discussed in Sec. VI.

B. The static potential and determining the lattice spacing

Since results of lattice QCD simulations are initially in units of the lattice spacing, knowing the lattice spacing is crucial to calculating any dimensionful quantity. Since ratios of dimensionful quantities (mass ratios) calculated on the lattice will only have their physical values at the physical quark masses and in the continuum limit, there is arbitrariness in the determination of the lattice spacing except in the physical limit. Some dimensionful quantity must be taken to be equal to its physical value or to some *a priori* model.

Following the practice of most current lattice simulation programs, we use a Sommer scale (Sommer, 1994) as the quantity kept fixed, and determine this scale from some well controlled measurement.

A Sommer scale is defined as the length where the force between a static (infinitely heavy) quark and antiquark satisfies $r^2F(r)=-C$, where C is a constant. Intuitively, this is a length where this static potential changes behavior from the short distance Coulomb form to the long distance linear form. In particular, the most common choice is r_0, defined by $C=1.65$. We have chosen to use r_1, defined by $C=1$. This choice was made based on early simulations at $a \approx 0.12$ fm where it was found that r_1 had smaller statistical errors than r_0 (Bernard *et al.*, 2000a).

The calculation of the static potential on the earlier ensembles is described in Bernard *et al.* (2000a). We begin by fixing the lattice to Coulomb gauge. In this gauge, we can evaluate the potential from correlators of (nonperiodic) Wilson lines, where the line at $(\vec{x},t)$ with length T is $W_T(\vec{x},t)=\Pi_{i=0}^{T-1}U_4(\vec{x},t+i)$. The Coulomb gauge fixing, which makes the spatial links as smooth as possible, is an implicit way of averaging over all spatial paths closing the loop at the top and bottom. Because we do not explicitly construct the spatial parts, it is easy to average over all lattice points $(\vec{x},t)$ and to get the potential at all spatial separations $\vec{R}$.

The first step in determining r_1 is to extract $V(\vec{R})$ from the expectation value of the correlators of Wilson lines. We expect

$$L(\vec{R},T) = \langle W_T^\dagger(\vec{x},t) W_T(\vec{x}+\vec{R},t)\rangle = Ae^{-V(\vec{R})T} + A'e^{-V'(\vec{R})T} + \cdots, \quad (113)$$

where V', etc. are potentials for excited states. For $a \geqslant 0.09$ fm, the excited states are negligible for fairly small T, and we simply take $V(\vec{R})=\ln(L(\vec{R},T)/L(\vec{R},T+1))$. Specifically, we use $T=3$ for $a \approx 0.15$ fm, $T=4$ for $a \approx 0.12$ fm, and $T=5$ for $a \approx 0.09$ fm. Figure 10 shows the resulting potential for the run at $a \approx 0.09$ fm and m_l

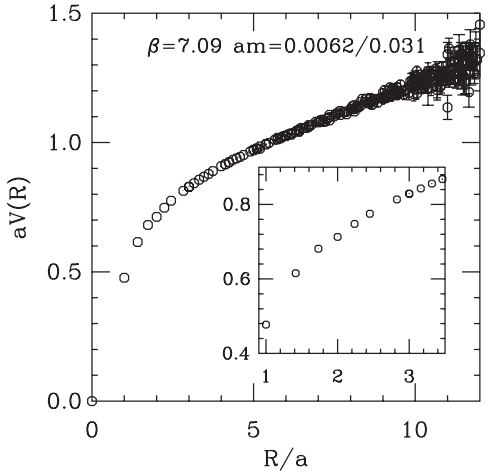

FIG. 10. The static quark potential for the ensemble with $a \approx 0.09$ fm and $m_l=0.2m_s$. This was obtained from time range five to six. The inset magnifies the short distance part, showing a lattice artifact which is discussed in the text.

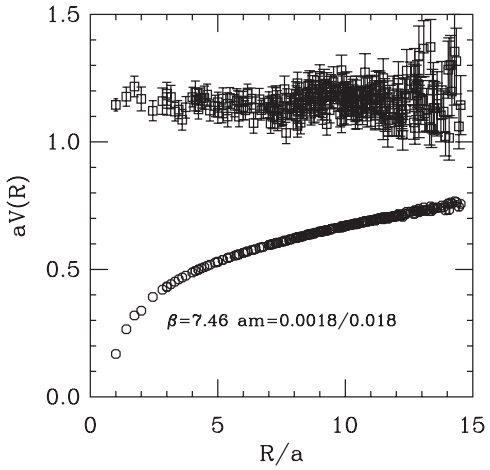

FIG. 11. The static quark potential and first excited state potential for the ensemble with $a \approx 0.06$ fm and $m_l = 0.1 m_s$. This was obtained from time range three to twenty, using the APE smeared time links discussed in the text.

$= 0.2 m_s$. The inset shows the short distance part of the potential. In this inset, there is a visible lattice artifact where the point at $R=2$, or separation (2,0,0) is slightly below a smooth curve through the nearby points with off-axis distances $\vec{R}$. However, at $R=3$ the lattice artifacts are quite small. In fact, what appears to be a single point at $R=3$ is actually two points, one for $\vec{R}=(3,0,0)$ and another for $\vec{R}=(2,2,1)$. The small objects in the center of the plot symbols are the statistical error bars on $V(R)$.

For $a \approx 0.06$ fm, the above procedure for finding $V(R)$ gave large statistical errors. This is primarily because a large constant term in the potential causes a rapid falloff of $L(\vec{R},T)$ with T. This constant can be considered a self-energy of the static quark, diverging as $1/a$. To fix this, the timelike links were smeared by adding a multiple of the three link "staples" (Albanese *et al.*, 1987), namely, fat3 links defined in Eq. (69) with $\omega = 0.1$. The Wilson line correlators $L(\vec{R},T)$ were computed from the smeared time direction links as described above. As expected, this reduces the constant term in $V(R)$, and comparison with the potential from unsmeared links suggests that any systematic effects on r_1/a are less than 0.005 at $a \approx 0.06$ fm, smaller than the statistical errors. With the smeared time links, the correlators $L(\vec{R},T)$ are statistically significant out to T as large as 20 (for small R). It is then advantageous to do a two state fit to $L(\vec{R},T)$. For the $a \approx 0.06$ fm ensembles, we generally fit these two states over a time range $3 \leqslant T \leqslant 20$. An example of the potential from this procedure is shown in Fig 11. The first excited state potential is also shown, but we caution the reader that in addition to having large statistical errors this excited state potential has not been carefully checked for stability under varying fit ranges, or under addition of a third state to the fit.

Once $V(R)$ is determined, we find r_1 by fitting $V(R)$ to a range of R approximately centered at r_1. We use a fit form

$$V(R) = C + \frac{B}{R} + \sigma R + \lambda \left(\left. \frac{1}{R} \right|_{lat} - \frac{1}{R} \right). \tag{114}$$

Here C is part of the quarks' self-energy, σ is the string tension and B is $-\frac{3}{4}\alpha_s$ for a potential definition of α_s. The last term, $\frac{1}{R}|_{lat} - \frac{1}{R}$, is the difference between the lattice Coulomb potential,

$$\left. \frac{1}{R} \right|_{lat} = 4\pi \int \frac{d^3p}{(2\pi)^3} D_{00}^{(0)}(p) e^{ipR}$$

with $D_{00}^{(0)}(p)$ the free lattice gluon propagator calculated with the Symanzik improved gauge action, and the continuum Coulomb potential $1/R$. Use of this correction term was introduced by the UKQCD Collaboration (Booth *et al.*, 1992). This correction was used for $R < 3$. The scale r_1 (or r_0) was then found from solving $r^2 F(r) = -C$ with λ set to zero, $r_1 = \sqrt{(1+B)/\sigma}$. Since we often want lattice spacing estimates from only a few lattices, and there are a large number of distances to be fit, these fits were generally done without including correlations among the different $\vec{R}$. Errors on r_1 are estimated by the jackknife method, where the size of the blocks eliminated ranges from 30 to 100 simulation time units. Spot checks comparing fits including the correlations confirmed that the jackknife errors are consistent with derivative errors in the correlated fits, and that the fit function does fit the data well over the chosen range.

For the $a \approx 0.18$ fm ensembles, we used the spatial range from 1.4 or 1.5 to 6.0; for the $a \approx 0.15$ fm ensembles, $\sqrt{2} \leqslant R \leqslant 5$; for the $a \approx 0.12$ fm ensembles, $\sqrt{2} \leqslant R \leqslant 6$; and for the $a \approx 0.09$ fm ensembles, $2 < R \leqslant 7$. For the $a \approx 0.06$ fm ensembles, where the two state fits with smeared links were used, the spatial range was $4 < R \leqslant 7$, and for the $a \approx 0.045$ fm run, it was $5 < R \leqslant 10$.

The static quark potentials for different lattice spacings can be overlaid after rescaling to check for lattice effects and to plot the potential over a large range. Figure 12 shows such a plot in units of r_1 for five different lattice spacings, using the ensembles with $m_l = 0.2 m_s$ at each lattice spacing. Bernard *et al.* (2000a), found that including the dynamical quarks modifies the static potential in the expected way. This can be seen by plotting dimensionless quantities such as r_0/r_1 or $r_1\sqrt{\sigma}$. When this is done in a region where the potential is approximated by Eq. (114) and r_1 is found from $r_1 = \sqrt{(1+B)/\sigma}$, this amounts to plotting the coefficient of $1/R$ in the fit.

Once r_1 is estimated for each ensemble, the estimate can be improved by fitting all values of r_1/a to a smooth function of the gauge coupling and quark masses. We have used two different forms for this smoothing. In the first form, we fit $\ln(r_1/a)$ to a polynomial in β and $2am_l + am_s$. The second form is a function based on work of Allton (1996):

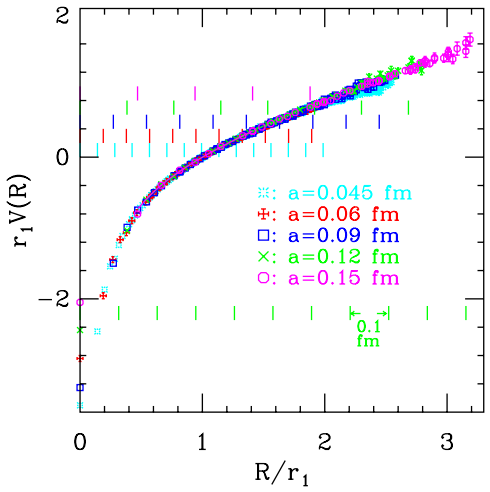

FIG. 12. (Color online) The static quark potential in units of r_1 for five different lattice spacings. In all cases, these are for light quark mass of two-tenths the simulation strange quark mass. For each lattice spacing, a constant has been subtracted to set $V(r_1)=0$. The ruler near the bottom of the plot shows distance in units of fm, using $r_1=0.318$ fm. The multiple rulers in the upper half of the plot show distance in units of the lattice spacings for the different ensembles.

$$a/r_1 = (C_0 f + C_2 g^2 f^3 + C_4 g^4 f^3)/(1 + D_2 g^2 f^2), \qquad (115)$$

where

$$f = (b_0 g^2)^{(-b_1/(2b_0^2))} \exp[-1/(2b_0 g^2)],$$

$$b_0 = (11 - 2n_f/3)/(4\pi)^2,$$

$$b_1 = (102 - 38n_f/3)/(4\pi)^4, \quad am_{tot} = 2am_l/f + am_s/f, \qquad (116)$$

$$C_0 = C_{00} + C_{01l} am_l/f + C_{01s} am_s/f + C_{02}(am_{tot})^2,$$

$$C_2 = C_{20} + C_{21} am_{tot}.$$

Here C_{00}, C_{01l}, C_{01s}, C_{02}, C_{20}, C_{21}, C_4, and D_2 are parameters. The second form is a slightly better fit, and we have used it for the r_1/a values in Table I. Errors on the smoothed r_1/a are estimated by a bootstrap for which artificial data sets were generated. In these data sets the value of r_1/a for each ensemble was chosen from a Gaussian distribution centered at the value for the ensemble given by the fit, and the standard deviation was given by the statistical error in r_1/a for the ensemble.

To find r_1 in physical units, we use a quantity that is both well-known experimentally and accurately determined in a lattice calculation. One such quantity, and the one used in most of our work, is the splitting between two energy levels of the $b\bar{b}$ mesons. These splittings have been calculated on several of the asqtad ensembles by the HPQCD/UKQCD Collaboration (Gray *et al.*, 2003, 2005; Wingate *et al.*, 2004). From fitting the 2S-1S splittings on the $a\approx 0.12$ fm ensembles with quark masses $am_l/am_s=0.01/0.05$, $0.02/0.05$, $0.03/0.05$, and $0.05/0.05$, and the $a\approx 0.09$ fm ensembles with light masses $am_l/am_s=0.0062/0.031$ and $0.0124/0.031$, to the form $r_1(a,am_l,am_s)=r_1^{\rm phys}+c_1a^2+c_2am_l/am_s$, we find $r_1^{\rm phys}=0.318$ fm with an error of 0.007 fm. [Gray *et al.* (2005) used a different fitting procedure to estimate $r_1^{\rm phys}=0.321(5)$ fm.]

More recently, analysis of the light pseudoscalar meson masses and decay constants gave an accurate value of f_π. The fitting procedure to arrive at this is complicated; see Sec. VI. Requiring that f_π in the continuum and chiral limits match its experimental value gives $r_1=0.3108(15)(^{+26}_{-79})$ fm, where the errors are statistical and systematic, respectively.

To summarize, we set the scale for each ensemble by $a\equiv(a/r_1)\times r_1^{\rm phys}$, where (a/r_1) is the output of the smoothing function, Eq. (115), at the ensemble values of am_l, am_s, and g^2, and $r_1^{\rm phys}$ is the physical value of r_1, obtained from either $b\bar{b}$ mesons splittings or f_π. The scheme is useful for generic chiral extrapolations, and tends to result in fairly small dependence of physical quantities on the sea-quark masses. However, chiral perturbation theory assumes a mass-independent scale setting scheme, because all dependence on quark masses is supposed to be explicit. So detailed fits to chiral perturbation theory forms require a mass-independent scale procedure, especially if one hopes to extract low-energy constants that govern mass dependence. Once the r_1 smoothing form is known, though, it is easy to modify the procedure to make it mass independent: instead of using the ensembles' values of am_l and am_s in the smoothing function, Eq. (115), use the physical values. This mass-independent scheme is used for the analysis of light pseudoscalars described in Sec. VI.

C. Tuning the strange quark mass

In most of these ensembles, the original intent was to fix the strange quark mass at its correct value, and to set the light quark mass to a fixed fraction of the strange quark mass. The correct strange quark mass, however, is actually not known until the lattices are analyzed. In practice, the best that can be done is to estimate the correct strange quark mass from short tuning runs or by scaling arguments from results of earlier runs. As described in Sec. VI, the physical strange and up-down quark masses are determined by demanding that the light pseudoscalar meson masses take their physical values. For the strange mass, we find $am_s=0.0439(18)$ at $a\approx 0.15$ fm, $am_s=0.0350(7)$ at $a\approx 0.12$ fm, $am_s=0.0261(5)$ at $a\approx 0.09$ fm, and $am_s=0.0186(4)$ at $a\approx 0.06$ fm. For the up-down mass, we find $am_l=0.00158(7)$ at $a\approx 0.15$ fm, $am_l=0.00126(2)$ at $a\approx 0.12$ fm, $am_l=0.000955(8)$ at $a\approx 0.09$ fm, and $am_l=0.000684(8)$ at $a\approx 0.06$ fm. The errors include statistical and systematic effects, but they are dominated by the systematic effects.

D. The topological susceptibility

The topological structure of the QCD vacuum is an important characteristic of the theory. A stringent test for lattice simulations consists in correctly capturing the dependence of the topological susceptibility on the number of quarks and their masses, since this susceptibility reveals the effect of the quarks on the nonperturbative vacuum structure. Chiral perturbation theory predicts $\chi_{\rm topo}(n_f,m_i)$ in the chiral limit (Leutwyler and Smilga, 1992). Lattice calculations, however, have struggled to reproduce this dependence satisfactorily because the topological charge is not uniquely defined and the fermion action typically breaks chiral symmetry. The asqtad action combined with rSχPT gives us good control over the taste and chiral symmetry breaking effects; thus we expect that a careful treatment of the topological charge will lead to an accurate computation of the topological susceptibility. This has been explored by Bernard *et al.* (2003c), Billeter *et al.* (2004), and Bernard *et al.* (2007c).

As explained by Aubin and Bernard (2003a) and Billeter *et al.* (2004), the chiral anomaly couples to the *taste-singlet* meson, not the Goldstone pion, which is the usual focus of hadron spectroscopy calculations. (Of course, in the continuum limit these mesons are degenerate.) To leading order in rSχPT, the topological susceptibility depends on this mass as

$$\chi_{\rm topo} = \frac{f_\pi^2 m_{\pi,I}^2/8}{1 + m_{\pi,I}^2/(2m_{ss,I}^2) + 3m_{\pi,I}^2/(2m_0^2)}, \tag{117}$$

where $m_{\pi,I}$ is the taste-singlet pion mass, and m_0 comes from the term representing the coupling of the anomaly to the η' in the chiral Lagrangian, Eq. (93). The strange flavor-singlet, taste-singlet meson mass is denoted $m_{ss,I}$.

Equation (117) interpolates smoothly between the infinite sea-quark-mass (quenched) prediction (Veneziano, 1979; Witten, 1979), $\chi = f_\pi^2 m_0^2/12$, which we can use to set m_0, and the chiral limit, $m_l \to 0$, which is dominated by the pion, $\chi = f_\pi^2 m_\pi^2/8$. Hence, to this order, we simply replace the Goldstone pion mass with the mass of the taste-singlet (non-Goldstone) pion in the Leutwyler-Smilga formula. Note that this means that, at nonzero lattice spacing, the topological susceptibility does not vanish as $m_l \to 0$, a reminder that the continuum limit must be taken before the $m_l \to 0$ extrapolation.

In order to compute the topological charge density $q(x)$ on our lattice ensembles, we use three iterations of the Boulder HYP smoothing method (DeGrand *et al.*, 1997; Hasenfratz and Knechtli, 2001), which we have found (Bernard *et al.*, 2003c, 2003d) compares well with the improved cooling method of de Forcrand *et al.* (1997). We define the topological susceptibility from the correlator of $q(x)$ via

$$\chi_{\rm topo} = \langle Q^2\rangle/V = \int d^4r \langle q(r)q(0)\rangle. \tag{118}$$

On our lattices, the short-distance part of the density correlator has a strong signal, but the correlator at large separation is noisy. To reduce the resulting variance, we define a cutoff distance r_c. In the integral above, for $r \le r_c$ where the signal is strong, we use the measured values of the correlator $\langle q(r)q(0)\rangle$. For $r > r_c$ we integrate a function obtained by fitting the measured correlator to a Euclidean scalar propagator

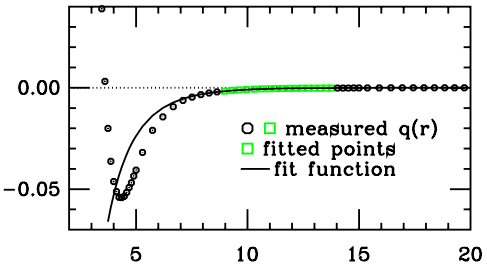

FIG. 13. (Color online) Points used to compute $\langle q(r)q(0)\rangle$. Measured points (open symbols) are used for $r \le r_c \sim 9a$. For $r > r_c$ the fit function (solid curve) is used in Eq. (118). From Bernard *et al.*, 2007c.

$$\langle q(r)q(0)\rangle \sim A_\eta K_1(m_\eta r)/r + A_{\eta'} K_1(m_{\eta'} r)/r, \tag{119}$$

where we use priors for the masses of the η and η', and K_1 is a Bessel function. This significantly reduces the variance in Q^2. An example of the measured values of $q(r)$, the fit function, and the fitting range are shown in Fig. 13.

Figure 14 shows this definition of $\chi_{\rm topo}$ computed on our coarse ($a \approx 0.12$ fm), fine ($a \approx 0.09$ fm), and superfine ($a \approx 0.06$ fm) lattices. The continuum limit is taken first by fitting the susceptibility data to

$$\frac{1}{\chi_{\rm topo} r_0^4}(m_{\pi,I}^2, a) = A_0 + A_1 a^2 + (A_2 + A_3 a^2 + A_4 a^4)/m_{\pi,I}^2. \tag{120}$$

The solid black line in Fig. 14 shows the $a \to 0$ form of this function. Some representative points along this line are shown with error bars reflecting the errors of the continuum extrapolation. Finally, the chiral perturbation

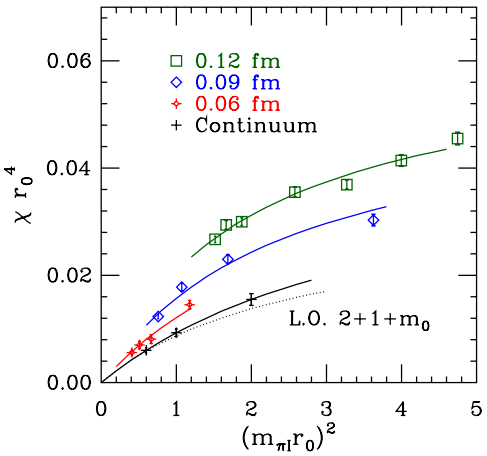

FIG. 14. (Color online) Topological susceptibility data, and its continuum extrapolation, compared with the prediction of Eq. (117). Adapted from Bernard *et al.*, 2007c.

theory prediction of Eq. (117), shown as a dotted line, is based on the value for m_0 set by the quenched data.

With the addition of the new $a \approx 0.06$ fm data, we see that the topological susceptibility is behaving as expected in the $m_{\pi,I}^2 \to 0$ limit of rooted staggered chiral perturbation theory.

These results lend further credibility to the use of the fourth-root procedure to simulate single flavors, since aberrant results from this procedure would be expected to arise first in anomalous behavior of topological quantities and correlations, as these are rather sensitive to the number of flavors.

V. SPECTROSCOPY OF LIGHT HADRONS

Computing the masses of the light hadrons is a classic problem for lattice QCD, since the masses and structures of these particles are highly nonperturbative. By this point, hadron mass computations, including the effects of light and strange dynamical quarks, have been done for several different lattice actions, including staggered quarks, Wilson quarks (Ukita *et al.*, 2007, 2009; Dürr *et al.*, 2008, 2009) and domain-wall quarks (Ukita *et al.*, 2007; Allton *et al.*, 2008) It has long been apparent from these and other studies that lattice QCD reproduces the experimental masses within the accuracy of the computations. For most of the light hadrons, however, this accuracy is not as good as for other quantities discussed in this review. The reasons for this are that these masses have a complicated dependence on the light quark mass, making the chiral extrapolation (to the physical light quark mass) difficult, and that all but a few of these hadrons decay strongly. Most of the lattice simulations are at heavy enough quark masses or small enough volumes that these decays cannot happen, so the chiral extrapolation crosses thresholds. With staggered quarks there is the additional technical complication that for all but the pseudoscalar particles with equal mass quarks the lattice correlators contain states with both parities, with one of the parities contributing a correlator that oscillates in time.

Masses of the lowest-lying light-quark hadrons have been computed on almost all of the MILC asqtad ensembles. Hadron masses from the $a \approx 0.12$ fm ensembles were reported by Bernard *et al.* (2001), masses from the $a \approx 0.09$ fm ensembles were added by Aubin *et al.* (2004a), and nucleon and Ω^- masses from the $a \approx 0.06$ fm ensembles by Bernard *et al.* (2007d). Simple extrapolations of these masses to the continuum limit and physical quark mass, including results from several of the $a \approx 0.06$ fm ensembles, are compared to experiment in Fig. 15. In addition, this figure shows charm and bottom meson mass splittings (Gray *et al.*, 2003, 2005; Wingate *et al.*, 2004) compared with experimental values (Amsler *et al.*, 2008).

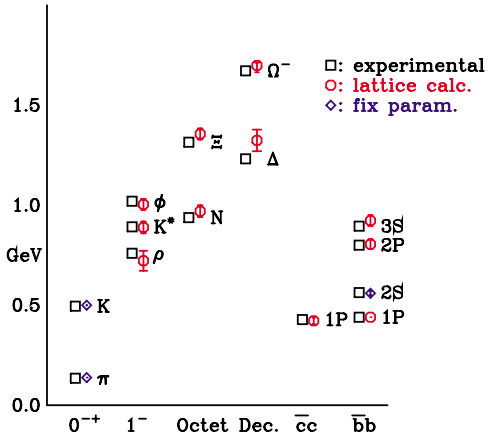

FIG. 15. (Color online) The "big picture"—comparison of masses calculated on the asqtad ensembles with experimental values. For the light quark hadrons we plot the hadron mass, and for the $\bar{c}c$ and $\bar{b}b$ masses the difference from the ground state ($1S$) mass. The continuum and chiral extrapolations of the pion and kaon masses are described in Sec. VI, and most other meson masses were extrapolated to the continuum and physical light quark masses using simple polynomials. Masses of hadrons containing strange quarks were adjusted for the difference in the strange quark mass used in generating the ensembles from the correct value. The nucleon mass extrapolation, described by Bernard *et al.* (2007d), used a one-loop chiral perturbation theory form. The charmonium mass splitting is from Follana *et al.* (2008) and the $\bar{b}b$ splittings from Gray *et al.* (2003, 2005) and Wingate *et al.* (2004). Experimental values are from Amsler *et al.* (2008). The Υ $2S$-$1S$ splitting and the π and K masses are shown with a different symbol since these quantities were used to fix r_1 in physical units and the light and strange quark masses. Earlier versions of the plot appeared in Aubin *et al.* (2004a) and the PDG "Review of Particle Physics" (Amsler *et al.*, 2008).

A. Hadron mass computations

The theory behind hadron mass computations with staggered quarks was developed by Kluberg-Stern, Morel, Napoly, and Petersson (1983), Golterman and Smit (1985), and Golterman (1986b) [see also Kilcup and Sharpe (1987)]. Early implementations, in which technical aspects were addressed, include Marinari *et al.* (1981a), Bowler *et al.* (1987), Gupta *et al.* (1991), and Fukugita *et al.* (1993).

The calculation begins with a Euclidean time correlation function for any operator that can produce the desired state from the vacuum. For instance, if an operator $\mathcal{O}$ can annihilate a particle p and the adjoint $\mathcal{O}^\dagger$ can create p, then we study the zero-momentum correlation function, or "correlator" $C_{\mathcal{O}^\dagger\mathcal{O}}$ given by

$$C_{\mathcal{O}^\dagger\mathcal{O}}(t) = \sum_x \langle \mathcal{O}(x,t)\mathcal{O}^\dagger(0,0)\rangle. \tag{121}$$

By putting in a complete set of states between the two operators, we find

$$C_{\mathcal{O}^\dagger\mathcal{O}}(t) = \sum_n \langle 0|\mathcal{O}|n\rangle\langle n|\mathcal{O}^\dagger|0\rangle \exp(-M_n t). \tag{122}$$

If the particle p is the lowest-energy state n, then for large Euclidean time the dominant contribution will be $|\langle 0|\mathcal{O}|p\rangle|^2 \exp(-M_p t)$. Generally, there will be additional

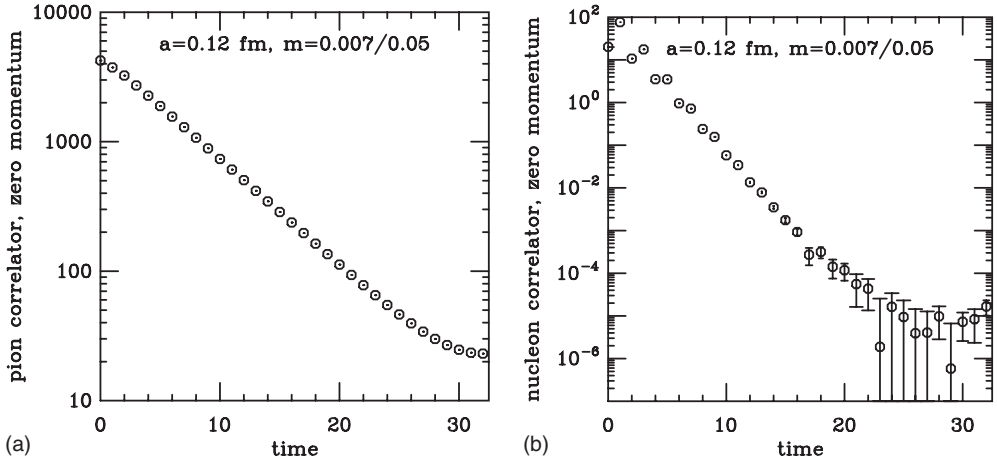

FIG. 16. Pion and nucleon correlators plotted vs the distance from the source. These correlators are from the $\beta=6.76$, $am_l/am_s=0.007/0.05$ ensemble. The small symbols in the center of the octagons in the pion correlator are error bars. Note the increasing fractional errors with distance in the nucleon correlator, and the constant fractional errors in the pion correlator.

contributions from higher mass states, and with staggered quarks there are usually contributions from opposite parity states of the form $(-1)^t\exp(-M't)$. In addition, because of the antiperiodic boundary conditions in time for the quarks, there will be additional terms of the form $\exp[-M_n(T-t)]$, where T is the time extent of the lattice. Thus, with staggered quarks a meson correlator generically has the form

$$C_{\mathcal{O}^\dagger\mathcal{O}}(t) = A_0(e^{-M_0 t} + e^{-M_0(T-t)}) + A_1(e^{-M_1 t} + e^{-M_1(T-t)}) + \cdots + (-1)^t A_0'(e^{-M_0' t} + e^{-M_0'(T-t)}) + \cdots . \tag{123}$$

Here the primed masses and amplitudes with the factor of $(-1)^t$ correspond to particles with parity opposite that of the unprimed. For baryons the form is similar, except that the backwards propagating terms $e^{-M(T-t)}$ have an additional factor of $(-1)^{t+1}$. Here the overall minus sign in the backwards propagating part is due to the antiperiodic boundary conditions for the quarks in the Euclidean time direction. Figure 16 shows correlators for the pion and nucleon in a sample asqtad ensemble. Statistical errors on the pion correlator are the small symbols in the center of the octagons. The effect of periodic (for a meson correlator) boundary conditions in time is clearly visible. For short times, there are contributions from heavier particles.

For hadrons other than glueballs, evaluating this correlator requires computing $M^{-1}_{x,y}$ where M is the matrix defining the quark action. This can be done by making a "source" vector b which is nonzero only at lattice point y, or in some small region, and solving the sparse matrix equation $Ma=b$, usually using the conjugate gradient algorithm. (Here a and b are vectors with one component for each color at each lattice site in the system—i.e., $3V$ complex components. With Wilson-type quarks there would also be four spin components per lattice site.)

The simplest possibility for $\mathcal{O}$ is an operator built from quarks and antiquarks located in the same 2^4 hypercube, often even on the same lattice site. This is usually called a point source. Because the point operator $\mathcal{O}_P$ tends to have a large overlap with excited states, it is usually advantageous to take a "smeared" source operator $\mathcal{O}^\dagger$, where the quarks in the hadron may be created at different lattice sites. One common approach is to choose a smeared operator that creates quarks and antiquarks with a distribution similar to that of the expected quark model wave function of the desired hadron. A cruder and simpler approach used in most of the MILC light hadron mass calculations is to take a "Coulomb wall" source, where the lattice is first gauge transformed to the lattice Coulomb gauge, making the spatial links as smooth as possible. Then a source is constructed which covers an entire time slice, for example, with a 1 in some corner of each 2^3 cube in the time slice. This works because with Coulomb gauge fixing contributions from source components within a typical hadronic correlation length interfere coherently, while contributions average to zero if the quarks created by $\mathcal{O}^\dagger$ are widely separated (although they do contribute to the statistical noise). In other words, $\langle M^{-1}_{\vec{x}_1,t_i;\vec{y},t_f} M^{-1}_{\vec{y},t_f;\vec{x}_2,t_i}\rangle$ is significant only when $|\vec{x}_1-\vec{x}_2|$ is less than a typical hadronic size. For example, a Coulomb wall operator appropriate for a Goldstone pion is

$$\mathcal{O}_W(t) = \sum_{\vec{x},\vec{y}} \bar{\chi}(\vec{x},t)(-1)^{\vec{x}+t}\chi(\vec{y},t). \tag{124}$$

In a mass calculation, we want the state with zero spatial momentum, which is isolated by summing the sink position over all spatial points on a time slice. In many matrix element studies, we need hadron states with nonzero momenta, and they are isolated by summing over the spatial slice with the appropriate phase factors.

Statistics are usually further enhanced by averaging correlators from wall sources, or other types of sources, from several time slices in the lattice. In general, each different source requires a new set of sparse matrix inversions.

For most hadrons, the statistical error is the limiting factor in the mass computations. At long Euclidean time t, a correlator with hadron H as its lowest mass constituent is proportional to $e^{-M_H t}$. The variance of this correlator can itself be thought of as the correlator of the square of the operator

$$\langle \mathcal{O}_H(x)\mathcal{O}_H^\dagger(x)\mathcal{O}_H^\dagger(y)\mathcal{O}_H(y)\rangle, \tag{125}$$

where in this correlator for flavor-nonsinglet hadrons it is understood that quark lines all run from the operators at x to those at y (Lepage, 1990). The behavior of the variance at long distances is dominated by the lowest mass set of particles created by $\mathcal{O}_H(x)\mathcal{O}_H^\dagger(x)$. Thus for mesons $\mathcal{O}_H(x)\mathcal{O}_H^\dagger(x)$ creates two quarks and two antiquarks which can propagate as two pseudoscalar mesons. Then the variance decreases approximately as $e^{-2M_{PS}t}$, where M_{PS} is the mass of the pseudoscalar meson made from the quarks in $\mathcal{O}_H^\dagger\mathcal{O}_H$. For baryons there are three quarks and three antiquarks, and the variance decreases approximately as $e^{-3M_{PS}t}$. This behavior can be seen in Fig. 16, where the fractional error on the pion correlator does not increase with distance, while the fractional error on the nucleon correlator grows quickly.

As discussed in Sec. II.B.3, hadrons with staggered quarks come with different tastes, all of which are degenerate in the continuum limit. For pseudoscalar mesons, the mass differences between different tastes are large, but they are well understood as discussed in Sec. III.A. For the other hadrons, for which chiral symmetry is not the most important factor in determining the mass, taste symmetry violations are much smaller. In particular, we have computed masses for four different tastes of the ρ meson on many of our ensembles, and have failed to find any statistically significant taste splittings. [See also Ishizuka *et al.* (1994).]

B. Correlated fits

There are several kinds of correlations in the numerical results of lattice gauge theory simulations. The Markov chain that produces the configurations produces correlated configurations. Thus, there are correlations in "simulation time." The correlations vary with the algorithm, and one can reduce them by increasing the simulation time gap between the configurations that are analyzed. Generation of configurations is computationally expensive, however, and the autocorrelation length is unknown until the run and some analysis is completed, so one usually saves configurations with some degree of correlation. A simple way to deal with these correlations is to block successive configurations together and then to estimate errors from the variance of blocks. However, if the number of blocks is not many times larger than the number of degrees of freedom, the finiteness of the sample size must be considered when estimating goodness-of-fit or statistical errors on the parameters in a fit (Michael, 1994; Toussaint and Freeman, 2008). In cases where blocking is not practical, notably the pseudoscalar meson analysis in Sec. VI, we have estimated elements of the covariance matrix using the measured autocorrelations in the data to rescale a covariance matrix based on unblocked data.

Even if successive configurations are not correlated, different physical quantities are correlated with each other. For example, if the pion correlator is larger than average at a separation t from the source on a particular configuration, it is likely to be larger at $t+1$. Thus, when extracting hadron masses, or other fit parameters, we must use the full correlation matrix in the fit model, not just the variance in each particular element fit. To be specific, let the values of the independent parameters be denoted x_i and corresponding lattice "measured" values be y_i. The fitting procedure requires varying the model parameters $\{\lambda\}$ that define the model function $y_M(x_i,\{\lambda\})$ in order to minimize χ^2. For uncorrelated data,

$$\chi^2 = \sum_i [y_M(x_i,\{\lambda\}) - y_i]^2/\sigma_i^2, \tag{126}$$

where σ_i is the standard deviation of y_i. When the data are correlated, let $C_{ij}=\mathrm{Cov}(y_i,y_j)$ and then

$$\chi^2 = \sum_{i,j} [y_M(x_i,\{\lambda\}) - y_i]C_{ij}^{-1}[y_M(x_j,\{\lambda\}) - y_j]. \tag{127}$$

(In practice C_{ij} is almost always estimated from the same data as the y_i, and in this case χ^2 is more properly called T^2.) Uncorrelated data reduce to $C_{ij}=\delta_{ij}\sigma_i^2$. If C_{ij} has positive off-diagonal entries, then the data will look smoother than it would if uncorrelated.

In Fig. 17 we show how the fitted pion and nucleon masses vary with the minimum distance from the source that is included in the fit. The octagons and squares are correlated fits, minimizing χ^2 in Eq. (127). For the pion, the octagons correspond to a single-particle (two-parameter) fit, and the squares correspond to a two-particle (four-parameter) fit. For the nucleon, the octagons are fits including one particle of each parity. We need to decide which fit is best, and we do that based on the confidence levels of the fits, which are roughly indicated by the symbol size. Figure 17 also contains fits ignoring correlations while minimizing the χ^2 in Eq. (126). It can be seen that the error bars on these points are in general incorrect—they are neither a correct estimate of how much the parameters would likely vary if the calculation were repeated nor of how much the parameters are likely to differ from the true value. We also see that the confidence levels are generally too large for the uncorrelated fits. In particular, based on its confidence level, one might accept the uncorrelated pion fit with minimum distance five. But in fact it can be seen that it differs significantly from the asymptotic value. The effects on the confidence level from ignoring correlations can be quite extreme. For example, in the single-particle pion fits with $D_{\min}=5$, the correlated fit has $\chi^2=180$ for 25 degrees of freedom, for a confidence of 10^{-24}, while the uncorrelated fit has $\chi^2=14$ for 25 degrees of freedom, or an (erroneous) confidence of 0.96.

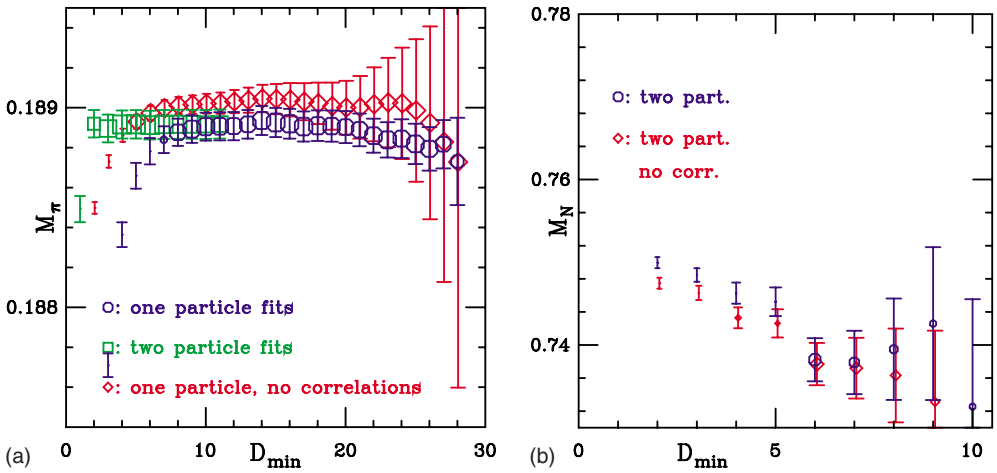

FIG. 17. (Color online) Result of fitting the correlators in Fig. 16 from a minimum distance to the center of the lattice (for the pion) or distance at which the correlator loses statistical significance (for the nucleon). For the pion correlator (left panel), octagons correspond to single-particle fits and squares to two-particle fits. The diamonds are from single-particle fits ignoring correlations among the data points. For the nucleon fits (right panel), all fits use two particles, one of each parity. Octagons are correlated fits, and diamonds are fits ignoring the correlations. The sizes of the symbols are proportional to the confidence level of the fits, with the symbol size in the legends corresponding to 50% confidence.

Jackknife or bootstrap methods are often used with correlated data. These methods give estimates of the errors in fit parameters, but they do not provide information about goodness of fit.

Once the hadron propagators are fit, we still need to perform chiral or continuum extrapolations. In these cases, it is also imperative to deal with the correlations among the fitted quantities that come from the same ensemble. With partial quenching these covariance matrices can become quite large, so it is essential to have enough configurations in each ensemble to be able to get a good estimate of the covariance matrix.

C. Results for some light hadrons

The pseudoscalar mesons are special for several reasons. First, very accurate mass computations are possible. This is because the statistical error in the correlator (square root of the variance) decreases with the same exponential as the correlator itself—the fractional error is nearly independent of t, and accurate correlators can be computed out to the full extent of the lattice. Second, for equal mass quarks the pseudoscalar correlator does not have oscillating contributions from opposite parity particles, and the oscillating contributions are negligible for the kaon. Third, because of the pions' role as the approximate Goldstone bosons for broken chiral symmetry, the breaking of taste symmetry leads to large mass splittings among the different taste combinations. Finally, because it is related to the decay constant of the meson, the amplitude of the pseudoscalar correlator is as interesting as the mass. Because of the exact U(1) chiral symmetry of the staggered quark action, the axial-vector current corresponding to the Goldstone (taste pseudoscalar) pion needs no renormalization, so the decay constants can also be calculated to high precision. For these reasons, discussion of the light pseudoscalar mesons is deferred to Sec. VI.

For the vector mesons, the fractional statistical error in the correlator increases as $e^{(M_V-M_{PS})t}$. Also, the vector mesons decay strongly. On the lattice, conservation of momentum and angular momentum forbids the mixing of a zero-momentum vector meson with two zero momentum pseudoscalars, so the vector meson is "stable on the lattice" for pion masses large enough that $2\sqrt{M_{PS}^2+(2\pi/L)^2} > M_V$. (Taste breaking adds some additional complications to this.) For all of the asqtad ensembles except those with the smallest quark masses, this condition is satisfied, and the vector meson masses can be easily, if not accurately, found. However, the problem of extrapolation through the decay threshold to the physical quark mass has not been fully addressed. Figure 18 shows the ρ meson mass as a function of light quark mass for three different lattice spacings. Results for the K^* and ϕ are similar, except that there is an added complication in that the mass needs to be adjusted to compensate for the fact that the strange quark mass used in the correlator computations differs from the physical m_s. While the values in Bernard *et al.* (2001) and Aubin *et al.* (2004a) used the same valence and sea strange quark masses, the masses in Fig. 15 have been interpolated to the correct valence strange quark mass.

The nucleon is stable and chiral perturbation theory is available to guide the extrapolation in quark mass. However, computation of reliable masses is difficult because the fractional error in the nucleon propagator increases as $e^{(M_N-3/2M_{PS})t}$. Also, there are excited states with masses not too far above the nucleon mass that contribute to the correlator. In fact, with staggered quarks the simplest baryon source operators couple to the Δ as well as the nucleon, so the lowest positive-parity excited state in the correlator is the Δ (Golterman and

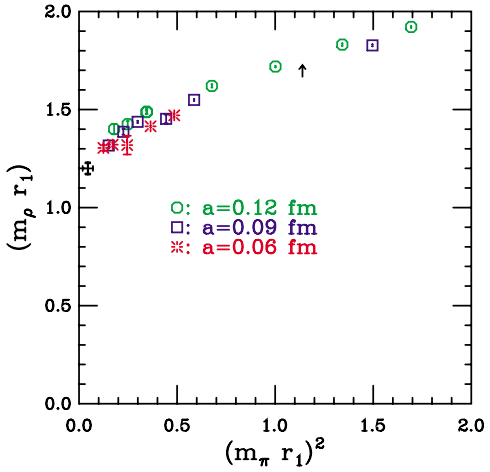

FIG. 18. (Color online) The ρ mass in units of r_1, plotted vs the squared pion mass. Since $m_\pi^2 \propto m_q$, this is effectively a plot vs light quark mass. The octagons are from ensembles with $a \approx 0.12$ fm, the squares from ensembles with $a \approx 0.09$ fm, and the bursts from ensembles with $a \approx 0.06$ fm. The decorated plus at the left is the physical ρ mass, with the error on this point coming from the error in r_1. For reference, the upward arrow indicates approximately where the quark mass equals the strange quark mass.

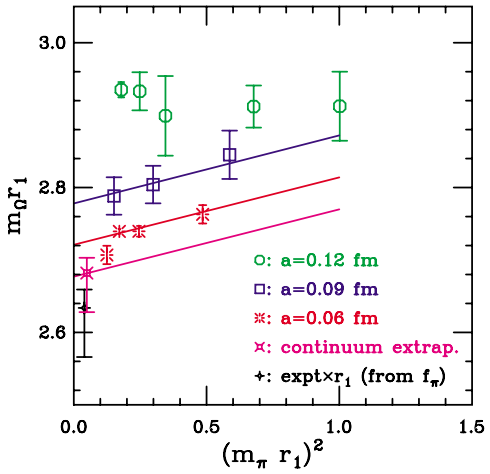

FIG. 20. (Color online) The Ω^- mass. Results are shown for three different lattice spacings. The points with $a \approx 0.09$ and ≈ 0.06 fm were fit to the form $M_\Omega r_1 = A + Ba^2\alpha_s + C(m_\pi r_1)^2$. The sloping lines show this fit form evaluated at the values of $a^2\alpha_s$ for these lattice spacings, and at $a=0$. Finally, the fancy cross with error bars is the fit form evaluated at the physical pion mass, and the small diamond is the experimental value. Note that in this case the vertical axis does not begin at zero. Adapted and updated from Toussaint and Davies, 2005 and Bernard *et al.*, 2007d.

Smit, 1985). Figure 19 shows nucleon masses for three lattice spacings versus quark mass, together with a continuum and chiral extrapolation.

Another hadron of particular interest is the Ω^- (Toussaint and Davies, 2005). This particle is stable against strong decays. In one-loop chiral perturbation theory there are no pion-baryon loops, so at this order there are also no logarithms of m_π in the chiral extrapolation of the mass. Therefore, we expect that a simple polynomial extrapolation in light quark mass should be good. Unfortunately, the Ω^- is a difficult mass computation with staggered quarks, first because it is a heavy particle and second because a baryon operator that has the Ω^- as its lowest-energy state has its three quarks at different lattice sites (Golterman and Smit, 1985; Gupta *et al.*, 1991). The Ω^- mass is strongly dependent on the strange quark mass, and in principle provides an independent way to determine the correct lattice strange quark mass. Figure 20 contains Ω^- mass estimates, using strange valence quark masses at each lattice spacing that were independently determined from the pseudoscalar meson analysis in Sec. VI. To do this, Ω^- correlators were generated using two different strange quark masses near the desired one, and the Ω^- mass was obtained by linearly interpolating to the strange quark mass determined separately. This plot also shows a continuum and chiral extrapolation using the simple form $M_\Omega r_1 = A + Ba^2\alpha_s + C(m_\pi r_1)^2$.

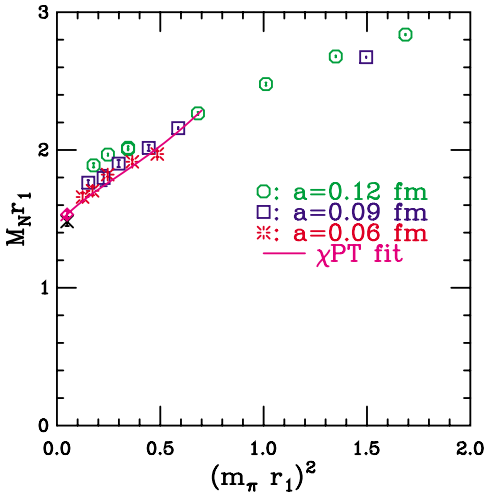

FIG. 19. (Color online) The nucleon and a chiral fit. Nucleon masses are shown for different light quark masses at three lattice spacings. The cross at the left is the experimental value. The slightly curved line and the diamond at the physical quark mass are a continuum and chiral extrapolation. Lattice spacing errors are assumed to be linear in $a^2\alpha_s$. The particular chiral form used here is a one-loop calculation with π-N and π-Δ intermediate states (Jenkins, 1992; Bernard, Kaiser, and Meissner, 1993). Adapted and updated from Bernard *et al.*, 2007d.

Masses of other particles, such as the a_1 and b_1 and particles including strange quarks, were calculated by Bernard *et al.* (2001) and Aubin *et al.* (2004a), and the excited state of the pion was identified by Aubin *et al.* (2004a) and Bernard *et al.* (2004). Light hybrid mesons with exotic quantum numbers were studied by Bernard *et al.* (2003a, 2003b), and exotic hybrid mesons with nonrelativistic heavy quarks by Burch *et al.* (2001, 2002) and Burch and Toussaint (2003).

D. Flavor singlet spectroscopy

Determining the masses of flavor-singlet mesons is perhaps the most challenging endeavor in lattice QCD light hadron spectroscopy. The difficulty in doing so has three main sources.

(i) Flavor-singlet correlators have two different contributions: quark-line connected and quark-line disconnected. The quark-line disconnected piece requires so-called "all-to-all" correlators. To avoid the $\mathcal{O}(V)$ inversions to compute these all-to-all propagators, stochastic methods are used. Kuramashi *et al.* (1994) used a unit source at each site and let gauge invariance do the averaging. More common now is the use of random sources (Dong and Liu, 1994; Venkataraman and Kilcup, 1997) similar to Eqs. (62) and (63), with various noise reduction techniques (Wilcox, 1999; McNeile and Michael, 2001; Struckmann *et al.*, 2001; Mathur and Dong, 2003; Foley *et al.*, 2005), including low-eigenmode preconditioning (Venkataraman and Kilcup, 1998; DeGrand and Heller, 2002).

(ii) While the stochastic noise of the quark-line connected correlators falls off exponentially (albeit with a smaller exponent than the signal), the noise in the quark-line disconnected part is constant. So the signal to noise ratio falls off much faster for the disconnected part.

(iii) The quark-line connected correlator is the same as for a flavor-nonsinglet meson—in particular the pion for the pseudoscalar channel. Therefore, the very noisy disconnected correlator first has to cancel the connected correlator before giving the desired singlet correlator whose falloff gives the flavor-singlet mass.

Since much larger statistics are needed for the computation of the flavor-singlet correlators, the UKQCD Collaboration has extended a couple of the MILC lattice ensembles to around 30 000 trajectories (Gregory *et al.*, 2007, 2008, 2009). Their simulations are still on-going. So far, the only result given is for the 0^{++} glueball, whose correlator can be constructed from gauge field operators and requires no noisy estimators and Dirac operator inversions. For two different lattice spacings, $a \approx 0.12$ and 0.09 fm, the UKQCD Collaboration finds $m_{0^{++}} = 1629(32)$ and 1600(71) MeV (Gregory *et al.*, 2009), respectively.

It is important to continue this investigation. In particular, obtaining the correct η' mass would further support the correctness of the rooting procedure to eliminate the unwanted tastes for staggered fermions.

E. Scalar mesons f_0 and a_0

In this section, we describe briefly the analysis of correlators for two light, unstable scalar mesons, namely, the isosinglet f_0 and the isovector a_0.

With the first good measurements of the a_0 channel in the staggered fermion formulation a peculiarity was encountered: it was found that on coarse lattices the a_0 correlator appeared to have a spectral contribution with an anomalously low mass, lighter than any physical decay channel (Aubin *et al.*, 2004a; Gregory *et al.*, 2006).

For sufficiently light u and d quark masses, the f_0 decays to two pions. Likewise, the isovector scalar meson a_0 decays to a pion and an η. On the lattice, the open decay channels complicate the analysis of the scalar meson correlators. They are dominated by the spectral contributions of the significantly lighter decay channels. As a flavor singlet, the f_0 also suffers from the quark-line disconnected contributions described in the previous subsection. Finally, with staggered fermions at nonzero lattice spacing, the splitting of the pseudoscalar meson taste multiplets in the decay channel deals a seeming *coup de grâce*.

Fortunately, one can make progress using rSχPT described in Sec. III.A (Bernard, DeTar, *et al.*, 2006, 2007; Prelovsek, 2006a, 2006b). The essential idea is to match definitions of the desired correlator of local interpolating operators in the lattice QCD formulation and in rSχPT. The lattice definition is the basis for the numerical simulation of the correlator, and the rSχPT definition provides a model for fitting the result of the simulation, including all taste-breaking effects in the decay channels. If we take the taste-multiplet masses from separate calculations, then, despite the rather complicated set of two-meson channels, that portion of the fit model depends on only three low-energy constants. In principle, even these constants can be determined from independent measurements, leaving no free parameters. So this fit provides a further test of the viability of rSχPT as a low-energy effective theory for the staggered action.

The hadron propagator from lattice site 0 to y is defined in the same way from the generating functionals for both QCD and the chiral theory,

$$\frac{\partial^2 \ln Z}{\partial m_{f,f'}(y) \partial m_{e',e}(0)}. \tag{128}$$

In QCD, the source $m_{f,f'}(y)$ generalizes the usual quark mass term and includes off-diagonal flavor mixing f,f'. The same correlator is defined in rSχPT, where the local source $m_{f,f'}(y)$ appears in the generalized meson mass matrix. This establishes a correspondence between the correlator defined in terms of the quark fields $\bar{q}(y)q(y)$ in QCD and in terms of the local meson fields $B\Phi^2(y)$.

To lowest order in rSχPT, the meson correlator is described by a bubble diagram, which gives the contributions of the two-pseudoscalar-meson intermediate states, including all taste multiplets and hairpins. These contributions are determined from the multiplet masses and the rSχPT low-energy constants B, δ'_A, and δ'_V described in Sec. III.A. In addition to the bubble diagram, one adds an explicit quark-antiquark a_0 or f_0 state to complete the fit model. Results are shown in Fig. 21, and results for the low-energy constants are listed in Table III.

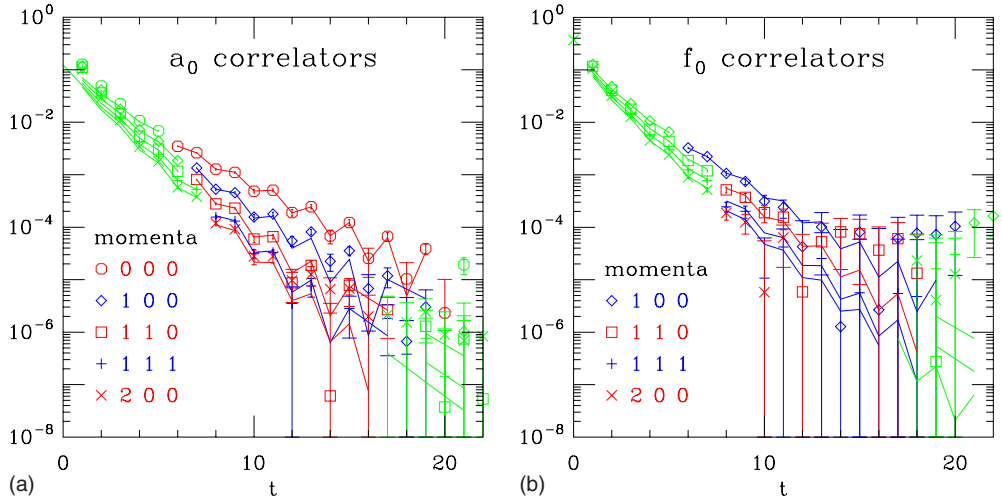

FIG. 21. (Color online) Best fit to the a_0 correlator (left panel) for five momenta and the f_0 correlator (right panel) for four momenta. The fitting range is indicated by darker points and lines. Occasional points with negative central values are not plotted. Data are determined from the $a \approx 0.12$ fm (coarse) ensemble with $am_l = 0.005$ and $am_s = 0.05$. From Bernard, DeTar, *et al.*, 2007.

It is particularly instructive to examine the variety of two-pseudoscalar-meson taste channels contributing to the scalar meson correlators. To be physical states, the external scalar mesons a_0 and f_0 must be taste singlets. Taste selection rules then require that they couple only to pairs of pseudoscalar mesons of the same taste. Thus, for example, for the a_0, each flavor channel, such as π-η, comes with a multiplicity of 16 taste pairs, although lattice symmetries reduce the number of distinct thresholds to 6. There is also a set of π-η' channels. To get the energies of the thresholds, we look at the taste splitting of the component hadrons. We have already seen how the pion taste multiplet splits into the Goldstone state and a variety of higher-lying states, all of which become degenerate in the continuum limit. η and η', on the other hand, have unusual splitting because they mix with the chiral anomaly. Since the anomaly is a taste singlet, only the taste-singlet η and η' mix with it in the usual way. Thus, in the continuum limit only the taste singlet states are expected to have the correct masses. They are the only physical states. The 15 taste non-singlet η's and η''s remain light. The pseudoscalar-taste eta pairs with the pseudoscalar-taste pion. The unphysical pseudoscalar-taste π-η channel gives an anomalously light spectral contribution to the a_0 correlator (Prelovsek, 2006a, 2006b). A similar complication occurs in the f_0 correlator, but it is masked by the expected physical two-pion intermediate state.

TABLE III. Comparison of our fit parameters for the rSχPT low energy constants with results from Aubin *et al.* (2004b).

	f_0 and a_0 correlators	Meson masses and decays
$r_1 m_\pi^2/(2m_{u,d})$	7.3(1.6)	6.7
δ_V	(prior)	−0.016(23)
δ_A	−0.056(10)	−0.040(6)

The unphysical taste contributions provide a concrete illustration of the breakdown of unitarity at nonzero lattice spacing as a result of the fourth root. The theory heals the scalar meson correlators in the continuum limit by a mechanism that parallels exactly the one described for the one-flavor model in Sec. III.C. The pseudoscalar meson bubble diagram contains a negative-norm channel. This unphysical ghost channel has the weight needed to cancel the contributions of all unphysical taste components in the continuum limit. Thus in the continuum limit only the physical intermediate two-meson states survive.

The behavior of the isovector scalar correlator has also been analyzed for the case of domain-wall valence quarks on the MILC staggered ensembles (Aubin *et al.*, 2008). In the mixed-action case, the a_0 correlator receives contributions from two-particle intermediate states with mesons composed of two domain-wall quarks, mixed mesons composed of one domain-wall and one staggered quark, and mesons composed of two staggered quarks. Because the symmetry of the external valence quarks restricts the sea-sea mesons to be taste singlets, the correlator does not receive contributions from all of the taste channels. As in the purely staggered case, the one-loop bubble contribution is determined by three low-energy constants (Prelovsek, 2006b), which are known from tree-level χPT fits to meson masses. For domain-wall quarks on the coarse and fine MILC lattices, the contribution from the bubble term is predicted to be large and negative for several time slices. Thus a comparison of the mixed-action χPT prediction for the behavior of the a_0 correlator with lattice data provides a strong consistency check.

Aubin *et al.* (2008) compared the mixed-action χPT prediction for the bubble contribution with the lattice a_0 correlator for several domain-wall valence masses on the coarse and fine MILC lattices. They found that in all cases the size of the bubble contribution is quantitatively

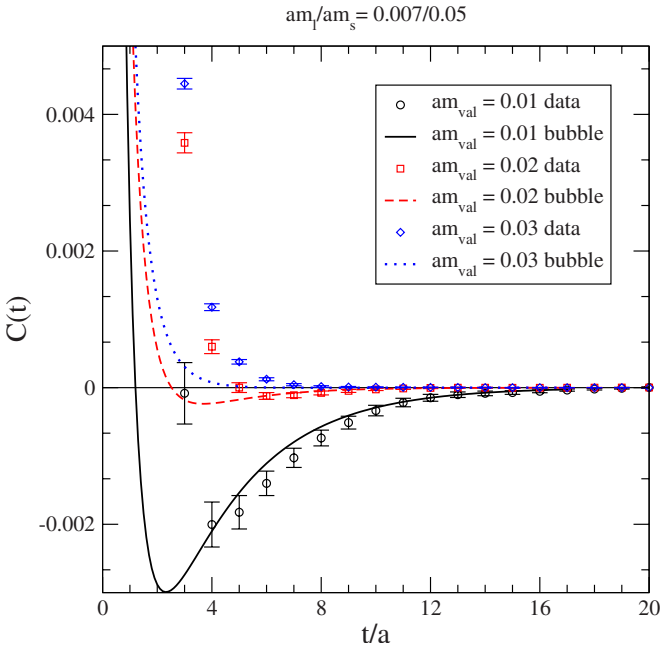

FIG. 22. (Color online) The isovector scalar (a_0) correlator on the MILC coarse $am_l/am_s=0.007/0.05$ ensemble with three different domain-wall valence masses. Overlaid on the data are the predicted bubble contributions, which should dominate over the exponentially decaying contributions at sufficiently large times. From Aubin *et al.*, 2008.

consistent with the data, and that the behavior of the data cannot be explained if mixed-action lattice artifacts are neglected. For fixed light sea-quark mass, the size of the bubble term decreases as the valence quark mass increases (see Fig. 22). The bubble contribution also decreases as $a\to 0$. These results of Aubin *et al.* (2008) support the claim that mixed-action χPT is indeed the low-energy effective theory of the domain-wall valence, staggered sea lattice theory. Furthermore, mixed-action χPT describes the dominant unitarity-violating effects in the mixed-action theory even when such effects are larger than the continuum full QCD contributions that one wishes to extract. Thus mixed-action χPT fits can be used to remove taste-breaking and unitarity-violating artifacts and recover physical quantities.

F. Summary

In general these and other lattice spectrum calculations confirm that QCD does predict the hadron spectrum. Although we can see the effects of decay thresholds as the quark mass is varied (e.g., Sec. V.E), and though some scattering lengths can be indirectly determined through chiral perturbation theory (Leutwyler, 2006), most hadronic decay rates and cross sections remain to be calculated in the future.

VI. RESULTS FOR THE LIGHT PSEUDOSCALAR MESONS

A. Motivation

Precise computations are possible for light pseudoscalar mesons (see Sec. V.C), and they lead to interesting physics. If lattice calculations of light pseudoscalar mesons and decay constants can approach the chiral and continuum limits, we can determine the up, down, and strange quark masses and many of the low-energy constants (LECs) of the chiral Lagrangian, including several combinations of the NLO Gasser-Leutwyler constants L_i (Gasser and Leutwyler, 1984). From the ratio f_K/f_π, we can extract $|V_{us}|$ from the kaon leptonic branching fraction, providing a test of CKM matrix unitarity for the first row of the matrix.

B. From correlators to lattice masses and decay constants

Study of the light pseudoscalar mesons on MILC lattices began in 2004 (Aubin *et al.*, 2004b) and has included several updates at the annual lattice conferences (Bernard *et al.*, 2006b, 2006c, 2007b). We first review the methodology of Aubin *et al.* (2004b). In the Goldstone (taste pseudoscalar) case, we can use the partially conserved axial-vector current relation to relate the decay constant f_{PS} to matrix elements of the spin- and taste-pseudoscalar operator $\mathcal{O}_P(t)=\bar{\psi}(\gamma_5\otimes\xi_5)\psi$ between the vacuum and the meson. In terms of the one-component staggered quark formalism,

$$\mathcal{O}_P(t)=\bar{\chi}^a(\vec{x},t)(-1)^{\vec{x}+t}\chi^a(\vec{x},t), \tag{129}$$

where a is the (summed) color index. As in Eqs. (121) and (122), we define a correlator by

$$C_{PP}(t)=\frac{1}{V_s}\sum_{\vec{y}}\langle\mathcal{O}_P(\vec{y},t)\mathcal{O}_P^\dagger(\vec{x},0)\rangle=c_{PP}e^{-m_{PS}t}+\cdots, \tag{130}$$

where m_{PS} is the mass of the (lightest) pseudoscalar and V_s is the spatial volume. After fitting the correlator to this form, we can find the decay constant from

$$f_{PS}=(m_x+m_y)\sqrt{\frac{V_s c_{PP}}{4m_{PS}^3}}, \tag{131}$$

where m_x and m_y are the two valence quark masses.

Although the decay constant is found from the overlap of the point-source operator with the meson state, most directly obtained from the point-point correlator Eq. (130), it is useful to use the Coulomb wall source Eq. (124) and point sink to calculate the correlator

$$C_{WP}=\langle\mathcal{O}_P(\vec{x},t)\mathcal{O}_W^\dagger(0)\rangle=c_{WP}e^{-m_{PS}t}+\cdots. \tag{132}$$

The advantage of this correlator is that it has less contamination from excited states than does C_{PP}, and helps in fixing the pseudoscalar mass.

A random-wall source can also be used instead of a point source to calculate C_{PP}, giving smaller statistical errors. The source for the quark on each site of a time slice is a three component complex unit vector with a random direction in color space. Thus, contributions where the quark and antiquark in a meson originate on different spatial sites average to zero. After dividing by the spatial lattice volume, this source is used instead of

$\mathcal{O}_P^\dagger$ in C_{PP}. The preferred method is then to fit C_{WP} and the random-wall point-sink C_{PP} with three free parameters A_{PP}, A_{WP}, and m_{PS},

$$C_{PP} = m_{PS}^3 A_{PP} e^{-m_{PS}t}, \quad C_{WP} = m_{PS}^3 A_{WP} e^{-m_{PS}t}, \quad (133)$$

so that A_{PP} is the desired combination c_{PP}/m_{PS}^3 that appears in Eq. (131). An appropriate range of Euclidean time must be selected to get a good confidence level of the fit. If the minimum distance from the source point is too small, there will be excited state contamination. It is essential to use the full correlation matrix of the data to get a meaningful confidence level and avoid contamination.

For chiral fits used to extract LECs that govern the mass dependence of physical quantities, it is important to fix the scale in a mass-independent manner. This is because all mass dependence should be explicit in χPT, and none should be hidden in the scale-fixing scheme. As described in Sec. IV.B, a mass independent method is used to determine a in which r_1/a is extrapolated to the physical, rather than simulated, quark masses on the given ensemble.

Partial quenching is very useful in order to obtain enough data to perform the required chiral fits. For the valence masses on a typical ensemble, nine different masses from $0.1m_s'$ to m_s' (m_s' is the simulated strange sea mass) may be used. This yields 45 distinct pairs of valence masses, and hence 90 values (meson masses and decay constants) for the chiral fit. Without partial quenching, we would have only four values. Of course, the correlations among the 90 values must be taken into account.

Finite volume corrections are included in the one-loop rSχPT forms used to fit the lattice data. Since the spatial box sizes are at least 2.4 fm, and for the smallest light sea-quark masses they are increased to about 2.9 fm or larger, these corrections are always less than 1.5%. Smaller, additional corrections representing "residual" effects from higher-loop contributions are applied at the end of the calculation, as described below. The results cannot be fit without the one-loop finite volume corrections, nor can they be fit with continuum χPT. Aubin *et al.* (2004b) fitted five coarse and two fine ensembles with continuum χPT; however, the confidence level of the fit was 10^{-250}.

We now present methods and results from Bernard *et al.* (2007b). A final version of the analysis, using added ensembles and two-loop chiral logarithms (Bijnens *et al.*, 2004, 2006; Bijnens and Lahde, 2005), is in progress.

The fitting is done in two stages. In the first stage, the leading order (LO) and next-to-leading order (NLO) low-energy constants (LECs) are determined by fitting a restricted set of data that is closer to the chiral and continuum limits than the additional points included later. Specifically, the largest lattice spacing ($a \approx 0.15$ fm) is omitted and the valence quark masses are required to obey $am_x + am_y \lesssim 0.39am_s$ (for $a \approx 0.12$ fm), $am_x + am_y \lesssim 0.51am_s$ (for $a \approx 0.09$ fm), and $am_x + am_y \lesssim 0.56am_s$ (for $a \approx 0.06$ fm). Further, for $a \approx 0.12$ fm three higher-mass

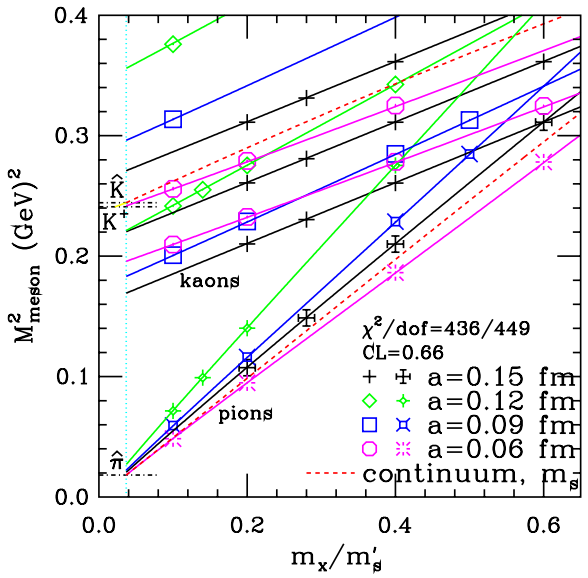

FIG. 23. (Color online) NNNLO fit to partially quenched squared meson masses. Only the lightest sea-quark ensemble for each lattice spacing is shown. The data fit includes the results for decay constants and is reflected in the number of degrees of freedom. From Bernard *et al.*, 2007b.

combinations of sea-quark masses are omitted. Despite the restrictions, it is found that due to the high precision of the data it is necessary to add NNLO analytic terms in order to get good fits. In the second stage, the range of valence and sea-quark masses is extended to include the region around the strange quark mass. The LO and NLO low energy constants are constrained to be within the range determined by the first stage of fitting. In this stage, NNNLO analytic terms are needed to get good fits.

In Fig. 23, we show the squared meson masses in units of (GeV)^2. For the pions $m_x = m_y$. For the kaons a few fixed values of m_y are picked for illustration, and m_x is varied. The horizontal axis is m_x/m_s'. Only a small fraction of the points used in the fit are shown. For each lattice spacing, the plot contains only the lightest sea-quark mass ensemble, and no decay constant data is plotted. For this fit, $\chi^2 = 436$ with 449 degrees of freedom, corresponding to a confidence level of 0.66. The dashed line shows the continuum prediction after all lattice spacing dependence in the fit parameters is extrapolated away, the strange sea-quark mass is fixed to its physical value and the light valence and sea masses are set equal. The physical values of m_s and $\hat{m} = (m_u + m_d)/2$ are required to simultaneously yield the kaon and pion masses denoted $\hat{K}$ and $\hat{\pi}$ in the figure. These masses correspond to what the kaon and pion masses would be with isospin and electromagnetic effects removed. Some phenomenological input is needed to account for the electromagnetic effects. This is explained in detail in Aubin *et al.* (2004b). The vertical dotted line is drawn at $\hat{m}/m_s$.

The residual finite volume corrections are then applied. Colangelo *et al.* (2005) showed that higher than

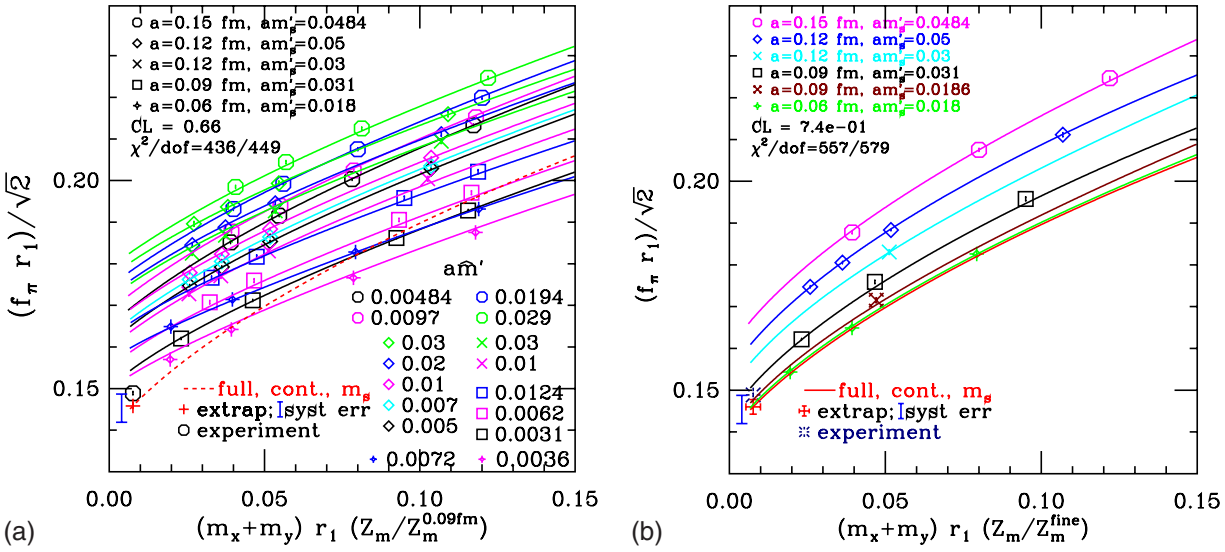

FIG. 24. (Color online) The meson decay constants are plotted along with the NNNLO fit that was shown for the masses in Fig. 23. The left plot shows partially quenched data from more ensembles than in Fig. 23, but still only a fraction of the data fit. On the right, still more ensembles are included, but only full QCD data points are plotted. From Bernard *et al.*, 2007b.

one-loop χPT corrections can be significant in the current range of quark masses and volumes. For $a \approx 0.12$ fm with sea masses $am_l/am'_s = 0.01/0.05$, there is a direct test of finite volume effects on 20^3 and 28^3 volumes that correspond to 2.4 and 3.4 fm box sides. Bernard *et al.* (2007b) detailed the comparison between these calculations and the one-loop result. On this basis, a small correction is applied to the continuum prediction. This amounts to 0.25% for f_π, 0.05% for f_K, −0.15% for m_π^2, and −0.10% for m_K^2. These values are also added to the systematic error.

By extending the kaon extrapolation line in Fig. 23, one finds the value of m_u that corresponds to the K^+ mass [see Aubin *et al.* (2004b)]. Two important mass ratios are determined,

$$m_s/\hat{m} = 27.2(1)(3)(0), \quad m_u/m_d = 0.42(0)(1)(4). \quad (134)$$

The errors are statistical, lattice systematic, and electromagnetic (from continuum estimates). Note that the $m_u = 0$ solution to the strong *CP* problem is ruled out at the 10σ level.

Having found the continuum fit parameters and the physical quark masses, the decay constants are predicted. Figure 24 (left) shows (some of) the decay constant data and the fit through the displayed data. For the continuum prediction (dashed line), the strange sea-quark mass is set to its physical value and the light valence and sea masses are set equal. The left end of the curve corresponds to $m_x = m_y = \hat{m}$. The vertical error bar to the left of the + shows the systematic error. The experimental result is shown as an octagon. It comes from the decay $\pi^+ \to \mu^+ \nu_\mu$ with the assumption that $|V_{ud}| = 0.973\,77(27)$ (Amsler *et al.*, 2008). Figure 24 (right) shows the full QCD points from a slightly different fit with data from additional ensembles. Note that the data points at $a \approx 0.06$ fm are quite close to the full QCD continuum extrapolated curve.

Up to this point, the lattice spacing is set by calculation of the heavy-quark potential parameter r_1, which yields relative lattice spacings between ensembles, and the continuum extrapolation of Υ splittings determined by the HPQCD Collaboration (Gray *et al.*, 2005), which gives an absolute scale. These results yield a value $r_1 = 0.318(7)$ fm. On this basis,

$$f_\pi = 128.3 \pm 0.5^{+2.4}_{-3.5}\ \text{MeV},$$
$$f_K = 154.3 \pm 0.4^{+2.1}_{-3.4}\ \text{MeV}, \quad (135)$$
$$f_K/f_\pi = 1.202(3)(^{+8}_{-14}),$$

where the errors are from statistics and lattice systematics. This value for f_π is consistent with the experimental result $f_\pi^{\text{expt}} = 130.7 \pm 0.1 \pm 0.36$ MeV (Amsler *et al.*, 2008).

An alternative approach is to set the scale from f_π itself. In this case, there are small changes in the quark masses and

$$r_1 = 0.3108(15)(^{+26}_{-79})\ \text{fm}, \quad (136)$$

which is 1σ lower (and with somewhat smaller errors) than the value from the Υ system. For the decay constants,

$$f_K = 156.5 \pm 0.4^{+1.0}_{-2.7}\ \text{MeV}, \quad f_K/f_\pi = 1.197(3)(^{+6}_{-13}), \quad (137)$$

where the errors are statistical and systematic.

Marciano (2004) noted that the lattice value of f_K/f_π can be combined with measurements of the kaon branching fraction (Ambrosino *et al.*, 2006a, 2006b) to obtain $|V_{us}|$. From Eq. (137),

$$|V_{us}| = 0.2246(^{+25}_{-13}), \tag{138}$$

which is consistent with (and competitive with) the world-average value $|V_{us}|=0.2255(19)$ (Amsler *et al.*, 2008) coming from semileptonic K decay coupled with nonlattice theory.

Using the two-loop perturbative calculation of the mass renormalization constant Z_m (Mason *et al.*, 2006),[11] absolute quark masses can be found,

$$\begin{aligned} m_s &= 88(0)(3)(4)(0)\ \text{MeV}, \\ \hat{m} &= 3.2(0)(1)(2)(0)\ \text{MeV}, \\ m_u &= 1.9(0)(1)(1)(1)\ \text{MeV}, \\ m_d &= 4.6(0)(2)(2)(1)\ \text{MeV}. \end{aligned} \tag{139}$$

The errors are statistical, lattice systematic, perturbative, and electromagnetic (from continuum estimates). Nonperturbative computations of Z_m are in progress.

The chiral fits also determine various Gasser-Leutwyler low-energy constants and chiral condensates,

$$\begin{aligned} &2L_6 - L_4 = 0.4(1)(^{+2}_{-3}), \quad 2L_8 - L_5 = -0.1(1)(1), \\ &L_4 = 0.4(3)(^{+3}_{-1}), \quad L_5 = 2.2(2)(^{+2}_{-1}), \\ &L_6 = 0.4(2)(^{+2}_{-1}), \quad L_8 = 1.0(1)(1), \\ &f_\pi/f_2 = 1.052(2)(^{+6}_{-3}), \\ &\langle \bar{u}u\rangle_2 = -(278(1)(^{+2}_{-3})(5)\ \text{MeV})^3, \\ &f_\pi/f_3 = 1.21(5)(^{+13}_{-3}), \\ &\langle \bar{u}u\rangle_3 = -(242(9)(^{+5}_{-17})(4)\ \text{MeV})^3, \\ &f_2/f_3 = 1.15(5)(^{+13}_{-3}), \quad \langle \bar{u}u\rangle_2/\langle \bar{u}u\rangle_3 = 1.52(17)(^{+38}_{-15}). \end{aligned} \tag{140}$$

The errors are statistical, lattice systematic, and perturbative for the condensates. f_2 (f_3) denotes the three-flavor decay constant in the two- (three-) flavor chiral limit, and $\langle \bar{u}u\rangle_2$ ($\langle \bar{u}u\rangle_3$) is the corresponding condensate. The low-energy constants L_i are in units of 10^{-3} and are evaluated at chiral scale m_η; the condensates and masses are in the modified minimal subtraction ($\overline{\text{MS}}$) scheme at scale 2 GeV. The indications are that the L_i will change significantly when the two-loop logarithms are included, just as they do in phenomenological estimates (Bijnens, 2007). Other results are very stable, however.

The rSχPT formalism relies on the replica procedure, and taking the fourth root corresponds to $n_r=1/4$, where n_r is the number of replicas. The fact that there are good fits with the rSχPT formulas, but not with continuum χPT, is a test of staggered chiral perturbation theory. A further test of rSχPT is to allow n_r to be a free parameter in the fits. For the low-mass data, $n_r=0.28(2)(3)$ where the first error is statistical and the second systematic coming from varying the details of the chiral fits. We are encouraged by this strong constraint on n_r, and the success of rSχPT in describing the MILC data.

C. Other computations of f_π and f_K

Since the MILC Collaboration's initial calculation of the light pseudoscalar meson masses, decay constants, and quark masses using the $a\approx 0.12$ and 0.09 fm lattices (Aubin *et al.*, 2004b), several others have also computed f_π and f_K on the MILC ensembles using different valence quark formulations. All of the results are consistent with those of the MILC Collaboration, Eq. (135), and with each other.

The HPQCD Collaboration uses HISQ staggered valence quarks and the MILC asqtad staggered sea-quark ensembles with lattice spacings $a\approx 0.15$, 0.12, and 0.09 fm (Follana *et al.*, 2008). They generate one pion point and one kaon point per ensemble, matching the masses of the Goldstone HISQ pion to the asqtad one, and the mass of the HISQ $s\bar{s}$ meson to 696 MeV, the χPT value. Although Follana *et al.* (2008) performed a mixed action lattice simulation, they extrapolated to the physical light quark masses and the continuum using continuum NLO χPT augmented by analytic terms constrained with Bayesian priors. Terms proportional to $\alpha_s a^2$ and a^4 are included to test for conventional discretization errors, while those proportional to $\alpha_s^3 a^2$, $\alpha_s^3 a^2 \ln(m_q)$, and $\alpha_s^3 a^2 m_q$ are intended to test for residual taste-changing interactions with the HISQ valence quarks. HPQCD obtains the following results for f_π, f_K, and the ratio:

$$\begin{aligned} &f_\pi = 132(2)\ \text{MeV}, \quad f_K = 157(2)\ \text{MeV}, \\ &f_K/f_\pi = 1.189(7), \end{aligned} \tag{141}$$

where the largest source of error is the uncertainty in the scale r_1 (1.4% for f_π and 1.1% for f_K).

The NPLQCD Collaboration used domain-wall valence quarks and four $a\approx 0.12$ fm ensembles with $m_l/m_s'=0.14$–0.6 (Beane, Bedaque, *et al.*, 2007). They tuned to match the valence pion and kaon to the corresponding asqtad particles. Due to the mixed action, there are still unitarity-violating artifacts that vanish only in the limit $a\to 0$. They computed only the ratio f_K/f_π, which has a milder dependence upon the quark mass than the individual decay constants, and extrapolated to the physical light quark masses using the NLO continuum χPT expression, which depends only on one free parameter, L_5. The result is

[11] With this two-loop Z_m factor a tadpole improved definition of the bare quark mass should be used, where am_q denoted throughout this review should be replaced by $u_0 am_q$. The tadpole factors for the various MILC ensembles are listed in Table I.

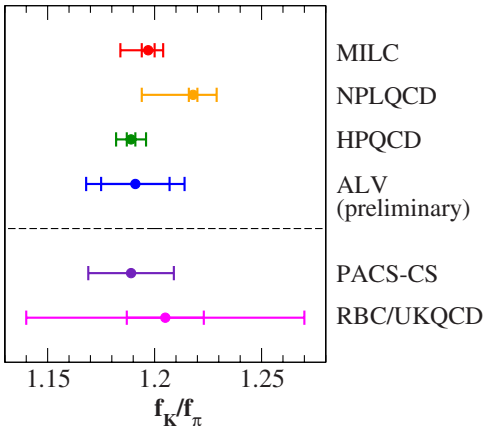

FIG. 25. (Color online) The ratio of light decay constants f_K/f_π from six calculations. The top four use MILC asqtad configurations and the lower two use other types of quarks. Details and references can be found in the text.

$$f_K/f_\pi = 1.218 \pm 0.002^{+0.011}_{-0.024},$$
$$L_5(m_\eta) = 2.22 \pm 0.02^{+0.18}_{-0.54} \times 10^{-3}, \tag{142}$$

where the first error is statistical and the second error is the sum of systematic errors added in quadrature. The dominant source of uncertainty is from the truncation of the χPT expression ($^{+0.011}_{-0.022}$ for the ratio), which they estimated by varying the fit function through the addition of NNLO analytic terms and double logarithms. Although they did not include an error due to their use of only a single lattice spacing, this is likely a small effect in the ratio f_K/f_π.

Aubin *et al.* (2009) also used domain-wall valence quarks. In contrast with NPLQCD, however, they computed many partially quenched points on the $a \approx 0.12$ and 0.09 fm ensembles, and used NLO mixed action χPT with higher-order analytic terms to extrapolate to physical quark masses and the continuum (Bär *et al.*, 2005). Their preliminary results for the light pseudoscalar meson decay constants are

$$f_\pi = 129.1(1.9)(4.0)\ \text{MeV},$$
$$f_K = 153.9(1.7)(4.4)\ \text{MeV}, \tag{143}$$
$$f_K/f_\pi = 1.191(16)(17),$$

where the first error is statistical and the second is the sum of systematic errors added in quadrature. The dominant source of error is from the chiral extrapolation procedure (2.2% for f_π and 2.3% for f_K), and is estimated by varying the analytic terms included in the fit function.

In Fig. 25, we compare results for f_K/f_π from a variety of (2+1)-flavor calculations. The top four results all use MILC aqstad configurations and were discussed above. The two lower results from the PACS-CS Collaboration (Aoki *et al.*, 2009) and the RBC/UKQCD Collaboration (Allton *et al.*, 2008) use clover quarks with the Iwasaki gauge action and domain-wall quarks, respectively.

VII. HEAVY-LIGHT MESONS: MASSES AND DECAY CONSTANTS

Calculations of B- and D-meson masses and decay constants using the (2+1)-flavor MILC configurations have been performed in joint work by the Fermilab Lattice and MILC Collaborations, and by the HPQCD Collaboration. Of quantities involving heavy b and c quarks, meson masses and decay constants are among the simplest quantities to compute numerically and are often well measured experimentally. Thus they provide valuable cross checks of lattice QCD methods. In particular, once the treatment of the light sea and valence quarks has been validated within the light pseudoscalar sector, calculations of heavy-light meson masses and decay constants allow tests of the various lattice QCD formalisms used for heavy quarks. In this section, we describe the (2+1)-flavor calculations by Fermilab/MILC and HPQCD of heavy-light meson masses and decay constants, and show that, with one exception, they are consistent with experiment. These results give confidence in other lattice QCD calculations involving b and c quarks, such as those of semileptonic form factors described in Sec. VIII.

A. Heavy quarks on the lattice

Heavy quarks, i.e., those for which the quark mass in lattice units am is large, present special challenges. As long as $am \ll 1$, heavy quarks on the lattice can be treated with light-quark formalisms such as staggered fermions. At the lattice spacings in common use, we have $am_c \sim 0.5$–1.0 and $am_b \sim 2$–3. For charm quarks, light-quark methods can only be used if they are highly improved to remove discretization errors. Bottom quarks still require special heavy-quark methods.

1. Nonrelativistic QCD

A straightforward way of formulating heavy quarks on the lattice is to rewrite the Dirac-like light-quark action as a sum in a nonrelativistic operator expansion, as is done in HQET (Isgur and Wise, 1992; Neubert, 1994) and in nonrelativistic expansions in QED (Caswell and Lepage, 1986; Lepage *et al.*, 1992),

$$S_{\text{NRQCD}} = \sum_x \phi^\dagger(x)\Bigg(-\nabla_0^{(+)} + \frac{1}{2m}\sum_i \Delta_i + \frac{1}{2m}\sigma\cdot B(x) + \frac{1}{8m^3}\Big(\sum_i \Delta_i\Big)^2 + \cdots\Bigg)\phi(x), \tag{144}$$

where

$$\nabla_\mu^{(+)}\phi(x) \equiv a^{-1}[U_\mu(x)\phi(x+a\hat{\mu}) - \phi(x)], \tag{145}$$

and ϕ denote two-component fermions representing the quarks. An analogous term in the action governs the antiquarks. The leading heavy-quark mass dependence is absorbed into the fermion field and vanishes from explicit calculations. For b quarks in particles with a single heavy quark, the first term in this action yields the

static approximation (Eichten and Hill, 1990). In heavy-light systems, the importance of operators in this expansion is ordered according to HQET power counting ($\lambda \sim \Lambda/m_Q$). In quarkonium systems, operators are ordered by the heavy-quark velocity.

2. Wilson fermions with the Fermilab interpretation

In NRQCD, the kinetic energy operator of the Dirac action, $\bar{\psi}(x)\Sigma_i \gamma_i \nabla_i \psi(x)$ is replaced by the leading kinetic energy operator $\phi^\dagger(x)(2m^{-1})\Sigma_i \Delta_i \phi(x)$ plus a series of higher dimension operators. The action for Wilson fermions contains the leading kinetic energy operators of both the Dirac and the nonrelativistic actions, as in Eq. (15),

$$S_W = \sum_x \bar{\psi}(x)\left(\sum_\mu \gamma_\mu \nabla_\mu - \frac{ar}{2}\sum_\mu \Delta_\mu + m\right)\psi(x). \quad (146)$$

The effects of the Laplacian term, which eliminates the doubler states, vanish in the limit $am \to 0$. As am becomes larger, the importance of the Laplacian term grows. When $am \gg 1$, the Laplacian term dominates the Dirac-like kinetic energy term, and the theory behaves like a type of nonrelativistic theory in which the rest mass $m_1 \equiv E(p^2=0)$ does not equal the kinetic mass $m_2 \equiv 1/(2\partial E/\partial p^2)$. (Note that we use lower case m to refer to quarks and capital M to refer to mesons in this section.) As $am \to 0$, the two masses converge to the bare quark mass m. For heavy quarks the kinetic mass controls the physics, and the rest mass may be absorbed into a field redefinition. This means that the Wilson action and related actions can be used as actions for heavy quarks as long as m_2, with contributions from both terms in the kinetic energy, is adjusted to equal the desired physical mass (El-Khadra *et al.*, 1997). It is possible to set $m_1 = m_2$ by breaking time-space axis-interchange symmetry in the Lagrangian. If this is not done, m_1 and m_2 have the tree-level form

$$am_1 = \ln(1 + am_0) \quad (147)$$

and

$$1/(am_2) = 2/[am_0(2 + am_0)] + 1/(1 + am_0). \quad (148)$$

The action of the nonrelativistic expansion can be viewed as arising from a field transformation of the Dirac field, the Foldy-Wouthuysen-Tani (FWT) transformation. The Wilson action, with both types of kinetic energy operators, can be viewed as arising from a partial FWT transformation. Like the action of NRQCD, it produces the same physics as the Dirac action as long as a series of correction operators is added to sufficient precision (Oktay and Kronfeld, 2008). The leading dimension-five correction operator has the same form for heavy Wilson fermions as for light Wilson-clover fermions [Eq. (19)], $S_{SW} = (iag/4)c_{SW}\Sigma_x \bar{\psi}(x)\sigma_{\mu\nu}\mathcal{F}_{\mu\nu}(x) \times \psi(x)$. All simulations to date using this approach to heavy quarks have therefore used Wilson-clover fermions. A systematic improvement program is possible as outlined in Sec. X.C.

3. The HISQ action

Because $0.5 \lesssim am_c \lesssim 1$ at currently accessible lattice spacings, it is possible to use ordinary light-quark actions to treat the charm quark. However, to obtain high precision it is necessary to correct the action to a high order in am. This approach is followed with "highly improved staggered quarks" (Follana *et al.*, 2007), as explained in Sec. II.E.

B. Lattice calculations of masses and decay constants

As in the light pseudoscalar meson case, the heavy-light decay constant is proportional to the matrix element of the axial current,

$$\langle 0|A_\mu|H_q(p)\rangle = if_{H_q}p_\mu, \quad (149)$$

where $A_\mu = \bar{q}\gamma_\mu\gamma_5 Q$. Because of the heavy-quark normalization in HQET, it is often useful to consider the combination decay amplitude

$$\phi_{H_q} = f_{H_q}\sqrt{M_{H_q}}, \quad (150)$$

which is computed from the correlators

$$C_0(t) = \langle O_{H_q}(t)O^\dagger_{H_q}(0)\rangle, \quad C_{A_4}(t) = \langle A_4(t)O^\dagger_{H_q}(0)\rangle. \quad (151)$$

For the case of Fermilab heavy quarks or NRQCD b quarks, the heavy-light meson mass is obtained from the kinetic mass (M_2) in the dispersion relation, whereas for HISQ charm quarks $M_1 = M_2$, so both are simultaneously set to the D- or D_s-meson mass.

The Fermilab lattice and MILC Collaborations' calculation of heavy-light meson decay constants (Aubin *et al.*, 2005a; Bernard *et al.*, 2009c) employed the Fermilab action for the heavy b and c quarks and the asqtad staggered action for the light u, d, and s quarks. They constructed the heavy-light meson interpolating operator and axial vector current A_μ using the method for combining four-component Wilson quarks with one-component staggered quarks described by Wingate *et al.* (2003). Their most recent determination from Lattice 2008 (Bernard *et al.*, 2009c) used data on the medium-coarse, coarse, and fine lattices, with 8–12 partially quenched valence masses per ensemble. The clover coefficient c_{SW} and hopping parameter κ in the Fermilab action are tuned to remove errors of $\mathcal{O}(1/m_Q)$ in the heavy-quark action. In particular, they set $c_{SW} = u_0^{-3}$, the value given by tree-level tadpole-improved perturbation theory (Lepage and Mackenzie, 1993). They chose the charm quark hopping parameter κ_c so that the spin-averaged (kinetic) D_s-meson mass is equal to its physical value, and chose the bottom quark hopping parameter κ_b to reproduce the B_s-meson mass in an analogous manner; this implicitly fixes the b and c quark masses. They also removed errors of $\mathcal{O}(1/m_Q)$ from the heavy-light axial vector current A_μ by rotating the heavy-quark field in the two-point correlation function,

$$\psi_b \to \Psi_b = (1 + ad_1 \vec{\gamma} \cdot \vec{D}_{\rm lat})\psi_b, \tag{152}$$

where $\vec{D}_{\rm lat}$ is the symmetric, nearest-neighbor, covariant difference operator, and the tadpole-improved tree-level value for d_1 is given by (El-Khadra *et al.*, 1997)

$$d_1 = u_0^{-1}\{1/(2 + am_0) + 1/[2(1 + am_0)]\}. \tag{153}$$

They obtained the renormalization factor needed to match the lattice heavy-light current onto the continuum using the method of Hashimoto *et al.* (1999),

$$Z_{A_4}^{Qq} = \rho_{A_4}^{Qq}\sqrt{Z_{V_4}^{QQ} Z_{V_4}^{qq}}, \tag{154}$$

where the flavor-conserving factors $Z_{V_4}^{QQ}$ and $Z_{V_4}^{qq}$ are determined nonperturbatively and the remaining factor is determined to one-loop in lattice perturbation theory (Lepage and Mackenzie, 1993; El-Khadra *et al.*, 2007).

The Fermilab/MILC Collaboration fits its decay constant data as a function of light-quark sea and valence masses to the one-loop form given by HMSχPT (see Sec. III.B), supplemented by analytic NNLO terms, which are quadratic in the light valence and/or sea masses. This is very similar to the approach taken in the light pseudoscalar sector, as described in Sec. VI. While pure NLO fits are adequate to describe the data for very light valence mass, once this mass gets to be roughly half the strange quark mass or higher, at least some NNLO terms are necessary to obtain acceptable fits.

Figure 26 shows the preferred HMSχPT fit to data at multiple lattice spacings for Φ_D and Φ_{D_s}, which are functions of the light valence mass, the light sea mass, and the strange sea mass. In addition to taste-breaking discretization effects that appear as taste-splittings, taste-hairpins, and taste-violating analytic terms, there are generic light-quark discretization effects, which can be thought of as changes in the physical LECs [such as Φ_0, the value of Φ in the SU(3) chiral limit] with lattice spacing. With the asqtad action, such effects are $\mathcal{O}(\alpha_s a^2)$. They can be (approximately) accounted for by adding additional parameters to the HMSχPT fit function, with variations limited by Bayesian priors, following Lepage *et al.* (2002). This is done in the fit shown in Fig. 26, although the effects are quite small, and fits without the additional parameters give almost the same results (and confidence levels), but with somewhat smaller statistical errors. Once the parameters of the HMSχPT fit are known, taste-violating and generic discretization effects through $\mathcal{O}(a^2)$ can be removed by setting $a=0$. After taking the continuum limit, the valence and sea-quark masses are set to their physical values in order to obtain the decay constants of a D^+ and D_s meson, up to small isospin violations in the sea sector.

The HPQCD Collaboration's calculation of the B- and B_s-meson decay constants (Gamiz *et al.*, 2009) employed the NRQCD action for the heavy b quarks and the asqtad staggered action for the light u, d, and s quarks. They used six data points in their analysis—four full QCD points on the coarse ensembles and two full QCD points on the fine ensembles. They fixed the

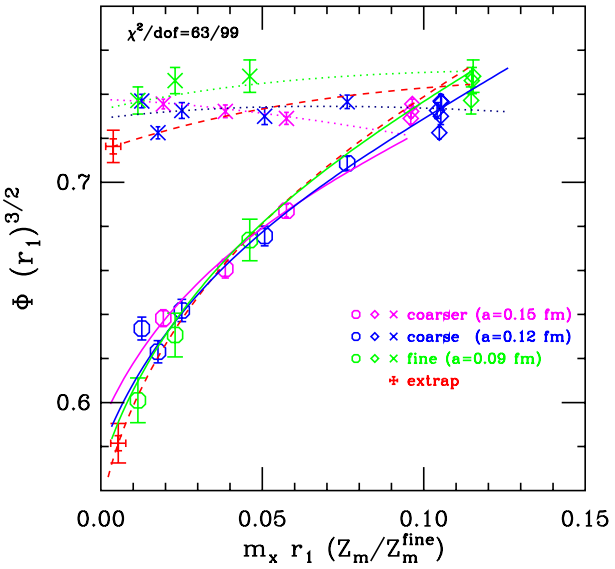

FIG. 26. (Color online) Chiral extrapolation for Φ_D (octagons) and Φ_{D_s} (crosses or diamonds) by the Fermilab/MILC Collaboration (Bernard *et al.*, 2009c). Solid lines are the HMSχPT fit to Φ_D; dotted lines, to Φ_{D_s}. Although the full set of partially quenched data is included in the fit, for Φ_D the plot shows only those full QCD points for which the light valence and sea masses are equal to m_x, the mass on the abscissa. For Φ_{D_s}, only points with the strange valence mass (m_{sv}) equal to the strange sea mass are shown, plotted either as a function of m_l (crosses), or at m_{sv} (diamonds). The dashed lines show the fit after removal of light-quark discretization errors, with the fancy plus signs giving the chirally extrapolated results with statistical errors.

b-quark mass so that the mass of a $b\bar{b}$ meson reproduces the physical m_Υ (Gray *et al.*, 2005). The HPQCD computation included all currents of $\mathcal{O}(1/m_b)$ (Morningstar and Shigemitsu, 1998) and used one-loop lattice perturbation theory to match onto the continuum (Dalgic *et al.*, 2004). Therefore, they included all corrections to the heavy-light current through $\mathcal{O}(\Lambda_{\rm QCD}/m_b)$, $\mathcal{O}(\alpha_s)$, $\mathcal{O}(a\alpha_s)$, $\mathcal{O}(\alpha_s/(am_b))$, and $O(\alpha_s\Lambda_{\rm QCD}/m_b)$. The HPQCD Collaboration used HMSχPT for the chiral extrapolations of Φ_B and Φ_{B_s} in a manner similar to Fermilab/MILC. They multiplied the NLO expression by $1+c\alpha_s a^2+c'a^4$ in order to parametrize higher-order discretization effects. They also included an additional NNLO analytic term $\propto(m_d-m_s)^2$ in the extrapolation of the ratio Φ_{B_s}/Φ_B.

The HPQCD Collaboration's calculation of the D- and D_s-meson decay constants (Follana *et al.*, 2008) employed the HISQ action (Follana *et al.*, 2007) (see Sec. II.E) for all of the u, d, s, and c valence quarks. Because they are treating the charm quark as a light quark, the computation is similar to the determinations of f_π and f_K described in Sec. VI, except for differences due to the fact that this is a mixed-action simulation with HISQ valence quarks and asqtad sea quarks. They used the medium-coarse, coarse, and fine MILC lattices, and included seven full QCD points in their analysis. They

fixed the c-quark mass so that the mass of the taste Goldstone η_c meson agrees with experiment. Because the HISQ axial current is partially conserved, it does not need to be renormalized. Therefore this method avoids the use of perturbation theory, whose truncation errors can be difficult to estimate. The HPQCD calculation does not use HMSχPT for the chiral extrapolations of f_D and f_{D_s}, but simply applies continuum χPT, supplemented by Bayesian fit parameters. These parameters test for the expected discretization effects of the form $\alpha_S a^2$, a^4, $\alpha_S^3 a^2$, $\alpha_S^3 a^2 \ln(m_{quark})$, and $\alpha_S^3 a^2 m_{quark}$ from the asqtad action, and the effects of residual taste-violating interactions with HISQ valence quarks.

All of the (2+1)-flavor calculations of heavy-light meson decay constants rely upon power counting in order to estimate the size of heavy-quark discretization errors. In the Fermilab method, heavy-quark discretization errors arise due to the short-distance mismatch of higher-dimension operators in the continuum and lattice theories. The sizes of these mismatches are estimated using HQET as a theory of cutoff effects, as described by Kronfeld (2000) and Harada *et al.* (2002). This typically leads to errors of a few percent on the fine MILC lattices. In simulations with NRQCD b quarks, relativistic errors arise from higher-order corrections to the NRQCD action and the heavy-light current. Although these are not all discretization errors proportional to powers of the lattice spacing, many are proportional to inverse powers of the heavy-meson mass, and hence should be considered heavy-quark errors. The leading relativistic error comes from radiative corrections to the $\sigma \cdot B$ term in the action, and is estimated to be of $\mathcal{O}(\alpha_s \Lambda_{\mathrm{QCD}}/M_B) \sim 3\%$ (Gamiz *et al.*, 2009). The HISQ action is highly improved, and the leading heavy-quark errors are formally of $\mathcal{O}(\alpha_s(m_c a)^2)$ and $\mathcal{O}((m_c a)^4)$ (Follana *et al.*, 2007), where $\alpha_s \sim 0.3$ and $am_c \sim 0.5$ on the fine MILC lattices. The HPQCD Collaboration, however, removed errors of $\mathcal{O}(\alpha_s(m_c a)^2)$ in the HISQ action by accounting for radiative corrections in the coefficient of the Naik term, and also extended the traditional Symanzik analysis to remove all $\mathcal{O}((m_c a)^4)$ errors to leading order in the charm quark's velocity. Thus the leading charm quark discretization errors should be of $\mathcal{O}((m_c a)^4 (v/c)^2) \sim 0.5\%$ or less for D mesons.

C. Results for masses and decay constants

Although the heavy-light meson decay constants, in combination with experimental measurements of leptonic branching fractions, can be used to extract CKM matrix elements via the relation

$$\Gamma(H \to \nu\ell) = (G_F^2 |V_{ab}|^2)/(8\pi) \times f_H^2 m_\ell^2 M_H (1 - m_\ell^2/M_H^2)^2, \tag{155}$$

the matrix elements $|V_{cd}|$, $|V_{cs}|$, and $|V_{ub}|$ can be obtained to better accuracy from other quantities such as neutrino scattering and semileptonic decays (Amsler *et al.*, 2008). Therefore lattice calculations of heavy-light meson decay constants provide good tests of lattice QCD methods, especially the treatment of heavy quarks on the lattice. Comparison of lattice calculations with experimental measurements, however, relies upon the assumption that, because leptonic decays occur at the tree level in the standard model, they do not receive large corrections from new physics. This is generally true of most beyond-the-standard model theories, but in a few models, such as those with leptoquarks, this is not necessarily the case (Dobrescu and Kronfeld, 2008).

CKM unitarity implies that $|V_{cd}| = |V_{us}|$ and $|V_{cs}| = |V_{ud}|$ up to corrections of $\mathcal{O}(|V_{us}|^4)$. Because both $|V_{ud}|$ and $|V_{us}|$ are known to subpercent accuracy, experimentalists use this relation to extract the D-meson decay constants from the measured branching fractions. The latest determinations of f_D (Eisenstein *et al.*, 2008) and f_{D_s} (Alexander, 2009) from the CLEO experiment are

$$f_{D^+} = 205.8 \pm 8.9 \text{ MeV}, \quad f_{D_s^+} = 259.5 \pm 7.3 \text{ MeV}. \tag{156}$$

These results used the determination of $|V_{ud}| = 0.974\,18(26)$ from superallowed $0^+ \to 0^+$ nuclear β decay (Towner and Hardy, 2008) and of $|V_{us}| = 0.2256$ (Eisenstein *et al.*, 2008).[12] The Fermilab Lattice and MILC Collaborations' preliminary determination of the D-meson decay constants are (Bernard *et al.*, 2009c)

$$f_D = 207(11) \text{ MeV}, \quad f_{D_s} = 249(11) \text{ MeV}, \tag{157}$$

where the dominant errors come from tuning the charm quark mass and from heavy-quark discretization effects, which are each $\sim 3\%$. Both of these results are consistent with experiment. The HPQCD Collaboration's determinations of the D-meson decay constants using HISQ fermions are more precise (Follana *et al.*, 2007),

$$f_D = 207(4) \text{ MeV}, \quad f_{D_s} = 241(3) \text{ MeV}, \tag{158}$$

with total errors each below 2%. The largest contribution to the errors comes from the uncertainty in the scale r_1, and is 1.4% (1%) for f_D (f_{D_s}). Although HPQCD's result for f_D is consistent with experiment, their value for f_{D_s} is $\sim 2.5\sigma$ below the CLEO measurement, where σ is dominated by the experimental uncertainty. A comparison of lattice QCD and experimental results for the D-meson decay constants is shown in the left panel of Fig. 27.

Many of the statistical and systematic uncertainties that enter the lattice calculations of f_D and f_{D_s} cancel in the ratio. Therefore the quantity f_D/f_{D_s} allows for a more stringent comparison between the results of Fermilab/MILC and HPQCD. The Fermilab Lattice and MILC Collaborations found (Bernard *et al.*, 2009c)

[12] Although Eisenstein *et al.* (2008) attributed $|V_{us}| = 0.2256$ to FlaviaNet (Antonelli, 2007), Antonelli (2007) gave $|V_{us}| = 0.2246(12)$ from $K_{\ell 3}$ decays plus lattice QCD, and $|V_{us}| = 0.2253(9)$ from $K_{\ell 2}$ and $K_{\ell 3}$ decays plus lattice QCD.

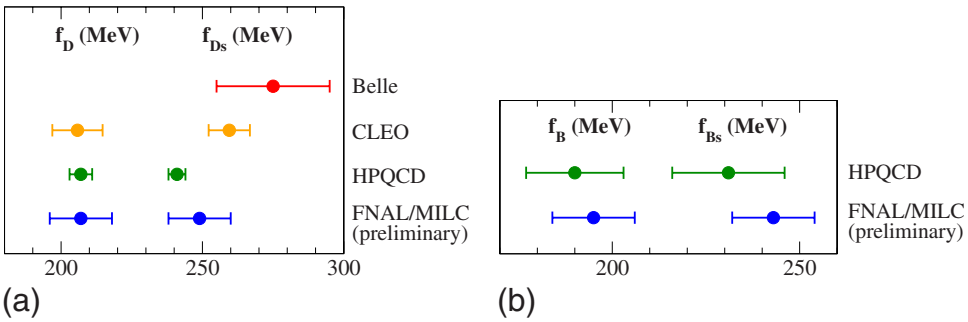

FIG. 27. (Color online) Comparison of lattice QCD and experimental results for f_D and f_{D_s} (left panel) and of lattice QCD results for f_B and f_{B_s} (right panel).

$$f_D/f_{D_s} = 0.833(19), \tag{159}$$

while the HPQCD Collaboration finds (Follana *et al.*, 2007)

$$f_D/f_{D_s} = 0.859(8). \tag{160}$$

The lattice results for the ratio disagree slightly, but only by $\sim 1.6\sigma$. The experimental uncertainties in f_D and f_{D_s} are largely independent, and therefore add in quadrature in the ratio (Alexander, 2009)

$$f_{D^+}/f_{D_s^+} = 0.793 \pm 0.040. \tag{161}$$

This increases the experimental errors and reduces the significance of the discrepancy with HPQCD.

The HPQCD Collaboration also used HISQ charm quarks to compute the D- and D_s-meson masses (Follana *et al.*, 2007),

$$M_D = 1.868(7)\ \text{GeV}, \quad M_{D_s} = 1.962(6)\ \text{GeV}, \tag{162}$$

and their results agree with the experimental values $M_D = 1.869$ GeV and $M_{D_s} = 1.968$ GeV (Amsler *et al.*, 2008). This lends credibility to their calculation of f_{D_s}, and suggests that both improved experimental measurements and lattice calculations are necessary to determine whether or not this discrepancy is new physics, a statistical fluctuation, or yet something else. Currently, Fermilab/MILC's determination of the D_s-meson decay constant lies between the experimental measurement and the calculation of HPQCD. Once the uncertainties in the calculation are reduced, which is expected to occur with the addition of statistics, finer lattice spacings, and a more sophisticated analysis, the Fermilab Lattice and MILC Collaborations hope to shed light on this intriguing puzzle.

B-meson leptonic decays are much more difficult to observe than D-meson decays because they are CKM suppressed ($\propto |V_{ub}|^2$). In addition, B decays to light leptons are suppressed by the factor m_ℓ^2 in Eq. (155), and only decays to τ's have been observed thus far. Furthermore, the branching fraction $\Gamma(B \to \tau\nu)$ is known only to $\sim 30\%$ accuracy (Amsler *et al.*, 2008). Thus there are no precise experimental determinations of the B-meson decay constants, and the lattice calculations of f_B and f_{B_s} should be considered predictions that have yet to be either confirmed or refuted by experiment.

The Fermilab Lattice and MILC Collaborations preliminary determinations of f_B, f_{B_s}, and the ratios are (Bernard *et al.*, 2009c)

$$f_B = 195(11)\ \text{MeV}, \quad f_{B_s} = 243(11)\ \text{MeV}, \quad f_B/f_{B_s} = 0.803(28). \tag{163}$$

The largest errors in the individual decay constants are due to scale and light-quark mass uncertainties, light-quark discretization effects, and heavy-quark discretization effects, all of which are $\sim 2\%$. The HPQCD Collaboration's determinations are consistent and have similar total uncertainties (Gamiz *et al.*, 2009),

$$f_B = 190(13)\ \text{MeV}, \quad f_{B_s} = 231(15)\ \text{MeV}, \quad f_B/f_{B_s} = 0.812(19). \tag{164}$$

Their largest source of error is the $\sim 4\%$ uncertainty from one-loop perturbative operator matching. A comparison of lattice QCD calculations of the B-meson decay constants is shown in the right panel of Fig. 27.

There are currently no calculations of the B- and B_s-meson masses using the (2+1)-flavor MILC lattices. This is, in part, because the staggered χPT expressions for heavy-light meson masses needed to extrapolate the numerical lattice data to the physical light-quark masses and the continuum are not known, and would require a nontrivial extension of the continuum expressions.

VIII. SEMILEPTONIC FORM FACTORS

Lattice calculations of semileptonic form factors allow the extraction of many of the CKM matrix elements from experiment. The processes we consider for this purpose are dominated by tree-level weak decays of quarks at short distances, but are dressed by the strong interactions at longer distances, such that only mesons appear on the external legs. Given the nonperturbative form factor that parameterizes the strong interactions of the mesons, one can extract the CKM parameters that accompany the flavor-changing weak vertex. With

enough processes one can overconstrain the four standard model parameters that appear in the CKM matrix, and thus test the standard model.

A. $D \to \pi \ell \nu$ and $D \to K \ell \nu$

Semileptonic decays of D mesons, $D \to K \ell \nu$ and $D \to \pi \ell \nu$, allow determinations of the CKM matrix elements $|V_{cs}|$ and $|V_{cd}|$, respectively. Since these CKM matrix elements are well determined within the standard model by unitarity, with results for other processes, the form factors can be obtained from experiment (assuming the standard model), and thus serve as a strong check of lattice calculations. Such calculations bolster confidence in similar calculations of $B \to \pi \ell \nu$, allowing a reliable determination of $|V_{ub}|$, one of the more important constraints on new physics in the flavor sector. Precise calculations of semileptonic form factors for charm decays are also interesting in their own right, given the discrepancy between the HPQCD and experimental values for the D_s leptonic decay.

The necessary hadronic amplitude $\langle P|V_\mu|D\rangle$ ($P=K,\pi$) is parametrized in terms of form factors by

$$\langle P|V_\mu|D\rangle = f_+(q^2)(p_D + p_P - \Delta)_\mu + f_0(q^2)\Delta_\mu, \tag{165}$$

where $q=p_D-p_P$, $\Delta_\mu=(m_D^2-m_P^2)q_\mu/q^2$, and $V_\mu=\bar{q}\gamma_\mu Q$. The differential decay rate $d\Gamma/dq^2$ is proportional to $|V_{cx}|^2|f_+(q^2)|^2$, with $x=d,s$. The CKM matrix element $|V_{cx}|$ is determined using the experimental decay rate and the integral over q^2 of the lattice determination of $|f_+(q^2)|$.

The matrix element $\langle P|V_\mu|D\rangle$ is extracted from the three-point function, where the P meson is given a nonzero momentum $\mathbf{p}$,

$$C_3^{D\to P}(t_x,t_y;\mathbf{p}) = \sum_{\mathbf{x},\mathbf{y}} e^{i\mathbf{p}\cdot\mathbf{y}}\langle O_P(0)V_\mu(y)O_D^\dagger(x)\rangle, \tag{166}$$

and O_D and O_P are the interpolating operators for the initial and final meson states. The calculation of this quantity by the Fermilab Lattice, MILC, and HPQCD Collaborations (Aubin *et al.*, 2005b) uses the Fermilab action [improved through $O(\Lambda_{\rm QCD}/m_c)$, with $\Lambda_{\rm QCD}$ in the HQET context] for the c quark and the asqtad action for the light valence quarks. The D meson and the heavy-light bilinears V_μ are constructed from a staggered light quark and a Wilson-type (Fermilab) heavy quark using the procedure described by Wingate *et al.* (2003) and Bailey *et al.* (2009). In order to extract the transition amplitude $\langle P|V_\mu|D\rangle$ from Eq. (166), we need the analogous two-point correlation function,

$$C_2^M(t_x,\mathbf{p}) = \sum_{\mathbf{x}} e^{i\mathbf{p}\cdot\mathbf{x}}\langle O_M(0)O_M^\dagger(x)\rangle \quad \text{with } M=D,P. \tag{167}$$

As in the case of decay constants, the renormalization factor matching the heavy-light currents on the lattice to the continuum is

$$Z_{V_{1,4}}^{Qq} = \rho_{V_{1,4}}^{Qq}\sqrt{Z_{V_4}^{QQ}Z_{V_4}^{qq}}, \tag{168}$$

where the factors $Z_{V_4}^{QQ}$ and $Z_{V_4}^{qq}$ are computed nonperturbatively, and the remaining factor $\rho_{V_{1,4}}^{Qq}$ (close to 1 by construction) is determined in one-loop perturbation theory (Harada, Hashimoto, *et al.*, 2002).

The quantities $f_\parallel$ and $f_\perp$ are more natural quantities than f_+ and f_0 in the heavy-quark effective theory, and are defined as

$$\langle P|V^\mu|D\rangle = \sqrt{2m_D}[v^\mu f_\parallel(E) + p_\perp^\mu f_\perp(E)], \tag{169}$$

where $v=p_D/m_D$, $p_\perp=p_P-Ev$, and $E=v\cdot p_P$ is the energy of the light meson. The chiral extrapolation and momentum extrapolation or interpolation are carried out in terms of these parameters, which are then converted into f_0 and f_+. The chiral extrapolation by Aubin *et al.* (2005b) was performed at fixed E, where $f_\parallel$ and $f_\perp$ were fit simultaneously to the parametrization of Becirevic and Kaidalov (2000) (BK),

$$f_+(q^2) = F/[(1-\tilde{q}^2)(1-\alpha\tilde{q}^2)], \quad f_0(q^2) = F/(1-\tilde{q}^2/\beta), \tag{170}$$

where $\tilde{q}^2=q^2/m_{D^*}^2$, and $F=f_+(0)$, α and β are fit parameters. The BK form contains the pole in $f_+(q^2)$ at $q^2=m_{D^*}^2$. Even so, the BK parametrization builds into the calculation unnecessary model dependence. The more recent calculation of the similar semileptonic process $B\to\pi\ell\nu$ does not make use of this assumption, as described next.

Aubin *et al.* (2005b) obtained for the form factors at $q^2=0$,

$$f_+^{D\to\pi}(0) = 0.64(3)(6), \quad f_+^{D\to K}(0) = 0.73(3)(7). \tag{171}$$

where the first error is statistical and the second is systematic. They also determined the shape dependence of the form factor as a function of q^2. This is shown in Fig. 28, along with experimental data from the Belle (Abe *et al.*, 2005), BABAR (Aubert *et al.*, 2007b) and CLEO (Cronin-Hennessy *et al.*, 2008; Ge *et al.*, 2009) Collaborations that confirms their prediction. Taking the most recent CLEO results (Ge *et al.*, 2009) $f_+^{D\to\pi}(0)|V_{cd}| = 0.143(5)(2)$ and $f_+^{D\to K}(0)|V_{cs}| = 0.744(7)(5)$ we obtain

$$|V_{cd}| = 0.223(8)(3)(23), \quad |V_{cs}| = 1.019(10)(7)(106), \tag{172}$$

where the first error is the (experimental) statistical error, the second is the (experimental) systematic error, and the third is the total lattice error. If we use unitarity along with $|V_{ud}|$ and $|V_{us}|$, then we can use the CLEO measurements to predict the form factors. We then obtain $f_+^{D\to\pi}(0)=0.634(25)$ and $f_+^{D\to K}(0)=0.764(9)$, in good agreement with the result in Eq. (171). Clearly, the lattice error still dominates the uncertainties. The largest errors in the lattice calculation are due to discretization errors and statistics. Improved calculations at finer lattice spacings and higher statistics are underway.

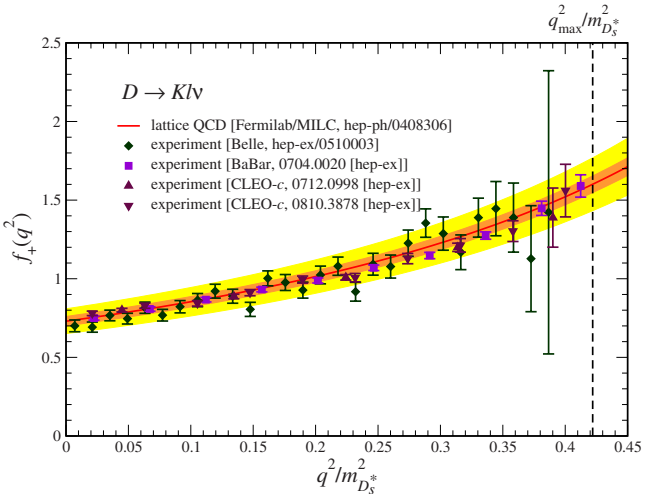

FIG. 28. (Color online) Comparison of the Fermilab/MILC/HPQCD lattice prediction for the normalized $D \to K\ell\nu$ form factor (bands) with the subsequent results from Belle (diamonds), BABAR (squares), and CLEO (triangles). The dark gray band is the 1σ error band from statistics, and the light gray band is the 1σ band for all errors added in quadrature. Adapted from Bernard *et al.*, 2009b. An earlier version appeared in Kronfeld (2006).

B. $B \to \pi\ell\nu$ and $|V_{ub}|$

Comparison between theory and experiment for $B \to \pi\ell\nu$ has been more troublesome than for other lattice calculations in CKM physics. Leptonic decays and $B\bar{B}$ mixing amplitudes are described by a single parameter. The semileptonic decays $B \to D^{(*)}\ell\nu$ and $K \to \pi\ell\nu$ can be described to high accuracy by a normalization and a slope. For $B \to \pi\ell\nu$, on the other hand, the form factors have a complicated q^2 dependence. Lattice data have covered only the low momentum, high q^2 end of the pion momentum spectrum, and errors are highly q^2 dependent and highly correlated between q^2 bins in both theory and experiment.

It has long been understood that analyticity, unitarity, and crossing symmetry can be used to constrain the possible shapes of form factors (Bourrely *et al.*, 1981; Boyd *et al.*, 1995; Lellouch, 1996; Boyd and Savage, 1997). This has been used recently to simplify the comparison of theory and experiment for $B \to \pi\ell\nu$. All form factors are analytic functions of q^2 except at physical poles and threshold branch points. In the case of the $B \to \pi l\nu$ form factors, $f(q^2)$ is analytic below the $B\pi$ production region except at the location of the B^* pole. The fact that analytic functions can always be expressed as convergent power series allows the form factors to be written in a particularly useful manner.

Consider mapping the variable q^2 onto a new variable, z, in the following way:

$$z(q^2,t_0) = \frac{\sqrt{1-q^2/t_+} - \sqrt{1-t_0/t_+}}{\sqrt{1-q^2/t_+} + \sqrt{1-t_0/t_+}}, \tag{173}$$

where $t_+ \equiv (m_B+m_\pi)^2$, $t_- \equiv (m_B-m_\pi)^2$, and t_0 is a free parameter. Although this mapping appears complicated, it actually has a simple interpretation in terms of q^2; this transformation maps $q^2 > t_+$ (the production region) onto $|z|=1$ and maps $q^2 < t_+$ (which includes the semileptonic region) onto real $z \in [-1,1]$. In the case of $B \to \pi\ell\nu$, the physical decay region is mapped into roughly $-0.3 < z < 0.3$. In terms of z, the form factors can be written in a simple form,

$$f(q^2) = \frac{1}{P(q^2)\phi(q^2,t_0)} \sum_{k=0}^{\infty} a_k(t_0) z(q^2,t_0)^k. \tag{174}$$

Most of the q^2 dependence is contained in the first two, perturbatively calculable, factors. The Blaschke factor $P(q^2)$ is a function that contains subthreshold poles and the outer function $\phi(q^2,t_0)$ is an arbitrary analytic function (outside the cut from $t_+ < q^2 < \infty$), which is chosen to give the series coefficients a_k a simple form; see Arnesen *et al.* (2005), Bailey *et al.* (2009), and references therein for the explicit forms of these expressions. With the proper choice of $\phi(q^2,t_0)$, analyticity and unitarity require the a_k to satisfy

$$\sum_{k=0}^{N} a_k^2 \lesssim 1. \tag{175}$$

The fact that $-0.3 < z < 0.3$ means that according to analyticity and unitarity only five or six terms are required to describe the form factors to 1% accuracy. (In $B \to D^{\{*\}}\ell\nu$ and $K \to \pi\ell\nu$, z is on the order of a few percent in the physics decay region, which is why these decays can be accurately described by just two parameters.) Becher and Hill (2006) have argued that the heavy-quark expansion implies that the bound is actually much tighter than analyticity and unitarity alone demand. They argued that $\Sigma_{k=0}^N a_k^2$ should be of order $(\Lambda_{\rm QCD}/m_b)^3$. This would lead to the expectation that only two or three terms will be sufficient to describe the form factors to 1% precision.

Calculations have been performed by the Fermilab Lattice and MILC Collaborations using Fermilab b quarks, and by the HPQCD Collaboration using NRQCD b quarks. Many of the details of the Fermilab/MILC calculations are the same as those for the Fermilab/MILC computation of heavy-light decay constants, described previously. For the semileptonic decays, only full QCD valence masses are used, as opposed to the partially quenched masses used in leptonic decays. The calculations used the $a \approx 0.12$ and 0.09 fm gauge field ensembles. The HMSχPT continuum and chiral extrapolations are done with the full NLO expressions plus additional NNLO analytic terms. These formulas allow the simultaneous interpolation in pion energy along with the continuum and chiral extrapolations, thus reducing the total systematic uncertainty.

Figure 29 shows the result of a fully correlated simultaneous z fit to the Fermilab/MILC lattice data and the BABAR 12-bin experimental results (Aubert *et al.*, 2007a), with $|V_{ub}|$ being a parameter in the fit.

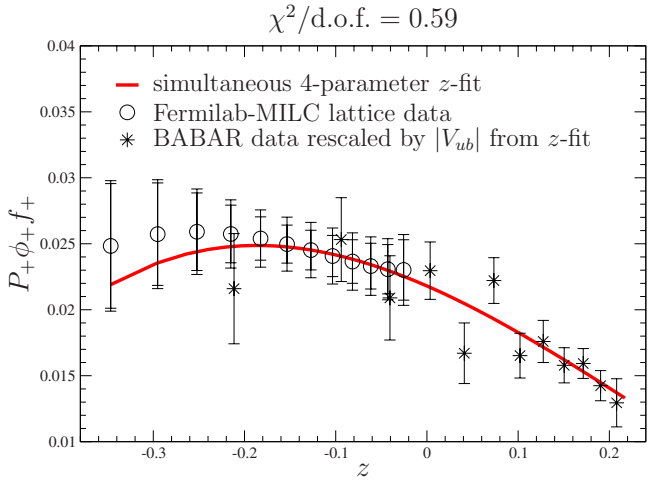

FIG. 29. (Color online) Results for the normalized $B\to\pi\ell\nu$ form factor $P_+\phi_+f_+$ from the Fermilab/MILC lattice calculations (circles) and BABAR (stars). The solid line is the results of a fully correlated simultaneous fit. Requiring that lattice and experiment have the same normalization yields $|V_{ub}|$. From Bailey *et al.*, 2009.

The resulting z-fit parameters are $a_0=0.0218\pm0.0021$, $a_1=-0.0301\pm0.0063$, $a_2=-0.059\pm0.032$, $a_3=0.079\pm0.068$, and

$$|V_{ub}| = (3.38 \pm 0.36) \times 10^{-3} \tag{176}$$

(Bailey *et al.*, 2009). The coefficients of z^n are indeed of order $(\Lambda_{\rm QCD}/m_b)^{3/2}$ as argued by Becher and Hill (2006). Because the ~11% uncertainty comes from a simultaneous fit of the lattice and experimental data, it contains both the experimental and theoretical errors in a way that is not simple to disentangle. If we make the assumption that the error in $|V_{ub}|$ is dominated by the most precisely determined lattice point, we can estimate that the contributions are roughly equally divided as ~6% lattice statistical and chiral extrapolation (combined), ~6% lattice systematic, and ~6% experimental. The largest lattice systematic uncertainties are heavy-quark discretization, the perturbative correction, and the uncertainty in $g_{B^*B\pi}$, all of which are about 3%. Our determination is $\sim(1-2)\sigma$ lower than most inclusive determinations of $|V_{ub}|$, where the values tend in the range $(4.0–4.5)\times10^{-3}$ (Di Lodovico, 2008). Our determination is, however, in good agreement with the preferred values from the CKMfitter Collaboration $[|V_{ub}|=(3.44^{+0.22}_{-0.17})\times10^{-3}$ (Charles *et al.*, 2008)] and the UTfit Collaboration $[|V_{ub}|=(3.48\pm0.16)\times10^{-3}$ (Silvestrini, 2008)].

Many of the details of the HPQCD calculation of $B\to\pi\ell\nu$ are the same as described previously for heavy-light decay constants. They used NRQCD b quarks and asqtad light quarks. On the coarse, $a\approx0.12$ fm ensembles, they performed the calculation on four unquenched ensembles plus an additional two partially quenched light quark masses on one ensemble. They also used full QCD data on two fine, $a\approx0.09$ fm ensembles in order to constrain the size of discretization effects. They used HMSχPT to perform the chiral extrapolations separately for various fiducial values of E_π after interpolating in E_π. They also showed that they obtained consistent results with simpler chiral extrapolation methods. They performed fits to their data using the z-fit method described above, as well as several other functional forms including the Becirevic-Kaidalov parametrization (Becirevic and Kaidalov, 2000) and Ball-Zwicky form (Ball and Zwicky, 2005). Note that they did not use a combined fit of experimental and lattice data using the z-fit method to extract $|V_{ub}|$. Rather, they used the various parametrizations to integrate the form factor $f_+(q^2)$ over q^2, and they showed that they obtain consistent results with all methods. Applying their results to 2008 data from the Heavy Flavor Averaging Group (HFAG) (Di Lodovico, 2008) yields

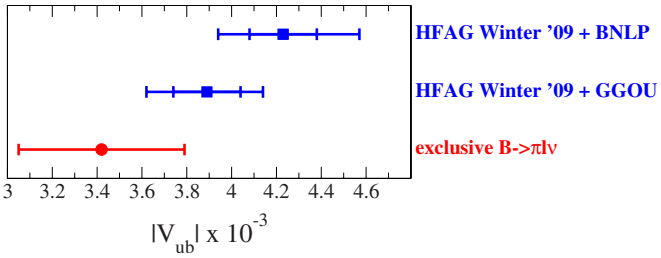

FIG. 30. (Color online) Values of $|V_{ub}|$ obtained from averaging the exclusive determinations compared with inclusive determinations using different theoretical inputs.

$$|V_{ub}| = (3.40 \pm 0.20^{+0.59}_{-0.39}) \times 10^{-3} \tag{177}$$

(Dalgic *et al.*, 2006), where the first error is experimental and the second is from the lattice calculation. Figure 30 shows the comparison between an average of the Fermilab/MILC and HPQCD results for $|V_{ub}|$ and two inclusive determinations of the same quantity using different theoretical inputs (Lange *et al.*, 2005; Gambino *et al.*, 2007).

C. $B\to D\ell\nu$ and $B\to D^*\ell\nu$

The CKM parameter $|V_{cb}|$ is important because it normalizes the unitarity triangle characterizing CP violation in the standard model, and must be determined precisely in order to constrain new physics in the flavor sector. The standard model prediction for kaon mixing contains $|V_{cb}|$ to the fourth power, for example. It is possible to obtain $|V_{cb}|$ from both inclusive and exclusive semileptonic B decays. The inclusive decays (Chay *et al.*, 1990; Bigi, Blok, *et al.*, 1992; Bigi, Uraltsev, and Vainshtein, 1992; Bigi, Shifman, *et al.*, 1993; Bigi, Shifman, and Uraltsev, 1997) make use of the heavy-quark expansion and perturbation theory, while the exclusive decays require the lattice calculation of the relevant form factors. Each of the exclusive channels $B\to D\ell\nu$ and $B\to D^*\ell\nu$ allows a lattice extraction of $|V_{cb}|$, and thus they provide a useful cross check, both of each other, and of the inclusive determination. We have so far considered the calculations of the necessary form factors only at zero recoil, as this leads to considerable simplification and

reduced theoretical errors (Hashimoto *et al.*, 2002).

The differential rate for the decay $B \to D\ell\nu$ is

$$\frac{d\Gamma(B \to D\ell\nu)}{dw} = \frac{G_F^2}{48\pi^3} m_D^3 (m_B + m_D)^2 (w^2-1)^{3/2} \times |V_{cb}|^2 |\mathcal{G}(w)|^2, \quad (178)$$

with

$$\mathcal{G}(w) = h_+(w) - [(m_B - m_D)/(m_B + m_D)] h_-(w), \quad (179)$$

where G_F is Fermi's constant, $h_+(w)$ and $h_-(w)$ are form factors, and $w = v' \cdot v$ is the velocity transfer from the initial state to the final state. The differential rate for the semileptonic decay $B \to D^*\ell\nu_\ell$ is

$$\frac{d\Gamma(B \to D^*\ell\nu)}{dw} = \frac{G_F^2}{4\pi^3} m_{D^*}^3 (m_B - m_{D^*})^2 \times \sqrt{w^2-1} |V_{cb}|^2 \chi(w) |\mathcal{F}(w)|^2, \quad (180)$$

where $\chi(w)|\mathcal{F}(w)|^2$ contains a combination of four form factors that must be calculated nonperturbatively. At zero recoil ($w=1$) we have $\chi(1)=1$, and $\mathcal{F}(1)$ reduces to a single form factor, $h_{A_1}(1)$.

We compute the form factor h_+ at zero recoil using the double ratio (Hashimoto *et al.*, 1999)

$$\frac{\langle D|\bar{c}\gamma_4 b|\bar{B}\rangle\langle\bar{B}|\bar{b}\gamma_4 c|D\rangle}{\langle D|\bar{c}\gamma_4 c|D\rangle\langle\bar{B}|\bar{b}\gamma_4 b|\bar{B}\rangle} = |h_+(1)|^2. \quad (181)$$

This double ratio has the advantage that the statistical errors and many of the systematic errors cancel. The discretization errors are suppressed by inverse powers of heavy-quark mass as $\alpha_s(\Lambda_{QCD}/2m_Q)^2$ and $(\Lambda_{QCD}/2m_Q)^3$ (Kronfeld, 2000), and much of the current renormalization cancels, leaving only a small correction that can be computed perturbatively (Harada, Hashimoto, *et al.*, 2002). The extra suppression of discretization errors by a factor of $\Lambda/2m_Q$ occurs at zero recoil for heavy-to-heavy transitions, and is a consequence of Luke's theorem (Luke, 1990).

In order to obtain h_-, it is necessary to consider nonzero recoil momenta. In this case, Luke's theorem does not apply, and the HQET power counting leads to larger heavy-quark discretization errors. However, this is mitigated by the small contribution of h_- to the branching fraction. The form factor h_- is determined from the double ratio (Hashimoto *et al.*, 1999)

$$\frac{\langle D|\bar{c}\gamma_j b|\bar{B}\rangle\langle D|\bar{c}\gamma_4 c|D\rangle}{\langle D|\bar{c}\gamma_4 b|\bar{B}\rangle\langle D|\bar{c}\gamma_j b|D\rangle} = \left[1 - \frac{h_-(w)}{h_+(w)}\right]\left[1 + \frac{h_-(w)}{2h_+(w)}(w-1)\right], \quad (182)$$

which is extrapolated to the zero-recoil point $w=1$. Combining the determinations of $h_+(1)$ and $h_-(1)$, we obtain the preliminary result $\mathcal{G}(1)=1.082(18)(16)$ (Okamoto, 2006), where the first error is statistical and the second is the sum of all systematic errors in quadrature, and where we have included a 0.7% QED correction (Sirlin, 1982). Combining this with the latest average from the HFAG, $\mathcal{G}(1)|V_{cb}| = (42.3 \pm 1.5) \times 10^{-3}$ (Di Lodovico, 2008), we obtain the preliminary result

$$|V_{cb}| = (39.1 \pm 1.4 \pm 0.9) \times 10^{-3}, \quad (183)$$

where the first error is experimental and the second is theoretical.

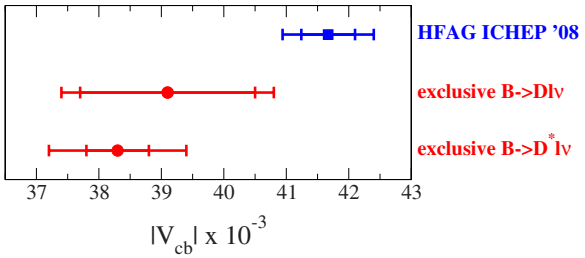

FIG. 31. (Color online) Values of $|V_{cb}|$ from the exclusive decays $B \to D\ell\nu$, $B \to D^*\ell\nu$, and the inclusive determination.

The form factor at zero-recoil needed for $B \to D^*\ell\nu$ is computed using the double ratio (Bernard *et al.*, 2009a)

$$\frac{\langle D^*|\bar{c}\gamma_j\gamma_5 b|\bar{B}\rangle\langle\bar{B}|\bar{b}\gamma_j\gamma_5 c|D^*\rangle}{\langle D^*|\bar{c}\gamma_4 c|D^*\rangle\langle\bar{B}|\bar{b}\gamma_4 b|\bar{B}\rangle} = |h_{A_1}(1)|^2, \quad (184)$$

where again, the discretization errors are suppressed by inverse powers of heavy-quark mass as $\alpha_s(\Lambda_{QCD}/2m_Q)^2$ and $(\Lambda_{QCD}/2m_Q)^3$, and much of the current renormalization cancels, leaving only a small correction that can be computed perturbatively (Harada, Hashimoto, *et al.*, 2002). We extrapolate to physical light quark masses using the appropriate rHMSχPT (Laiho and Van de Water, 2006).

Including a QED correction of 0.7% (Sirlin, 1982), we obtain $\mathcal{F}(1)=0.927(13)(20)$ (Bernard *et al.*, 2009a), where the first error is statistical and the second is the sum of systematic errors in quadrature. Taking the latest HFAG average of the experimental determination $\mathcal{F}(1)|V_{cb}| = (35.49 \pm 0.48) \times 10^{-3}$ (Di Lodovico, 2008), we obtain

$$|V_{cb}| = (38.3 \pm 0.5 \pm 1.0) \times 10^{-3}. \quad (185)$$

The experimental average includes all available measurements of $\mathcal{F}(1)|V_{cb}|$, but we point out that the global fit is not very consistent [$\chi^2/\text{dof} = 39/21$ (CL = 0.01%)]. The Particle Data Group handles this inconsistency by inflating the experimental error by 50% (Amsler *et al.*, 2008). The dominant lattice errors are discretization errors and statistics, and work is in progress to reduce these. Note that there is some tension between this and the inclusive determination of $|V_{cb}| = 41.6(6) \times 10^{-3}$ (Barberio *et al.*, 2007), as shown in Fig. 31.

IX. OTHER COMPUTATIONS USING MILC LATTICES

In this section, we describe a variety of additional results based on the MILC ensembles. Over 85 physicists outside the MILC Collaboration, at nearly 40 institutions throughout the world, have used the MILC configurations in their research. Their research covers a

broad range of topics including determinations of the strong coupling constant, the quark masses, the quarkonium spectrum and decay widths, the mass spectrum of mesons with a heavy quark and a light antiquark, the masses of baryons with one or more heavy quarks, studies of the weak decays of mesons containing heavy quarks, the mixing of neutral K and B mesons with their antiparticles, the quark and gluon structure of hadrons, the scattering lengths of pions, kaons and nucleons, the hadronic contributions to the muon anomalous magnetic moment, and meson spectral functions.

A. Determination of the strong coupling constant and the charm quark mass

1. The strong coupling constant from small Wilson loops

The HPQCD Collaboration used MILC lattice ensembles to compute the strong coupling constant α_s (Mason *et al.*, 2005; Davies *et al.*, 2008). They compute nonperturbatively (i.e., numerically on the MILC lattices) a variety of short-distance quantities Y, each of which has a perturbative expansion of the form

$$Y = \sum_{n=1}^{\infty} c_n \alpha_V^n(d/a), \tag{186}$$

where c_n and d are dimensionless a-independent constants and $\alpha_V(d/a)$ is the running QCD coupling constant in the so-called V scheme (Lepage and Mackenzie, 1993) for $n_f=3$ flavors of light quarks.

The coupling $\alpha_V(d/a)$ is determined by matching the perturbative expansion, Eq. (186), to the nonperturbative value for Y. Perturbatively converting from the V to the $\overline{\text{MS}}$ scheme and running up to the Z boson mass, switching to $n_f=4$ and then 5 at the c and b quark masses, gives a determination of the strong coupling constant $\alpha_{\overline{\text{MS}}}(M_Z,n_f=5)$.

The HPQCD Collaboration considered 22 short distance quantities Y, consisting of the logarithms of small Wilson loops and ratios of small Wilson loops (Davies *et al.*, 2008). The scales d in Eq. (186) are determined perturbatively by the method of Lepage and Mackenzie (1993), c_n for $n=1$, 2, and 3 were computed in lattice perturbation theory (Mason, 2004), and higher orders, up to $n=10$ were included in a constrained fitting procedure. In practice, $\alpha_V(d/a)$ for all different scales d/a used was run to a common scale of 7.5 GeV, and $\alpha_0 \equiv \alpha_V$ (7.5 GeV) was used as a free fitting parameter in the constrained fits for each of the observables.

Corrections to the perturbative form, Eq. (186), from condensates appearing in an operator product expansion (OPE) for short-distance objects, were included in the constrained fitting procedure. Other systematic errors such as finite lattice spacing effects and scale-setting uncertainties were considered. As their final result, the HPQCD Collaboration quotes

$$\alpha_V(7.5\ \text{GeV}, n_f=3) = 0.2120(28) \quad \text{and} \tag{187}$$

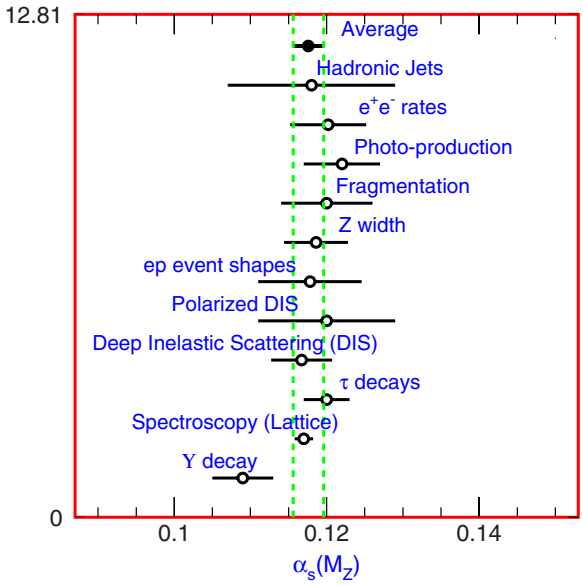

FIG. 32. (Color online) Summary of determinations of the strong coupling constant $\alpha_s(M_Z)$. The lattice QCD determination is the most precise one. From Amsler *et al.*, 2008.

$$\alpha_{\overline{\text{MS}}}(M_Z,n_f=5) = 0.1183(8).$$

The lattice determination of $\alpha_{\overline{\text{MS}}}(M_Z)$ is compared to other determinations in Fig. 32.

Maltman *et al.* (2008) performed a reanalysis of three of the short distance quantities used by the HPQCD Collaboration with the result

$$\alpha_{\overline{\text{MS}}}(M_Z,n_f=5) = 0.1192(11), \tag{188}$$

in good agreement with other next-to-next-to-leading-order determinations (Bethke, 2007). The two analyses differ in the way the perturbative running and matching was done, the value of the gluon condensate used in the OPE subtraction, the way the scale setting for each lattice ensemble is treated, and a slight difference of the value used for the scale setting. For more details see Maltman *et al.* (2008).

2. The charm quark mass and the strong coupling constant from current-current correlators

A new approach to extract α_s and to determine the charm quark mass m_c was used by Allison *et al.* (2008). It consists of comparing moments of charmonium current-current correlators computed nonperturbatively on the lattice with high-order continuum QCD perturbation theory. Vector current-current correlators have previously been used to obtain some of the most precise determinations of m_c from the experimental $e^+e^- \rightarrow$hadrons cross section (Kühn and Steinhauser, 2001; Kühn *et al.*, 2007). On the lattice, many types of correlators are available that are not accessible to experiment. In particular, the pseudoscalar current-current correlator can be computed to very high statistical accuracy, and the presence of a partially conserved axial vector current makes current renormalization unnecessary.

Consider the η_c current-current correlator

$$G(t) = a^6 \sum_{\vec{x}} (am_{0,c})^2 \langle 0|j_5(\vec{x},t) j_5(0,0)|0\rangle, \tag{189}$$

with moments

$$G_n = \sum_{t=-T/2}^{T/2} (t/a)^n G(t). \tag{190}$$

In the continuum limit, these moments can be computed perturbatively as

$$G_n(a=0) = g_n(\alpha_{\overline{\rm MS}}(\mu), \mu/m_c)/[(am_c(\mu))^{n-4}], \tag{191}$$

where g_n is known to $\mathcal{O}(\alpha_s^3)$ for $n=4$, 6, and 8. The approach to the continuum limit is improved by dividing by the tree-level results, and tuning errors in m_c and errors in the scale setting are ameliorated by multiplying with factors of the lattice η_c mass

$$R_4 = G_4/G_4^{(0)} \quad \text{and}$$
$$R_n = \left[\frac{(am_{\eta_c})}{(2am_{0c})}\right](G_n/G_n^{(0)})^{1/(n-4)} \quad \text{for } n>4. \tag{192}$$

The ratios R_n are extrapolated to the continuum limit using constrained fits. Comparing with continuum perturbative ratios $r_4 = g_4/g_4^{(0)}$ and $r_n = (g_n/g_n^{(0)})^{1/(n-4)}$ for $n>4$ allows $\alpha_{\overline{\rm MS}}$ to be extracted from R_4 and ratios R_n/R_{n+2} given the charm quark mass, and the charm quark mass can be obtained from the R_n with $n>4$, given the value of the strong coupling constant,

$$m_c(\mu) = \frac{m_{\eta_c}^{\rm exp}}{2} \frac{r_n(\alpha_{\overline{\rm MS}}, \mu/m_c)}{R_n(a=0)}. \tag{193}$$

Allison *et al.* (2008) used eight MILC lattice ensembles with four different lattice spacings. The charm correlators were computed using HISQ staggered quarks (Follana *et al.*, 2008, 2007). They obtained for m_c,

$$m_c(3\ \text{GeV}, n_f=4) = 0.986(10)\ \text{GeV} \quad \text{or}$$
$$m_c(m_c, n_f=4) = 1.268(9)\ \text{GeV}. \tag{194}$$

This is in good agreement, and about twice as precise as the best previous determination (Kühn *et al.*, 2007). They obtained for α_s

$$\alpha_{\overline{\rm MS}}(M_Z, n_f=5) = 0.1174(12), \tag{195}$$

in good agreement with the lattice determination described earlier and with other NNLO determinations (Bethke, 2007).

B. Onia and other heavy mesons

Heavy quarkonia were important in the early days of QCD because potential models could be used to approximately understand their dynamics before first-principles calculations were possible. The approximate validity of potential models helps in the selection of operators needed in the improvement program for quarkonia. The different methods for formulating heavy quarks on the lattice have various advantages and disadvantages for quarkonia. NRQCD employs the operators of the nonrelativistic, heavy-quark expansion. The operator expansion converges poorly for charmonium, and fails when $\Lambda_{\rm QCD}/m_q$ is not small. The Fermilab interpretation of Wilson fermions interpolates between a nonrelativistic type of action at $ma \gg 1$ and the usual Wilson-type action at $ma \ll 1$. It can be used for all ma, but has a more cumbersome set of operators, and has been less highly improved than other heavy-quark actions. The HISQ action is a light quark action that fails when $ma \gg 1$, but has been improved at tree level to high orders in ma and works well for ma close to 1.

1. Bottomonium with NRQCD heavy quarks

The HPQCD and UKQCD Collaborations have studied bottomonium spectroscopy on several MILC ensembles with lattice spacings $a \approx 0.18$, 0.12, and 0.09 fm (Gray *et al.*, 2005). Even on the finest of these ensembles, $am_b \sim 2$. They used lattice NRQCD to formulate the b quarks in the regime $am > 1$ (Thacker and Lepage, 1991; Lepage *et al.*, 1992; Davies *et al.*, 1994). The form of the action of NRQCD was shown in Eq. (144). The b quark is nonrelativistic inside the bottomonium bound states, with velocity $v_b^2 \sim 0.1$. NRQCD, as an effective field theory, can be matched order by order to full QCD in an expansion in v^2 and α_s. The action currently in use includes corrections of $\mathcal{O}(v^2)$ beyond leading order. Discretization errors have also been corrected to the same order in v^2.

The spin-averaged Υ mass splittings are expected to be quite insensitive to many lattice uncertainties, such as light sea-quark masses and normalization of correction operators. They are, therefore, expected to be calculable to high accuracy on the lattice. Gray *et al.* (2005) computed spin-averaged mass splittings, $1P$-$1S$ (i.e., $1\,^1P_1$-$1\,^3S_1$), $2S$-$1S$ (i.e., $2\,^3S_1$-$1\,^3S_1$), $2P$-$1S$, and $3S$-$1S$ in lattice units, and then use the experimental splittings to determine the lattice scale, as described in Sec. IV.B. Figure 33 shows the results, where the lattice spacing has been set by the $2S$-$1S$ splitting, and m_b has been set from M_Υ. The left-hand figure compares the results in GeV at two lattice spacings, for quenched and unquenched calculations. The right-hand figures show the splittings calculated on the lattice divided by experiment, in the quenched approximation (left narrow figure) and unquenched (right narrow figure). Clear disagreements with experiment in the quenched approximation are removed in the unquenched calculations.

As for the $\Upsilon(1S)$ hyperfine splitting, Gray *et al.* (2005) quoted $\Delta M = 61(14)$ MeV, corresponding to $r_1 \Delta M = 0.099(22)$, following an extrapolation to the physical point. This result is consistent with the recent observation of the η_b by the BABAR Collaboration (Aubert *et al.*, 2008, 2009) who found a splitting of 71(4) MeV from the $\Upsilon(1S)$.

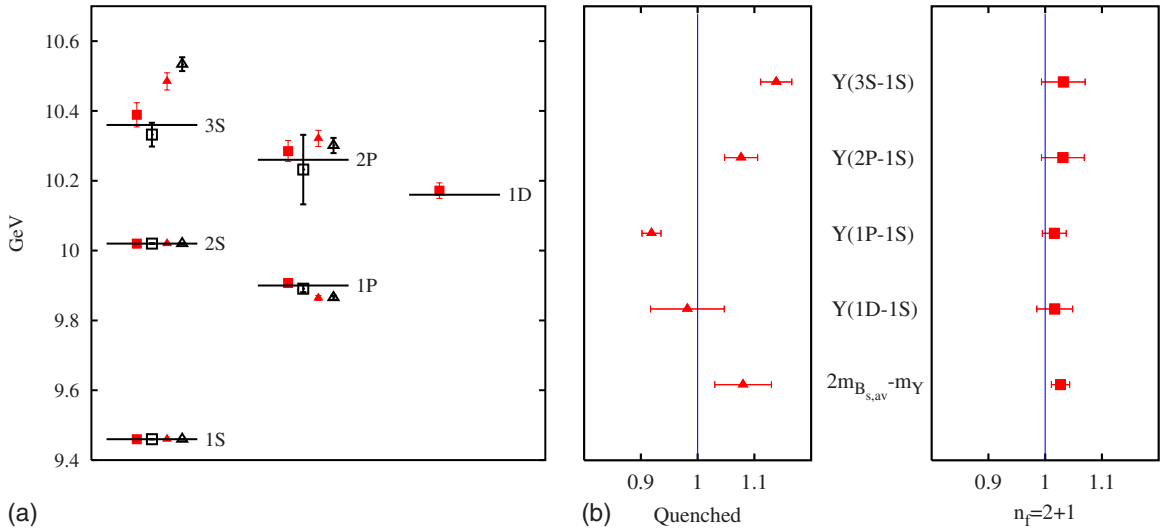

FIG. 33. (Color online) The Υ spectrum. Left: spin-averaged radial and orbital levels in GeV. Closed and open symbols are from coarse and fine lattices, respectively. Squares and triangles denote unquenched and quenched results, respectively. Lines represent experiment. Right: Spin-averaged mass differences from the same data divided by experiment, in the quenched approximation (left narrow figure) and unquenched (right narrow figure). From Gray *et al.*, 2005.

2. Onia with Fermilab quarks

The Fermilab and MILC Collaborations have computed charmonium and bottomonium masses on many of the MILC lattice ensembles with lattice spacings from $a \approx 0.18$ to $a \approx 0.09$ fm (di Pierro *et al.*, 2004; Gottlieb *et al.*, 2006a, 2006b). For the heavy charm and bottom quarks they use Fermilab quarks (El-Khadra *et al.*, 1997). An updated study is underway (Burch *et al.*, 2009).

In Fig. 34 (Burch *et al.*, 2009) all resulting masses for charmonium and bottomonium are shown as splittings from the spin-averaged $1S$ state. The chirally extrapolated values for each lattice spacing are plotted. They are compared with the experimental values given by solid lines, where the experimental results are known. In the cases where they are not known and are estimated from potential models, they are shown as dashed lines. The charmonium spectrum shows good agreement with experiment for the ground states, except for the χ_{c0}, which may be slightly heavier than the experimentally measured value. The excited S-wave states are also heavier than their respective experimental results, but one has to remember that these states are difficult to determine without careful consideration of finite-volume effects since they are close to the $D\bar{D}$ threshold. The bottomonium summary panel shows the general tendency of the result to approach the experimental values as the lattice spacing decreases.

Charm annihilation processes give a possible additional correction to the charmonium hyperfine splitting. DeTar and Levkova (2007) and Levkova and DeTar (2009) have started to study these quark-line disconnected diagrams using MILC ensembles with lattice spacings $a \approx 0.06$ and 0.09 fm. They used stochastic estimators with unbiased subtraction (Mathur and Dong, 2003) to compute the disconnected contribution to the η_c propagator. They found that annihilation processes *increase* the η_c mass a small amount [by 5.5(8) MeV for a fine lattice and 3.4(3) MeV for superfine], thereby de-

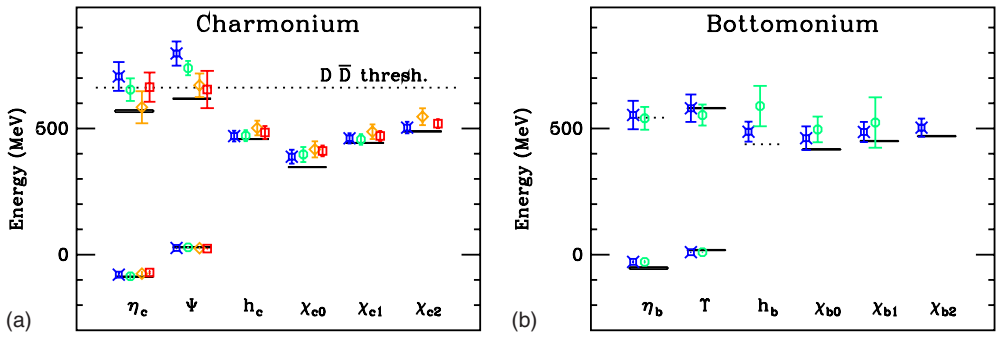

FIG. 34. (Color online) Summary of the charmonium (left) and bottomonium (right) spectra. The fine ensemble results are in fancy squares, the coarse in circles, the medium coarse are in diamonds, and the extracoarse results are in squares. Included in the error budget is an estimated systematic uncertainty from setting the heavy quark masses.

creasing slightly the predicted hyperfine splitting (Levkova and DeTar, 2009).

3. Charmonium with highly improved staggered quarks

The HPQCD and UKQCD Collaborations studied charmonium spectroscopy on MILC ensembles using the HISQ action for the valence quarks. They used MILC ensembles with lattice spacings $a \approx 0.12$ and 0.09 fm, where $am_c = 0.66$ and 0.43, respectively, to demonstrate the advantages of the HISQ action, and computed the charmonium spectrum, using the η_c mass to tune the input value for am_c. They corrected discretization errors in am up to order $(am)^4$, and showed that this produces a speed of light that is independent of p and equal to 1, within errors, in $E^2 = p^2c^2 + m^2c^4$. The results are shown in Fig. 7 of Follana *et al.* (2007). In particular, they found for the hyperfine mass splitting $M_{J/\psi} - M_{\eta_c} = 109(5)$ MeV. This result is the closest to the physical value of 117(1) MeV that has yet been achieved.

4. The B_c meson

The HPQCD, Fermilab Lattice and UKQCD Collaborations used MILC ensembles to predict the mass of the B_c meson (Allison *et al.*, 2005) before it was accurately measured. They used two different fermion actions for the heavy bottom and charm valence quarks, choosing the more optimal action in each case. For the bottom quark, they used lattice NRQCD (Thacker and Lepage, 1991; Lepage *et al.*, 1992; Davies *et al.*, 1994), because it has a better treatment of the v^4 interactions, where v is the velocity of the heavy quark. For the charm quark, they used the relativistic Fermilab action (El-Khadra *et al.*, 1997; Kronfeld, 2000), which treats higher-order effects in v^2 better. This is appropriate, since the velocity of the c quark in B_c is not particularly small, $v_c^2 \sim 0.5$.

Allison *et al.* (2005) calculated mass splittings, for which many of the systematic errors cancel, namely,

$$\Delta_{\psi Y} = m_{B_c} - (\bar{m}_\psi + m_\Upsilon)/2,$$
$$\Delta_{D_sB_s} = m_{B_c} - (\bar{m}_{D_s} + \bar{m}_{B_s}), \tag{196}$$

where $\bar{m}_\psi = (m_{\eta_c} + 3m_{J/\psi})/4$, $\bar{m}_{D_s} = (m_{D_s} + 3m_{D_s^*})/4$, and $\bar{m}_{B_s} = (m_{B_s} + 3m_{B_s^*})/4$ are spin-averaged masses. They found no visible lattice-spacing dependence using ensembles with $a \approx 0.18$, 0.12, and 0.09 fm. Extrapolating the $a \approx 0.12$ fm results linearly in the light sea-quark mass they obtained

$$\Delta_{\psi Y} = 39.8 \pm 3.8 \pm 11.2^{+18}_{-0}\ \text{MeV},$$
$$\Delta_{D_sB_s} = -[1238 \pm 30 \pm 11^{+0}_{-37}]\ \text{MeV}. \tag{197}$$

The errors are from statistics, tuning of the heavy-quark masses, and heavy-quark discretization effects. Since the statistical error on the first splitting is smaller, Allison *et al.* (2005) used that to predict the B_c mass as

$$m_{B_c} = 6304 \pm 4 \pm 11^{+18}_{-0}\ \text{MeV}. \tag{198}$$

Shortly after the lattice calculation was published, the CDF Collaboration announced their precise mass measurement (Abulencia *et al.*, 2006)

$$m_{B_c} = 6287 \pm 5\ \text{MeV}, \tag{199}$$

in good agreement with the lattice prediction, i.e., slightly more than 1σ away.

C. Heavy baryons

Baryons containing a heavy quark comprise a rich set of states. For example, there are currently 17 known charmed baryons (Amsler *et al.*, 2008). However, for bottom baryons, there are only a few known states. Thus, it is possible both to verify calculations by comparison with known masses and to make predictions for as yet undiscovered states.

Many of the heavy baryons contain one or more u or d quarks, thus requiring a chiral extrapolation. Although some early work on MILC configurations (Tamhankar, 2002; Gottlieb and Tamhankar, 2003) used clover quarks for u, d, and s, this limited how closely one could approach the chiral limit, and recent work has used staggered light quarks instead (Na and Gottlieb, 2006, 2007, 2009). The heavy quark is dealt with as in Sec. VII.A.

The pioneering lattice work on heavy baryons by the UKQCD Collaboration (Bowler *et al.*, 1996) considered two operators $O_5 = \varepsilon_{abc}(\psi_1^{aT} C\gamma_5 \psi_2^b)\Psi_H^c$ and $O_\mu = \varepsilon_{abc}(\psi_1^{aT} C\gamma_\mu \psi_2^b)\Psi_H^c$, where ε_{abc} is the Levi-Cività tensor, ψ_1 and ψ_2 are light valence quark fields for up, down, or strange quarks, Ψ_H is the heavy valence quark field for the charm or the bottom quark, C is the charge conjugation matrix, and a, b, and c are color indices. The former operator can be used to study the spin-1/2 baryons Λ_h and Ξ_h. The latter can be used, in principle, for both spin-1/2 and spin-3/2 baryons. However, with the current formalism, for operators with two staggered quarks, there are cancellations in the spin-3/2 sector and O_μ can only be used for spin-1/2 baryons (Na and Gottlieb, 2007). Gottlieb *et al.* (2008) considered the taste properties of staggered di-quark operators in much the way that Bailey (2007) studied staggered baryon operators. However, this method has not yet been applied in calculations. For states with two heavy quarks, both spin-1/2 and spin-3/2 states have been studied.

Another issue when dealing with states containing heavy quarks is the distinction between the rest and kinetic masses (see Sec. VII). Calculation of kinetic masses requires looking at states with nonzero momentum and fitting a dispersion relation. This has not yet been done for the heavy baryons, which means that we are restricted to reporting mass splittings.

So far ensembles with three lattice spacings have been studied (Na and Gottlieb, 2009). With $a \approx 0.15$ fm, three ensembles with $m_l/m_s = 0.2$, 0.4, and 0.6 were used. With $a \approx 0.12$ fm, $m_l/m_s = 0.007$, 0.01, and 0.02, and with $a \approx 0.09$ fm, only $m_l/m_s = 0.2$ and 0.4 were studied. Seven

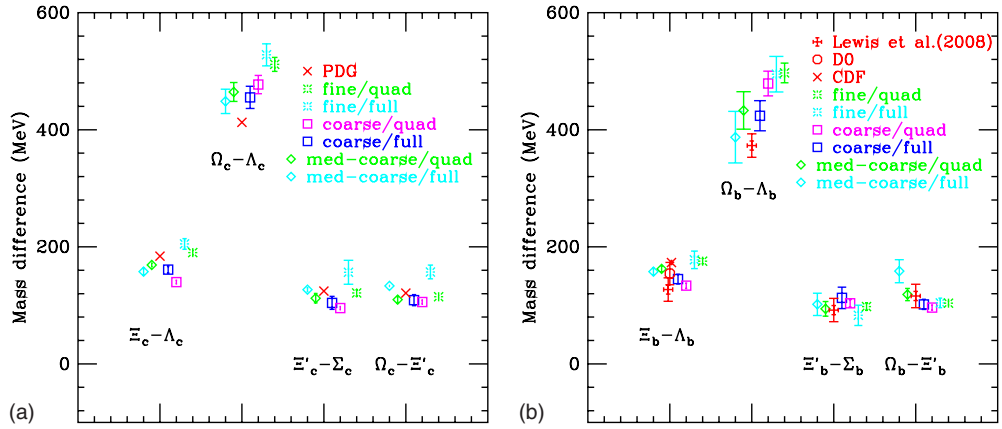

FIG. 35. (Color online) Independent mass differences of $J^P=\frac{1}{2}^+$ singly charmed baryons (a) and singly bottom baryons (b). From Na and Gottlieb, 2009.

to nine light quark masses are used to allow for chiral extrapolation. The charm and bottom quark masses are the same as in the meson work. Since mass splittings are desired, ratios of hadron propagators are fit in preference to fitting each hadron and subtracting the masses. For baryons with a heavy quark, rSχPT has not been worked out yet, so the chiral extrapolation is based on a polynomial in the valence and sea masses,

$$P_{\text{quad}} = c_0 + c_1 m_l + c_2 m_l^2 + c_3 m_s + c_4 m_{\text{sea}}, \tag{200}$$

where c_0 to c_4 are the fitting parameters, m_l is the light valence quark mass, m_s is the strange valence quark mass, and m_{sea} is the light sea-quark mass. These fits are denoted quad in the figures. Alternative chiral extrapolations use only the full QCD points, i.e., those in which the valence and sea light quark masses are equal. These are denoted full in the figures.

For the singly-charmed baryons in Fig. 35(a), three of the four differences are in good agreement with the experimental results. The result that is not in good agreement is one that involves one hadron from O_5 and one from O_μ. The other differences come from particles that are both determined using the same operator. This behavior is a mystery.

In Fig. 35(b), we consider the singly-bottom baryons and find good agreement for the one observed difference for $\Xi_b-\Lambda_b$. Also shown is the comparison with a recent lattice calculation of Lewis and Woloshyn (2009). The large value for the $\Omega_b-\Lambda_b$ splitting is again noticeable.

In Fig. 36, we compare with the results of Lewis *et al.* (2001) and Lewis and Woloshyn (2009) for both spin-1/2 and spin-3/2 baryons. The earlier calculation of charmed baryons used quenched anisotropic lattices generated with an improved gauge action. The more recent calculation of bottom baryons uses configurations containing the effects of dynamical quarks. In order to compare the two calculations, and because kinetic masses are not available in the calculation on MILC configurations, a constant was added to the static masses that depends on lattice spacing and whether the state contains charm or bottom quarks, but not upon spin or light quark content.

There are a number of ways to improve upon the current work including increasing statistics, extending the calculations to the finer ensembles, studying the kinetic masses and studying new operators that will allow us to explore the properties of the spin-3/2 baryons. It is also

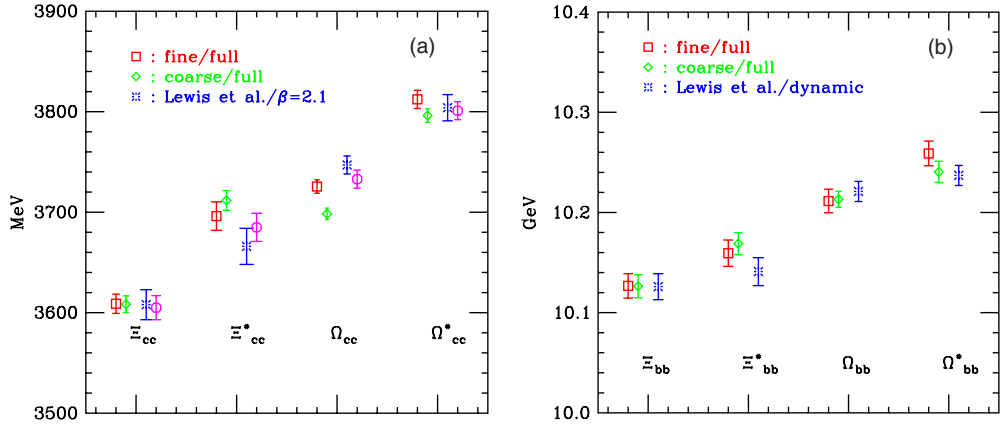

FIG. 36. (Color online) The mass spectrum of doubly charmed (a) and bottom (b) baryons. The error bars are statistical only. From Na and Gottlieb, 2009.

possible to use HISQ quarks for all of u, d, s, and c quarks to explore the charm sector using only staggered operators.

D. K^0-$\bar{K}^0$ mixing: B_K

Experimental measurements of the size of indirect CP violation in the neutral kaon system ε_K can be combined with theoretical input to constrain the apex of the CKM unitarity triangle (Buras, 1998). Because ε_K has been measured to better than a percent accuracy (Amsler *et al.*, 2008), the dominant sources of error in this procedure are the theoretical uncertainties in the CKM matrix element $|V_{cb}|$, which enters the constraint as the fourth power, and in the lattice determination of the nonperturbative constant B_K.

The kaon bag parameter B_K encodes the hadronic contribution to K^0-$\bar{K}^0$ mixing (Buchalla *et al.*, 1996; Buras, 1998),

$$B_K(\mu) \equiv \frac{\langle \bar{K}^0 | Q_{\Delta S=2}(\mu) | K^0 \rangle}{(8/3)\langle \bar{K}^0 | \bar{s}\gamma_0\gamma_5 d | 0 \rangle \langle 0 | \bar{s}\gamma_0\gamma_5 d | K^0 \rangle}, \tag{201}$$

where $Q_{\Delta S=2}$ is the effective weak four-fermion operator

$$Q_{\Delta S=2}(x) = [\bar{s}\gamma_\mu d]_{V-A}(x)[\bar{s}\gamma_\mu d]_{V-A}(x) \tag{202}$$

and μ is a renormalization scale. The dependence on μ cancels that of a Wilson coefficient $C(\mu)$ that multiplies $B_K(\mu)$ in physical observables such as the mass difference between K_S and K_L. The denominator in Eq. (201) is the value of the matrix element with vacuum saturation of the intermediate state. Often quoted is the value of the renormalization group invariant form of B_K, $\hat{B}_K$, defined by

$$\hat{B}_K = C(\mu) B_K(\mu). \tag{203}$$

Gamiz *et al.* (2006) carried out a calculation of B_K using two MILC ensembles with lattice spacing $a \approx 0.12$ fm. They employed asqtad valence quarks with valence kaons made of degenerate quarks of mass $m_s/2$. Using one-loop matching with the coupling taken as $\alpha_V(1/a)$ they found the following value for B_K in the naive dimensional regularization scheme:

$$B_K^{\overline{\text{MS}}\text{-}NDR}(2\ \text{GeV}) = 0.618(18)(19)(30)(130), \tag{204}$$

where the errors are from statistics, the chiral extrapolation (Van de Water and Sharpe, 2006), discretization errors, and the perturbative conversion to the $\overline{\text{MS}}$-NDR scheme. The value Eq. (204) corresponds to $\hat{B}_K = 0.83 \pm 0.18$. The error is dominated by the uncertainty from $\mathcal{O}(\alpha_s^2)$ corrections to the perturbative lattice-to-continuum matching.

Because the matching coefficients are known only to one loop, the result in Eq. (204) is not competitive with the published domain-wall fermion calculation by the RBC and UKQCD Collaborations, in which the operator renormalization is done nonperturbatively using the method of Rome-Southampton (Martinelli *et al.*, 1995) and mixing is suppressed due to the approximate chiral symmetry. They obtained, using a single, comparable lattice spacing $\hat{B}_K = 0.720 \pm 0.019$ (Allton *et al.*, 2008), where the dominant uncertainty is due to discretization errors, and is estimated to be ~4% from the scaling behavior of quenched data.

Recently Aubin, Laiho, and Van de Water obtained the first unquenched determination of B_K at two lattice spacings using domain-wall valence quarks on the MILC ensembles (Aubin *et al.*, 2010). Because dynamical domain-wall lattice simulations are computationally expensive, this mixed-action approach is an affordable compromise that takes advantage of the best properties of both fermion formulations. Since the MILC ensembles are available at several lattice spacings with light pion masses and large physical volumes, this allows for good control of the chiral extrapolation in the sea sector and the continuum extrapolation. Domain-wall fermions do not carry taste quantum numbers, so there is no mixing with operators of other tastes. Furthermore, the approximate chiral symmetry of domain-wall fermions suppresses the mixing with wrong-chirality operators and allows the use of nonperturbative renormalization in the same manner as in the purely domain-wall case. Finally, the expression for B_K in mixed action χPT contains only two more parameters than in continuum χPT (Aubin *et al.*, 2007b), both of which are known and are, therefore, not free parameters in the chiral and continuum extrapolation. Aubin *et al.* (2010) obtained

$$B_K^{\overline{\text{MS}}\text{-}NDR}(2\ \text{GeV}) = 0.527(6)(20), \tag{205}$$

where the first error is statistical and the second is systematic. With data on the coarse and fine MILC lattices, Aubin *et al.* (2010) found that the discretization errors in B_K are small. The largest error in B_K is ~3% and is from the renormalization factor Z_{B_K}, which is computed nonperturbatively in the RI/MOM scheme, but must be converted to the $\overline{\text{MS}}$ scheme using one-loop continuum perturbation theory.

Bae *et al.* (2009) also computed B_K with a mixed-action approach using HYP-smeared staggered valence quarks (Hasenfratz and Knechtli, 2001) on the MILC ensembles. They have preliminary data on the coarse, fine, and superfine MILC ensembles and are computing Z_{B_K} nonperturbatively in the RI/MOM scheme using the Rome-Southampton method. When completed, their result should be competitive with those of RBC/UKQCD and Aubin *et al.* (2010).

E. B^0-$\bar{B}^0$ mixing

The mass differences between the heavy and light B_q^0, $q = d, s$, are given in the standard model by (Buras *et al.*, 1990)

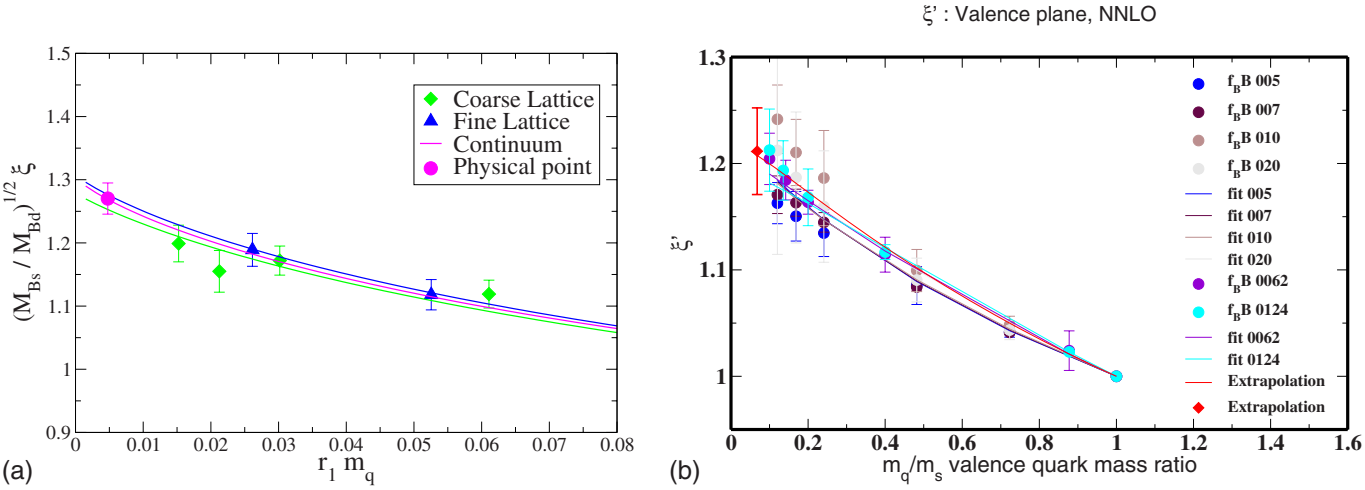

FIG. 37. (Color online) The ratio $\xi' = \xi\sqrt{M_{B_s}/M_{B_d}} = f_{B_s}\sqrt{M_{B_s}B_{B_s}}/f_{B_d}\sqrt{M_{B_d}B_{B_d}}$ as a function of the light valence quark mass together with rSχPT fits and the chiral and continuum extrapolation. The left panel is from the HPQCD Collaboration (Gamiz *et al.*, 2009) and the right panel from the Fermilab/MILC Collaboration (Evans *et al.*, 2009).

$$\Delta M_q^{\text{theor}} = (G_F^2 M_W^2/6\pi^2)|V_{tq}^* V_{tb}|^2 \times \eta_2^B S_0(x_t) M_{B_q} f_{B_q}^2 \hat{B}_{B_q}, \tag{206}$$

where η_2^B is a perturbative QCD correction factor and S_0 is the Inami-Lim function of $x_t = m_t^2/M_W^2$. $\hat{B}_{B_q}$ is the renormalization group invariant B_q^0 bag parameter that can be computed in lattice QCD.

The four-fermion operators whose matrix elements between B_q^0 and $\bar{B}_q^0$ are needed to study B_q^0 mixing in the standard model are

$$\begin{aligned} OL^q &\equiv [\bar{b}^a q^a]_{V-A}[\bar{b}^c q^c]_{V-A}, \\ OS^q &\equiv [\bar{b}^a q^a]_{S-P}[\bar{b}^c q^c]_{S-P}, \\ O3^q &\equiv [\bar{b}^a q^c]_{S-P}[\bar{b}^c q^a]_{S-P}, \end{aligned} \tag{207}$$

where a,c are color indices. The leading-order B_q^0-$\bar{B}_q^0$ mixing matrix element is parametrized by the product $f_{B_q}^2 B_{B_q}^{\overline{\text{MS}}}$,

$$\langle \bar{B}_q^0 | OL^q | B_q^0 \rangle^{\overline{\text{MS}}}(\mu) = \tfrac{8}{3} M_{B_q}^2 f_{B_q}^2 B_{B_q}^{\overline{\text{MS}}}(\mu), \tag{208}$$

where $B_{B_q}^{\overline{\text{MS}}}$ is related to $\hat{B}_{B_q}$ in Eq. (206) in an analogous manner to Eq. (203). Beyond tree level, the operator OL^q mixes with OS^q, both on the lattice and in the continuum. Including the one-loop correction, the renormalized matrix element is given by

$$\frac{a^3}{2M_{B_q}} \langle OL^q \rangle^{\overline{\text{MS}}}(\mu) = [1 + \alpha_s \cdot \rho_{LL}(\mu, m_b)] \langle OL^q \rangle^{\text{lat}}(a) + \alpha_s \cdot \rho_{LS}(\mu, m_b) \langle OS^q \rangle^{\text{lat}}(a). \tag{209}$$

The operator $O3^q$ is only needed to compute the width difference $\Delta\Gamma_q$ (Lenz and Nierste, 2007).

The HPQCD Collaboration calculated B_{B_q}, with $q = d,s$ on four MILC ensembles with $a \approx 0.12$ fm and two ensembles with $a \approx 0.09$ fm, using an asqtad light valence quark and lattice NRQCD for the bottom quark (Dalgic *et al.*, 2007; Gamiz *et al.*, 2009). With NRQCD for the heavy quark, a dimension seven operator contributes to the relevant matrix element at order $\mathcal{O}(\Lambda^{\text{QCD}}/M_B)$, which was also taken into account. The HPQCD Collaboration found (Gamiz *et al.*, 2009)

$$\begin{aligned} f_{B_s}\sqrt{\hat{B}_{B_s}} &= 0.266(6)(17)\ \text{GeV}, \\ f_{B_d}\sqrt{\hat{B}_{B_d}} &= 0.216(9)(12)\ \text{GeV}, \end{aligned} \tag{210}$$

and for the ratio

$$\xi = f_{B_s}\sqrt{B_{B_s}}/f_{B_d}\sqrt{B_{B_d}} = 1.258(25)(21), \tag{211}$$

where the errors are from statistics plus chiral extrapolation and from all other systematic errors added in quadrature, respectively. The chiral and continuum extrapolation is shown in the left panel of Fig. 37. Using the result in Eq. (211) and the experimentally measured mass differences ΔM_x, $x = s,d$ (Amsler *et al.*, 2008) they found

$$|V_{td}|/|V_{ts}| = 0.214(1)(5), \tag{212}$$

where the errors are experimental and theoretical, respectively.

A similar calculation is being performed by the Fermilab Lattice and MILC Collaborations (Evans *et al.*, 2007, 2009). They used Fermilab fermions for the heavy quarks, and, like HPQCD, asqtad fermions for the light valence quarks. The preliminary chiral and continuum extrapolation is shown in the right panel of Fig. 37. As a preliminary result they found $\xi = 1.205(52)$, with the statistical and systematic errors added in quadrature (Evans *et al.*, 2009).

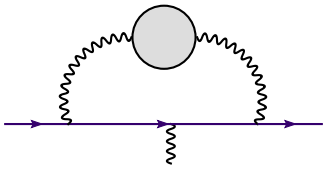

FIG. 38. (Color online) The lowest-order diagram for the QCD correction to the muon anomalous magnetic moment at $\mathcal{O}(\alpha^2)$. The bubble represents all possible hadronic states. From Aubin and Blum, 2007.

F. Hadronic contribution to the muon anomalous magnetic moment

One of the most precisely measured quantities, and hence an astonishingly accurate test of QED, is the anomalous magnetic moment of the muon, $a_\mu=(g-2)/2$. The QED contribution is known to four loops, with the five-loop term having been estimated; see Jegerlehner (2007, 2008) for recent reviews. With the experimental precision to which a_μ is known, QCD corrections are important at leading order via the QCD contribution to the vacuum polarization, shown in Fig. 38.

This leading contribution can be estimated from the experimental values of the $e^+e^-\to$hadrons total cross section, $a_\mu^{\mathrm{HLO}}=(692.1\pm5.6)\times10^{-10}$ (Jegerlehner, 2007, 2008). Using this value the difference between the experimental and theoretical value is

$$\delta a_\mu = a_\mu^{\mathrm{exp}} - a_\mu^{\mathrm{the}} = (287\pm91)\times10^{-11}, \tag{213}$$

about a 3.1σ effect and a possible hint at effects from physics beyond the standard model. The leading hadronic contribution can also be estimated from $\tau\to\nu_\tau+$hadrons, giving a result of $10\text{–}20\times10^{-10}$ higher than from the e^+e^- cross section, but this estimate is on somewhat weaker footing due to isospin-breaking effects. A purely theoretical calculation of a_μ^{HLO} is thus desirable.

The muon anomalous magnetic moment can be extracted from the full muon-photon vertex. The first effects from QCD, at order $\mathcal{O}(\alpha^2)$, are shown in Fig. 38, and can be computed from the vacuum polarization of the photons $\Pi(q^2)$ via (Blum, 2003)

$$a_\mu^{\mathrm{HLO}} = \left(\frac{\alpha}{\pi}\right)^2 \int_0^\infty dq^2 f(q^2)\Pi(q^2), \tag{214}$$

with the kernel $f(q^2)$ given by Blum (2003). The kernel $f(q^2)$ diverges as $q^2\to0$. This makes a precise calculations of $\Pi(q^2)$ at low momentum necessary, and, in particular, makes perturbative computations unreliable.

Aubin and Blum (2007) described such a calculation based on three MILC ensembles with lattice spacing $a\approx0.09$ fm, and three different light quark masses. The vacuum polarization $\Pi(q^2)$ is computed from the correlator of the electromagnetic current in terms of quark fields. Aubin and Blum used rSχPT to fit $\Pi(q^2)$ at low q (see Fig. 39), and used the result in the integral in Eq. (214).

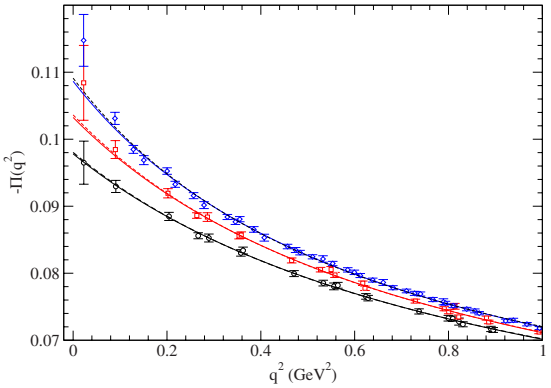

FIG. 39. (Color online) Two different rSχPT fits to $\Pi(q^2)$ for three light masses: $am_l=0.0031$ (diamonds), 0.0062 (squares), and 0.0124 (circles) with $am_s=0.031$. From Aubin and Blum, 2007, which contains the details.

Finally, they extrapolated to the physical light quark mass, obtaining

$$a_\mu^{\mathrm{HLO}} = (721\pm15)\times10^{-10} \quad \text{and}$$
$$a_\mu^{\mathrm{HLO}} = (748\pm21)\times10^{-10} \tag{215}$$

with a linear and quadratic fit, respectively. The errors are statistical only. Systematic errors in Eq. (215) other than due to the quark mass extrapolation come from finite lattice spacing and finite volume effects. Given this, the lattice result should be taken as in broad agreement with the estimate from the e^+e^- cross section. Further improvements need to be made before the lattice calculation becomes competitive with other determinations.

G. Quark and gluon propagators in Landau gauge

Quark and gluon propagators contain perturbative and nonperturbative information about QCD. Quark propagators play a crucial role in hadron spectroscopy and the study of three- and four-point functions used in form factor and matrix element calculations. The propagators are not gauge invariant, and thus have to be studied in a fixed gauge, usually the Landau gauge. Nevertheless, they contain gauge independent information on confinement, dynamical mass generation and spontaneous chiral symmetry breaking. Quark and gluon propagators can be studied on the lattice. They are often treated semianalytically in the context of Dyson-Schwinger equations, see Fischer (2006) and Roberts (2008) for recent reviews.

The Landau gauge gluon propagator has been studied in full QCD using MILC lattices by Bowman *et al.* (2004, 2007). In the continuum, the Landau gauge gluon propagator has the tensor structure

$$D^{ab}_{\mu\nu}(q) = [\delta_{\mu\nu} - (q_\mu q_\nu)/q^2]\delta^{ab}D(q^2), \tag{216}$$

where at tree level $D(q^2)=1/q^2$. The bare propagator is related to the renormalized propagator $D_R(q^2;\mu)$ by the renormalization condition

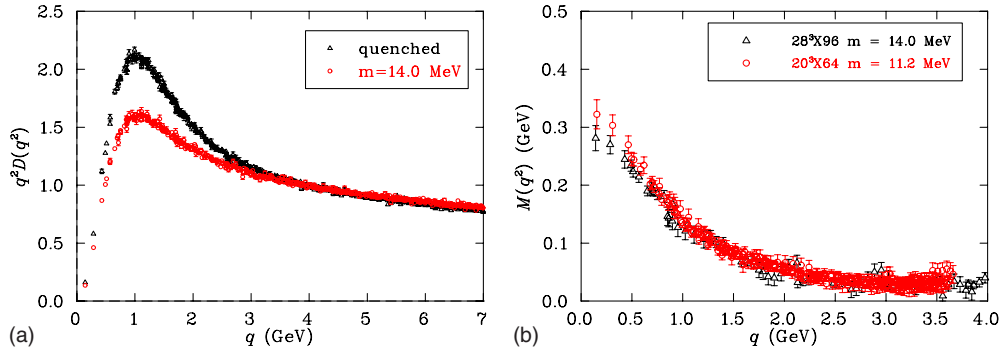

FIG. 40. (Color online) The gluon dressing function $q^2D(q^2)$ for quenched and dynamical configurations with $a \approx 0.09$ fm, from Bowman *et al.*, 2007 (left), and the quark mass function for light sea-quark mass in full QCD at $a \approx 0.12$ and 0.09 fm, from Parappilly *et al.*, 2006 (right).

$$D(q^2,a) = Z_3(a;\mu)D_R(q^2;\mu),$$
$$D_R(q^2;\mu)|_{q^2=\mu^2} = 1/\mu^2. \tag{217}$$

The gluon propagator in full QCD is somewhat less enhanced for momenta around 1 GeV than the quenched propagator, see Fig. 40 (left), and shows good scaling behavior (Bowman *et al.*, 2007). The gluon spectral function shows clear violations of positivity in qualitative agreement with Dyson-Schwinger equation studies [see Fischer (2006), and references therein].

The quark propagator has been studied in full QCD using MILC lattice ensembles with lattice spacings $a \approx 0.12$ and 0.09 fm by Bowman *et al.* (2005), Furui and Nakajima (2006), and Parappilly *et al.* (2006). The bare propagator can be parametrized, and related to the renormalized propagator, by

$$S(p^2;a) = Z(p^2;a)[i\gamma\cdot p + M(p^2)]^{-1}$$
$$= Z_2(a;\mu)S_R(p^2;\mu), \tag{218}$$

where $Z_2(a;\mu) = Z(p^2;a)|_{p^2=\mu^2}$ and the mass function $M(p^2)$ is renormalization point independent. Its asymptotic behavior as $p \to \infty$ is related via the OPE to the RGI quark mass and the chiral condensate, see, e.g., Bowman, Heller, *et al.* (2005).

The quark mass function for light sea-quark mass in full QCD simulations at two different lattice spacings is shown in Fig. 40 (right). It shows good scaling and clear indication of dynamical mass generation ("constituent mass") at low momenta.

H. Further uses of MILC lattices

Besides the calculations previously described, the MILC lattice ensembles have been used in other QCD calculations. These include the study of hadronic scattering lengths and n-body interactions, reviewed by Beane, Orginos, *et al.* (2008). Furthermore, computations of nucleon structure, moments of parton and generalized parton distribution functions, axial nucleon couplings, electromagnetic form factors, and nucleon transition amplitudes have been done using MILC lattice ensembles; see Orginos (2006), Hägler (2007), and Zanotti (2009) for recent reviews of lattice computations of these quantities.

X. FURTHER IMPROVEMENTS: A LOOK TO THE FUTURE

While the lattice QCD simulations described here are quite mature, the errors of many of the observables computed can be reduced in various ways. Many of the calculations have omitted some of the available MILC ensembles, in particular the more challenging ones with small lattice spacings. Sometimes, not all available configurations in an ensemble have been analyzed. Electromagnetic effects, where needed, have been taken from nonlattice estimates (see Sec. VI). They can be included directly in lattice simulations. Discretization effects coming from the fermion actions used can be further reduced using improvements to the Fermilab action for heavy quarks, and using highly improved staggered quarks for both valence and sea light quarks. These improvements are outlined in this section.

A. Impact of new ensembles

The superfine ($a \approx 0.06$ fm) and ultrafine ($a \approx 0.045$ fm) ensembles listed in Table I were recently completed, as was the coarse ($a \approx 0.12$ fm) ensemble with three degenerate light quarks. The fine ensembles with $m_l/m_s = 0.05$ and with three degenerate light quarks are still running, but should be completed soon. We have presented here some preliminary results from the superfine ensembles for the hadron spectrum, the light pseudoscalar mesons, and the topological susceptibility, and the HPQCD/UKQCD Collaboration has recently used some of the superfine ensembles in its studies of charmed physics (Davies, 2008); however, the physics analysis of the new ensembles is in a very early stage. When it is completed, we expect these ensembles to have a major impact on many of the calculations described above.

As indicated earlier, the leading finite lattice spacing artifacts for the asqtad action are of order $a^2/\ln(a)$. So

these artifacts for the superfine and ultrafine ensembles are down from those of the fine ensembles by factors of 2.6 and 5.2, respectively. As one can see from Figs. 14, 19, and 24, results obtained to date from the superfine ensembles are close to the rSχPT continuum extrapolations, which should reduce discretization errors in calculations that make use of them. Furthermore, as shown in Fig. 6, the decrease in taste splitting among the pions with decreasing lattice spacing is consistent with $a^2/\ln(a)^2$, as expected. Thus, this major source of systematic error will be significantly reduced using superfine ensembles.

The $a \approx 0.045$ fm, $m_l = 0.2 m_s$ ensemble will provide an anchor point for extrapolations to the continuum limit, and is particularly important for calculations which use the Fermilab method for heavy valence quarks. For many of these quantities the discretization errors in the heavy-quark action are the largest single source of systematic error. Although the size of heavy-quark discretization errors can be estimated using power-counting arguments, the precise form of the lattice spacing dependence is not explicitly known. It is thus important to have a range of lattice spacings in order to study the heavy-quark discretization effects. The heavy-quark errors decrease as $a/\ln(a)$ at the worst, so we expect the 0.045 fm ensemble to reduce the heavy-quark errors by a factor of 2 in quantities of interest involving B and D mesons, which thus far have only been computed on ensembles with lattice spacings $a \approx 0.09$ fm and larger. The reduction of the heavy-quark discretization errors does not require the full set of light-quark masses that we calculated at coarser lattice spacings; thus, we generated only one ensemble at $a \approx 0.045$ fm. By including the superfine and ultrafine ensembles into our work on heavy-light mesons, in conjunction with improving the statistics, we expect to determine the leptonic decay constants, the mixing parameters, and the corresponding semileptonic form factors to an accuracy of better than 5%.

The physical strange quark mass is not light enough for chiral perturbation theory to converge rapidly in its vicinity. To anchor chiral fits and to test the convergence of chiral perturbation theory, it is therefore extremely helpful to have ensembles with the strange sea-quark mass held fixed at a value well below the physical strange quark mass. Furthermore, with three dynamical quark flavors, there are two interesting chiral limits to be considered: the two-flavor limit, in which the u and d quarks become massless while the s stays at its physical mass, and the three-flavor chiral limit, where all three quarks become massless. The difference of various quantities in these two limits is an important probe of the nature of chiral symmetry breaking in QCD. The extrapolation to $m_s = 0$ necessary for the three-flavor chiral limit is a long one, with attendant large errors. The new ensembles with three degenerate light quarks were created to help address these issues. We estimate that incorporating all superfine ensembles into the analysis, as well as all configurations with the strange sea-quark mass held fixed below its physical value, will allow us to reduce the systematic errors on f_π and f_K to 2% or better, and should dramatically reduce the errors in low-energy constants and quantities such as the ratio of the two-flavor to three-flavor condensates $\langle \bar{u}u \rangle_2 / \langle \bar{u}u \rangle_3$. This would be an important milestone for lattice QCD calculations. We also expect corresponding improvements in other physical quantities of interest. In particular, our evaluation of $|V_{us}|$ should become significantly more accurate than the current world average.

B. Electromagnetic and isospin breaking effects

Most lattice calculations have not included electromagnetic or isospin breaking effects. However, as the precision of calculations increases, including these effects will become increasingly important. In fact, we have already seen in Sec. VI that electromagnetic effects are important in the determination of the u and d quark masses. Another interesting challenge for lattice QCD would be to determine the proton-neutron mass difference, which will require accounting for the differences of both the u and d quark masses and their charges.

The pioneering work by Duncan *et al.* (1996, 1997) regarding electromagnetic effects was done with quenched U(1) and quenched SU(3) fields. More recently, the RBC Collaboration has been pursuing such calculations but with domain-wall dynamical quarks. Yamada *et al.* (2006) and Blum *et al.* (2007) calculated electromagnetic effects on π and K meson masses in $N_f = 2$ configurations. Beane, Orginos, and Savage (2007) used MILC configurations with $a \approx 0.12$ fm to study isospin breaking for the nucleons using domain-wall valence quarks.

Electromagnetic effects in lowest order chiral perturbation theory were first studied some 40 years ago by Dashen (1969). A key result known as Dashen's theorem is that electromagnetic splittings of the pions and kaons are equal at this order, i.e.,

$$\Delta M_D^2 = \Delta M_K^2 - \Delta M_\pi^2 = (M_{K^\pm}^2 - M_{K^0}^2)_{\rm em} - (M_{\pi^\pm}^2 - M_{\pi^0}^2)_{\rm em} \quad (219)$$

vanishes.

Recently, Bijnens and Danielsson (2007) calculated electromagnetic corrections in partially quenched perturbation theory, which are particularly pertinent for analysis of lattice QCD calculations. They emphasized that a combination of meson masses with varying charges and quark masses is a close approximation to ΔM_D^2,

$$\Delta M^2 = M^2(\chi_1,\chi_3,q_1,q_3) - M^2(\chi_1,\chi_3,q_3,q_3) - M^2(\chi_1,\chi_1,q_1,q_3) + M^2(\chi_1,\chi_1,q_3,q_3). \quad (220)$$

Here $\chi_i = 2Bm_{q_i}$, where B is the continuum version of the low-energy constant defined in Eq. (39), and q_i is the quark charge. In their notation, $i=1$ (3) refers to the valence u (d) quark, respectively.

MILC has recently begun to explore electromagnetic effects on the pseudoscalar masses (Basak *et al.*, 2009),

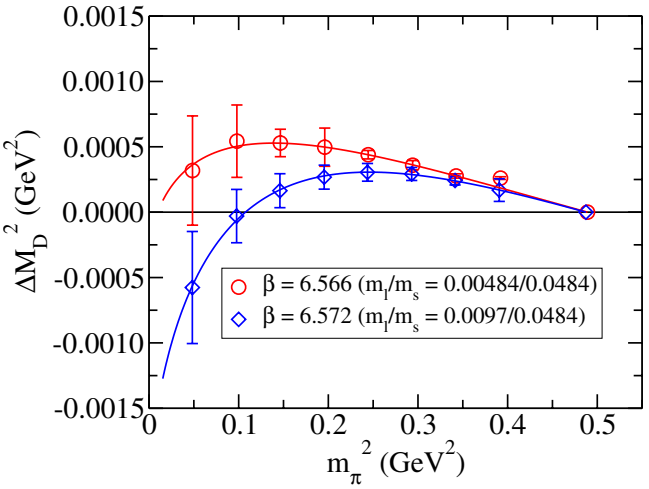

FIG. 41. (Color online) Correction to Dashen's theorem, as a function of the LO π mass squared (equivalent to the pion mass squared with $e^2=0$). From Basak *et al.*, 2009.

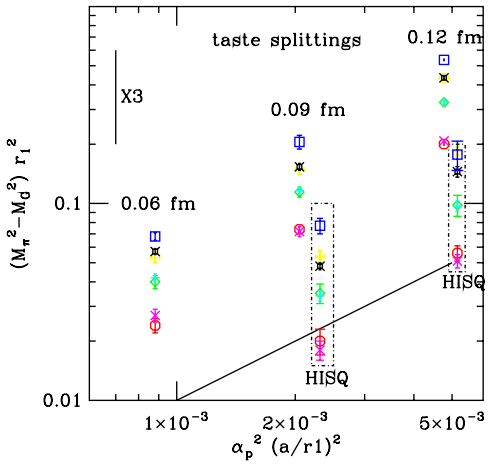

FIG. 42. (Color online) The taste splittings as function of $\alpha^2 a^2$ for the asqtad and HISQ actions (with the latter indicated by dashed boxes).

using the quenched approximation for electromagnetism. The initial study on $a \approx 0.15$ fm ensembles yielded promising results. The key result is a rough estimate of the correction to Dashen's theorem. In Fig. 41, we show results for two dynamical ensembles for various light valence masses. After fitting the results and performing the chiral extrapolation, we found that $0.7\times10^{-3} < \Delta M_D^2 < 1.8\times10^{-3}$ GeV^2. A recent phenomenological estimate is 1.07×10^{-3} GeV^2 (Bijnens and Danielsson, 2007).

It will be interesting to extend this work to smaller lattice spacings and eventually to include dynamical electromagnetic effects. There is also the prospect of including isospin breaking in the generation of the configurations.

C. Heavy Wilson fermion improvement program

The leading discretization errors contained in the Wilson-clover action applied to heavy quarks have been analyzed by Oktay and Kronfeld (2008), in an extension to the original Fermilab formalism. Since the heavy quarks introduce an additional scale $1/m_Q$, they consider all operators which have power counting of λ^3 ($\lambda \sim \Lambda a$ or Λ/m_Q) and v^6 for the heavy-light (HQET) and heavy-heavy (NRQCD) systems, respectively. This leads to actions containing all possible dimension six and some dimension seven operators. Many of these are redundant and may be chosen for calculational convenience by considering field transformations. For example, multihop time derivative operators (which spoil the properties of the transfer matrix) may be eliminated in this way. Tree-level matching of observables in the continuum and lattice QCD actions shows that six new operators beyond the original Fermilab action are required at this level of improvement, four of dimension six and two of dimension seven. In all, there are a total of 19 nonredundant operators at this level, and one-loop matching will presumably introduce more of these. One can estimate the uncertainties due to nonzero lattice spacing by calculating the mismatch between the lattice short-distance coefficients and their continuum counterparts. Initial estimates show that the new lattice action reduces the errors to the few percent level.

D. Preliminary studies of the HISQ action

As discussed in Sec. II, the HISQ action improves taste symmetry and is well suited for future studies with dynamical quarks. Subtleties with dynamical HISQ simulations, in particular from the reunitarization step, Eq. (85), which can lead to large contributions to the force, are described by Bazavov *et al.* (2009).

The first study of how the HISQ action reduces the splitting between different tastes of pions was undertaken by the HPQCD and UKQCD Collaborations by Follana *et al.* (2007). They used valence HISQ on the asqtad sea-quark configurations generated by MILC. Similar findings for HISQ sea quarks were reported by Bazavov *et al.* (2009). The results of a more recent study are shown in Fig. 42: The splittings between the Goldstone and the other pion tastes for the HISQ action are reduced by a factor of 2.5–3 compared to asqtad (notice a vertical line that indicates a factor of 3 in logarithmic scale in Fig. 42). Two HISQ ensembles, with $a \approx 0.09$ and 0.12 fm, are shown. The difference between the results presented here and in Bazavov *et al.* (2009) is that the current study uses the improved gauge action with the one-loop fermion corrections induced by the HISQ fermions (Hart *et al.*, 2009a, 2009b), and the ensembles were tuned to be close to the line of constant physics with $m_l = 0.2 m_s$.

XI. SUMMARY AND CONCLUSIONS

There has been a dramatic improvement in the accuracy of lattice QCD calculations over the past decade due to a combination of developments:

- The use of improved actions significantly reduces finite lattice spacing artifacts, improving the accuracy of extrapolations to the continuum limit. The asqtad improved staggered quark action the MILC Collaboration used provides a particularly strong reduction in taste symmetry breaking, the most challenging finite lattice spacing artifact for staggered quarks. The HISQ action improves on asqtad in this respect by an additional factor of 3. In general, one finds that a HISQ ensemble has lattice artifacts approximately half the size of an asqtad ensemble with the same lattice spacing.
- The inclusion of up, down and strange sea quarks with realistic masses is critical for reducing errors to the few percent level, as is shown in Fig. 1.
- The use of partially quenched chiral perturbation theory and, for staggered quarks, rooted staggered chiral perturbation theory have greatly improved the accuracy of the extrapolation of lattice data to the physical masses of the up, down, and strange quarks.
- Improved algorithms, such as RHMC, have enabled the generation of gauge field ensembles with significantly smaller lattice spacings and lighter quark masses than had previously been possible. These new algorithms have changed the balance between gauge field configuration generation and physics analysis on the configurations. Whereas the former used to take the bulk of the computing resources, now the resources required for an analysis project often rival those that went into the generation of the configurations.
- The vastly increased computing resources available to lattice gauge theorists over the past decade have enabled us to take advantage of the developments enumerated above. For example, between 1999 and 2008 the total floating point operations used per year by the MILC Collaboration increased by approximately three orders of magnitude.

The MILC Collaboration has taken advantage of these developments to generate, over the past ten years, the ensembles of asqtad gauge field configurations detailed in Table I. This is the first set of ensembles to have a wide enough range of small lattice spacings and light quark masses to enable controlled extrapolations of physical quantities to the continuum and chiral limits. These ensembles are publicly available, and we and others are using them to calculate a wide range of physical quantities of interest in high energy and nuclear physics. This work has included calculations of the strong coupling constant, the masses of light quarks and hadrons, the properties of light pseudoscalar mesons, the topological susceptibility, the masses, decays and mixings of heavy-light mesons, the charmonium and bottomonium spectra, the K^0-$\bar{K}^0$ mixing parameter B_K, the mass of the B_c meson, the π-π and N-N scattering lengths, generalized parton distributions, and hadronic contributions to the muon anomalous magnetic moment. The errors in these quantities have typically decreased by an order of magnitude as the library of ensembles has grown, with further improvements expected as the superfine and ultrafine ensembles are fully analyzed, and HISQ ensembles become available.

A number of quantities have been calculated to an accuracy of a few percent, and some predictions have been made that were later verified by experiment. The work of the Fermilab Lattice, MILC, and HPQCD/UKQCD Collaborations on the decays and mixings of heavy-light mesons and the decays of light pseudoscalar mesons has reached a level of accuracy where it is having a significant impact on tests of the standard model and the search for new physics. However, high precision has been obtained only for quantities that are most straightforward to calculate. There are many quantities, such as scattering phase shifts, the masses and widths of hadrons that are unstable under the strong interactions, and parton distribution functions, which are of great interest, but continue to pose major challenges.

Because it is relatively inexpensive to simulate, the asqtad quark action was the first to produce a set of gauge field ensembles with a wide enough range of lattice spacings and sea-quark masses to enable controlled extrapolations to the continuum and chiral limit. However, such ensembles are also being produced with other quark actions, such as Wilson clover, twisted mass, domain wall, and overlap. These ensembles are already producing impressive results. Over the next few years one can expect major advances on a wide variety of calculations with critical checks coming from the use of different lattice formulations of QCD. Finally, the techniques that have been developed for the study of QCD can be applied to study many of the theories that have been proposed for physics beyond the standard model. Such work is just beginning, but appears to have a bright future.

ACKNOWLEDGMENTS

We thank Maarten Golterman for careful reading of this manuscript and helpful suggestions. We are also grateful to Yigal Shamir for suggested clarifications to Sec. III.C. We thank Heechang Na for help with the heavy baryon section and Subhasish Basak for help with the section on electromagnetic effects. This work was supported in part by the United States Department of Energy under Grants No. DE-FG02-91ER-40628, No. DE-FG02-91ER-40661, No. DE-FG02-04ER-41298, No. DE-FC02-06ER-41443, No. DE-FC-06ER-41446, and No. DE-AC-02-98CH10886, and by the National Science Foundation under Grants No. PHY05-55234, No. PHY05-55235, No. PHY05-55243, No. PHY05-55397, No. PHY07-03296, No. PHY07-04171, No. PHY07-57035, and No. PHY07-57333. Fermilab is operated by Fermi Research Alliance, LLC, under Contract No. DE-AC02-07CH11359 with the United States Department of Energy. Computations for this work were carried out in part on facilities of the NSF Teragrid under allocation TG-MCA93S002, facilities of the USQCD Collabora-

tion, which are funded by the Office of Science of the United States Department of Energy, at the Argonne Leadership Class Computing Facility under an Incite grant to the USQCD Collaboration, at the National Energy Research Scientific Computing Center, at Los Alamos National Lab, and at the University of Arizona, the CHPC at the University of Utah, Indiana University, and the University of California, Santa Barbara.

REFERENCES

Abe, K., *et al.* (BELLE), 2005, e-print arXiv:hep-ex/0510003.
Abulencia, A., *et al.* (CDF), 2006, Phys. Rev. Lett. **96**, 082002.
Adams, D. H., 2005, Phys. Rev. D **72**, 114512.
Adams, D. H., 2008, Phys. Rev. D **77**, 105024.
Albanese, M., *et al.* (APE), 1987, Phys. Lett. B **192**, 163.
Alexander, J. P. (CLEO), 2009, Phys. Rev. D **79**, 052001.
Alford, M. G., W. Dimm, G. P. Lepage, G. Hockney, and P. B. Mackenzie, 1995, Phys. Lett. B **361**, 87.
Allison, I., *et al.* (HPQCD), 2008, Phys. Rev. D **78**, 054513.
Allison, I. F., *et al.* (HPQCD), 2005, Phys. Rev. Lett. **94**, 172001.
Allton, C., *et al.* (RBC-UKQCD), 2008, Phys. Rev. D **78**, 114509.
Allton, C. R., 1996, e-print arXiv:hep-lat/9610016.
Ambrosino, F., *et al.* (KLOE), 2006a, Phys. Lett. B **632**, 76.
Ambrosino, F., *et al.* (KLOE), 2006b, Phys. Lett. B **632**, 43.
Amsler, C., *et al.* (Particle Data Group), 2008, Phys. Lett. B **667**, 1.
Antonelli, M., 2007, e-print arXiv:0712.0734.
Aoki, S., *et al.* (PACS-CS), 2009, Phys. Rev. D **79**, 034503.
Arnesen, M. C., B. Grinstein, I. Z. Rothstein, and I. W. Stewart, 2005, Phys. Rev. Lett. **95**, 071802.
Aubert, B., *et al.* (BABAR), 2007a, Phys. Rev. Lett. **98**, 091801.
Aubert, B., *et al.* (BABAR), 2007b, Phys. Rev. D **76**, 052005.
Aubert, B., *et al.* (BABAR), 2008, Phys. Rev. Lett. **101**, 071801; **102**, 029901(E) (2009).
Aubert, B., *et al.* (BABAR), 2009, Phys. Rev. Lett. **103**, 161801.
Aubin, C., and C. Bernard, 2003a, Phys. Rev. D **68**, 034014.
Aubin, C., and C. Bernard, 2003b, Phys. Rev. D **68**, 074011.
Aubin, C., and C. Bernard, 2004, Nucl. Phys. B, Proc. Suppl. **129**, 182.
Aubin, C., and C. Bernard, 2006, Phys. Rev. D **73**, 014515.
Aubin, C., and C. Bernard, 2007, Phys. Rev. D **76**, 014002.
Aubin, C., and T. Blum, 2007, Phys. Rev. D **75**, 114502.
Aubin, C., J. Laiho, and R. S. Van de Water, 2007a, PoS LAT **2007**, 375.
Aubin, C., J. Laiho, and R. S. Van de Water, 2007b, Phys. Rev. D **75**, 034502.
Aubin, C., J. Laiho, and R. S. Van de Water, 2008, Phys. Rev. D **77**, 114501.
Aubin, C., J. Laiho, and R. S. Van de Water, 2009, PoS LAT **2008**, 105.
Aubin, C., J. Laiho, and R. S. Van de Water, 2010, Phys. Rev. D **81**, 014507.
Aubin, C., *et al.*, 2004a, Phys. Rev. D **70**, 094505.
Aubin, C., *et al.* (MILC), 2004b, Phys. Rev. D **70**, 114501.
Aubin, C., *et al.*, 2005a, Phys. Rev. Lett. **95**, 122002.
Aubin, C., *et al.* (Fermilab Lattice, HPQCD, MILC), 2005b, Phys. Rev. Lett. **94**, 011601.
Bae, T., *et al.*, 2009, PoS LAT **2008**, 275.
Bailey, J., *et al.*, 2009, Phys. Rev. D **79**, 054507.
Bailey, J. A., 2007, Phys. Rev. D **75**, 114505.
Ball, P., and R. Zwicky, 2005, Phys. Rev. D **71**, 014015.
Banks, T., L. Susskind, and J. B. Kogut, 1976, Phys. Rev. D **13**, 1043.
Banks, T., *et al.*, 1977, Phys. Rev. D **15**, 1111.
Bär, O., C. Bernard, G. Rupak, and N. Shoresh, 2005, Phys. Rev. D **72**, 054502.
Bär, O., G. Rupak, and N. Shoresh, 2003, Phys. Rev. D **67**, 114505.
Bär, O., G. Rupak, and N. Shoresh, 2004, Phys. Rev. D **70**, 034508.
Barberio, E., *et al.* (Heavy Flavor Averaging Group), 2007, e-print arXiv:0704.3575.
Basak, S., *et al.*, 2009, PoS LAT **2008**, 127.
Bazavov, A., *et al.*, 2009, PoS LAT **2008**, 033.
Beane, S. R., P. F. Bedaque, K. Orginos, and M. J. Savage, 2007, Phys. Rev. D **75**, 094501.
Beane, S. R., K. Orginos, and M. J. Savage, 2007, Nucl. Phys. B **768**, 38.
Beane, S. R., K. Orginos, and M. J. Savage, 2008, Int. J. Mod. Phys. E **17**, 1157.
Beane, S. R., *et al.* (NPLQCD), 2007, Nucl. Phys. A **794**, 62.
Beane, S. R., *et al.*, 2008a, Phys. Rev. Lett. **100**, 082004.
Beane, S. R., *et al.*, 2008b, Phys. Rev. D **77**, 014505.
Beane, S. R., *et al.* (NPLQCD), 2008c, Phys. Rev. D **77**, 094507.
Becher, P., and H. Joos, 1982, Z. Phys. C **15**, 343.
Becher, T., and R. J. Hill, 2006, Phys. Lett. B **633**, 61.
Becirevic, D., and A. B. Kaidalov, 2000, Phys. Lett. B **478**, 417.
Bernard, C. (MILC), 2002, Phys. Rev. D **65**, 054031.
Bernard, C., 2005, Phys. Rev. D **71**, 094020.
Bernard, C., 2006, Phys. Rev. D **73**, 114503.
Bernard, C., C. E. DeTar, Z. Fu, and S. Prelovsek, 2006, PoS LAT **2006**, 173.
Bernard, C., C. E. DeTar, Z. Fu, and S. Prelovsek, 2007, Phys. Rev. D **76**, 094504.
Bernard, C., and M. F. L. Golterman, 1994, Phys. Rev. D **49**, 486.
Bernard, C., and M. F. L. Golterman, 2009, unpublished.
Bernard, C., M. Golterman, and Y. Shamir, 2006, Phys. Rev. D **73**, 114511.
Bernard, C., M. Golterman, and Y. Shamir, 2008, Phys. Rev. D **77**, 074505.
Bernard, C., M. Golterman, Y. Shamir, and S. R. Sharpe, 2007, Phys. Lett. B **649**, 235.
Bernard, C., M. Golterman, Y. Shamir, and S. R. Sharpe, 2008a, Phys. Rev. D **78**, 078502.
Bernard, C., M. Golterman, Y. Shamir, and S. R. Sharpe, 2008b, Phys. Rev. D **77**, 114504.
Bernard, C., *et al.* (MILC), 1998, Phys. Rev. D **58**, 014503.
Bernard, C., *et al.*, 2000a, Phys. Rev. D **62**, 034503.
Bernard, C., *et al.* (MILC), 2000b, Phys. Rev. D **61**, 111502.
Bernard, C., *et al.*, 2001, Phys. Rev. D **64**, 054506.
Bernard, C., *et al.*, 2003a, Nucl. Phys. B, Proc. Suppl. **119**, 260.
Bernard, C., *et al.*, 2003b, Phys. Rev. D **68**, 074505.
Bernard, C., *et al.*, 2003c, Phys. Rev. D **68**, 114501.
Bernard, C., *et al.* (MILC), 2003d, Nucl. Phys. B, Proc. Suppl. **119**, 769.
Bernard, C., *et al.* (MILC), 2004, Nucl. Phys. Proc. Suppl. **129**, 230.
Bernard, C., *et al.* (MILC), 2005, Phys. Rev. D **71**, 034504.
Bernard, C., *et al.*, 2006a, PoS LAT **2005**, 114.
Bernard, C., *et al.* (MILC), 2006b, PoS LAT **2005**, 025.
Bernard, C., *et al.* (MILC), 2006c, PoS LAT **2006**, 163.

Bernard, C., *et al.*, 2007a, Phys. Rev. D **75**, 094505.
Bernard, C., *et al.*, 2007b, PoS LAT **2007**, 090.
Bernard, C., *et al.*, 2007c, PoS LAT **2007**, 310.
Bernard, C., *et al.* (MILC), 2007d, PoS LAT **2007**, 137.
Bernard, C., *et al.*, 2009a, Phys. Rev. D **79**, 014506.
Bernard, C., *et al.*, 2009b, Phys. Rev. D **80**, 034026.
Bernard, C., *et al.* (Fermilab Lattice and MILC), 2009c, PoS LAT **2008**, 278.
Bernard, V., N. Kaiser, and U. G. Meissner, 1993, Z. Phys. C **60**, 111.
Bethke, S., 2007, Prog. Part. Nucl. Phys. **58**, 351.
Bigi, I. I. Y., B. Blok, M. A. Shifman, N. G. Uraltsev, and A. I. Vainshtein, 1992, in *The Fermilab Meeting: DPF 92*, edited by C. H. Albright *et al.* (World Scientific, Singapore), p. 610.
Bigi, I. I. Y., M. A. Shifman, and N. Uraltsev, 1997, Annu. Rev. Nucl. Part. Sci. **47**, 591.
Bigi, I. I. Y., M. A. Shifman, N. G. Uraltsev, and A. I. Vainshtein, 1993, Phys. Rev. Lett. **71**, 496.
Bigi, I. I. Y., N. G. Uraltsev, and A. I. Vainshtein, 1992, Phys. Lett. B **293**, 430; **297**, 477(E) (1993).
Bijnens, J., 2007, PoS LAT **2007**, 004.
Bijnens, J., and N. Danielsson, 2007, Phys. Rev. D **75**, 014505.
Bijnens, J., N. Danielsson, and T. A. Lahde, 2004, Phys. Rev. D **70**, 111503.
Bijnens, J., N. Danielsson, and T. A. Lahde, 2006, Phys. Rev. D **73**, 074509.
Bijnens, J., and T. A. Lahde, 2005, Phys. Rev. D **71**, 094502.
Billeter, B., C. E. DeTar, and J. Osborn, 2004, Phys. Rev. D **70**, 077502.
Blum, T., 2003, Phys. Rev. Lett. **91**, 052001.
Blum, T., T. Doi, M. Hayakawa, T. Izubuchi, and N. Yamada, 2007, Phys. Rev. D **76**, 114508.
Blum, T., *et al.*, 1997, Phys. Rev. D **55**, R1133.
Booth, S. P., *et al.* (UKQCD), 1992, Phys. Lett. B **294**, 385.
Borici, A., 1999, Phys. Lett. B **453**, 46.
Borici, A., 2000, in *Lattice Fermions and Structure of the Vacuum*, edited by V. Mitrjushkin and G. Schierholz (Kluwer, Dordrecht), p. 41.
Bourrely, C., B. Machet, and E. de Rafael, 1981, Nucl. Phys. B **189**, 157.
Bowler, K. C., C. B. Chalmers, R. D. Kenway, G. S. Pawley, and D. Roweth, 1987, Nucl. Phys. B **284**, 299.
Bowler, K. C., *et al.* (UKQCD), 1996, Phys. Rev. D **54**, 3619.
Bowler, K. C., *et al.* (UKQCD), 2000, Phys. Rev. D **62**, 054506.
Bowman, P. O., U. M. Heller, D. B. Leinweber, M. B. Parappilly, and A. G. Williams, 2004, Phys. Rev. D **70**, 034509.
Bowman, P. O., U. M. Heller, D. B. Leinweber, A. G. Williams, and J. B. Zhang, 2005, Lect. Notes Phys. **663**, 17.
Bowman, P. O., *et al.*, 2005, Phys. Rev. D **71**, 054507.
Bowman, P. O., *et al.*, 2007, Phys. Rev. D **76**, 094505.
Boyd, C. G., B. Grinstein, and R. F. Lebed, 1995, Phys. Rev. Lett. **74**, 4603.
Boyd, C. G., and M. J. Savage, 1997, Phys. Rev. D **56**, 303.
Bratt, J. D., *et al.* (LHP), 2009, PoS LAT **2008**, 141.
Buchalla, G., A. J. Buras, and M. E. Lautenbacher, 1996, Rev. Mod. Phys. **68**, 1125.
Buras, A. J., 1998, in *Probing the Standard Model of Particle Interactions*, edited by F. David and R. Gupta (Elsevier Science, New York).
Buras, A. J., M. Jamin, and P. H. Weisz, 1990, Nucl. Phys. B **347**, 491.
Burch, T., K. Orginos, and D. Toussaint, 2001, Phys. Rev. D **64**, 074505.
Burch, T., K. Orginos, and D. Toussaint, 2002, Nucl. Phys. B, Proc. Suppl. **106**, 382.
Burch, T., and D. Toussaint (MILC), 2003, Phys. Rev. D **68**, 094504.
Burch, T., *et al.* (Fermilab Lattice and MILC), 2009, PoS LAT **2009**, 115.
Callaway, D. J. E., and A. Rahman, 1982, Phys. Rev. Lett. **49**, 613.
Callaway, D. J. E., and A. Rahman, 1983, Phys. Rev. D **28**, 1506.
Caswell, W. E., and G. P. Lepage, 1986, Phys. Lett. B **167**, 437.
Charles, J., *et al.*, 2008, preliminary results for Summer 2008, http://ckmfitter.in2p3.fr/plots_Summer2008/ckmEval_results.html.
Chay, J., H. Georgi, and B. Grinstein, 1990, Phys. Lett. B **247**, 399.
Chen, J.-W., M. Golterman, D. O'Connell, and A. Walker-Loud, 2009, Phys. Rev. D **79**, 117502.
Chen, J.-W., D. O'Connell, R. S. Van de Water, and A. Walker-Loud, 2006, Phys. Rev. D **73**, 074510.
Chen, J.-W., D. O'Connell, and A. Walker-Loud, 2007, Phys. Rev. D **D75**, 054501.
Chen, J.-W., D. O'Connell, and A. Walker-Loud, 2009, J. High Energy Phys. **04**, 090.
Clark, M. A., and A. D. Kennedy, 2004, Nucl. Phys. B, Proc. Suppl. **129**, 850.
Clark, M. A., and A. D. Kennedy, 2005, Nucl. Phys. B, Proc. Suppl. **140**, 838.
Colangelo, G., S. Dürr, and C. Haefeli, 2005, Nucl. Phys. B **721**, 136.
Collins, S., R. G. Edwards, U. M. Heller, and J. H. Sloan, 1997, Nucl. Phys. B, Proc. Suppl. **53**, 877.
Creutz, M., 1980, Phys. Rev. D **21**, 2308.
Creutz, M., 2006a, PoS LAT **2006**, 208
Creutz, M., 2006b, e-print arXiv:hep-lat/0603020.
Creutz, M., 2007a, Phys. Lett. B **649**, 241.
Creutz, M., 2007b, Phys. Lett. B **649**, 230.
Creutz, M., 2007c, PoS LAT **2007**, 007.
Creutz, M., 2008a, Phys. Rev. D **78**, 078501.
Creutz, M., 2008b, PoS CONFINEMENT **8**, 016.
Cronin-Hennessy, D., *et al.* (CLEO), 2008, Phys. Rev. Lett. **100**, 251802.
Dalgic, E., J. Shigemitsu, and M. Wingate, 2004, Phys. Rev. D **69**, 074501.
Dalgic, E., *et al.*, 2006, Phys. Rev. D **73**, 074502; **75**, 119906(E) (2007).
Dalgic, E., *et al.*, 2007, Phys. Rev. D **76**, 011501.
Dashen, R. F., 1969, Phys. Rev. **183**, 1245.
Dashen, R. F., 1971, Phys. Rev. D **3**, 1879.
Davies, C. T. H. (HPQCD), 2008, e-print arXiv:0810.3309.
Davies, C. T. H., *et al.*, 1994, Phys. Rev. D **50**, 6963.
Davies, C. T. H., *et al.* (HPQCD, UKQCD, Fermilab Lattice, MILC), 2004, Phys. Rev. Lett. **92**, 022001.
Davies, C. T. H., *et al.* (HPQCD), 2008, Phys. Rev. D **78**, 114507.
Davies, C. T. H., *et al.* (HPQCD), 2009, PoS LAT **2008**, 118.
de Forcrand, P., P. M. Garcia Perez, and I.-O. Stamatescu, 1997, Nucl. Phys. B **499**, 409.
DeGrand, T. A., A. Hasenfratz, and T. G. Kovacs, 1997, Nucl. Phys. B **505**, 417.
DeGrand, T. A., and U. M. Heller (MILC), 2002, Phys. Rev. D **65**, 114501.
DeTar, C., and U. M. Heller, 2009, Eur. Phys. J. A **41**, 405.

DeTar, C. E., and L. Levkova (Fermilab Lattice and MILC), 2007, PoS LAT **2007**, 116.
Detmold, W., *et al.*, 2008a, Phys. Rev. D **78**, 054514.
Detmold, W., *et al.*, 2008b, Phys. Rev. D **78**, 014507.
Di Lodovico, F., 2008, update presented at ICHEP 2008, http://www.slac.stanford.edu/xorg/hfag/semi/ichep08/home.shtml
di Pierro, M., *et al.*, 2004, Nucl. Phys. B, Proc. Suppl. **129**, 340.
Dobrescu, B. A., and A. S. Kronfeld, 2008, Phys. Rev. Lett. **100**, 241802.
Dong, S.-J., and K.-F. Liu, 1994, Phys. Lett. B **328**, 130.
Duane, S., A. D. Kennedy, B. J. Pendleton, and D. Roweth, 1987, Phys. Lett. B **195**, 216.
Duane, S., and J. B. Kogut, 1985, Phys. Rev. Lett. **55**, 2774.
Duane, S., and J. B. Kogut, 1986, Nucl. Phys. B **275**, 398.
Duncan, A., E. Eichten, and H. Thacker, 1996, Phys. Rev. Lett. **76**, 3894.
Duncan, A., E. Eichten, and H. Thacker, 1997, Phys. Lett. B **409**, 387.
Duncan, A., R. Roskies, and H. Vaidya, 1982, Phys. Lett. B **114**, 439.
Dürr, S., and C. Hoelbling, 2005, Phys. Rev. D **71**, 054501.
Dürr, S., and C. Hoelbling, 2006, Phys. Rev. D **74**, 014513.
Dürr, S., C. Hoelbling, and U. Wenger, 2004, Phys. Rev. D **70**, 094502.
Dürr, S., *et al.*, 2008, Science **322**, 1224.
Dürr, S., *et al.*, 2009, Phys. Rev. D **79**, 014501.
Edwards, R. G., and U. M. Heller, 2001, Phys. Rev. D **63**, 094505.
Edwards, R. G., U. M. Heller, and R. Narayanan, 1999, Nucl. Phys. B **540**, 457.
Edwards, R. G., *et al.* (LHPC), 2006a, PoS LAT **2006**, 195.
Edwards, R. G., *et al.* (LHPC), 2006b, Phys. Rev. Lett. **96**, 052001.
Eichten, E., and B. R. Hill, 1990, Phys. Lett. B **234**, 511.
Eisenstein, B. I., *et al.* (CLEO), 2008, Phys. Rev. D **78**, 052003.
El-Khadra, A. X., E. Gamiz, A. S. Kronfeld, and M. A. Nobes, 2007, PoS LAT **2007**, 242.
El-Khadra, A. X., A. S. Kronfeld, and P. B. Mackenzie, 1997, Phys. Rev. D **55**, 3933.
Evans, R. T., A. X. El-Khadra, and E. Gamiz, 2009, PoS LAT **2008**, 052.
Evans, R. T., E. Gamiz, A. X. El-Khadra, and M. Di Pierro, 2007, PoS LAT **2007**, 354.
Fischer, C. S., 2006, J. Phys. G **32**, R253.
Foley, J., *et al.*, 2005, Comput. Phys. Commun. **172**, 145.
Follana, E., C. T. H. Davies, G. P. Lepage, and J. Shigemitsu (HPQCD), 2008, Phys. Rev. Lett. **100**, 062002.
Follana, E., A. Hart, and C. T. H. Davies (HPQCD), 2004, Phys. Rev. Lett. **93**, 241601.
Follana, E., *et al.* (HPQCD), 2007, Phys. Rev. D **75**, 054502.
Frezzotti, R., P. A. Grassi, S. Sint, and P. Weisz, 2000, Nucl. Phys. B, Proc. Suppl. **83**, 941.
Frezzotti, R., P. A. Grassi, S. Sint, and P. Weisz (Alpha), 2001, J. High Energy Phys. **08**, 058.
Frezzotti, R., and G. C. Rossi, 2004, J. High Energy Phys. **08**, 007.
Frommer, A., B. Nöckel, S. Güsken, T. Lippert, and K. Schilling, 1995, Int. J. Mod. Phys. C **6**, 627.
Fukugita, M., N. Ishizuka, H. Mino, M. Okawa, and A. Ukawa, 1993, Phys. Rev. D **47**, 4739.
Furman, V., and Y. Shamir, 1995, Nucl. Phys. B **439**, 54.
Furui, S., and H. Nakajima, 2006, Phys. Rev. D **73**, 074503.
Gambino, P., P. Giordano, G. Ossola, and N. Uraltsev, 2007, J. High Energy Phys. **10**, 058.
Gamiz, E., C. T. H. Davies, G. P. Lepage, J. Shigemitsu, and M. Wingate (HPQCD), 2009, Phys. Rev. D **80**, 014503.
Gamiz, E., *et al.* (HPQCD), 2006, Phys. Rev. D **73**, 114502.
Gasser, J., and H. Leutwyler, 1984, Ann. Phys. **158**, 142.
Gasser, J., and H. Leutwyler, 1985, Nucl. Phys. B **250**, 465.
Gattringer, C., 2001, Phys. Rev. D **63**, 114501.
Ge, J., *et al.* (CLEO), 2009, Phys. Rev. D **79**, 052010.
Ginsparg, P. H., and K. G. Wilson, 1982, Phys. Rev. D **25**, 2649.
Gliozzi, F., 1982, Nucl. Phys. B **204**, 419.
Göckeler, M., 1984, Phys. Lett. B **142**, 197.
Golterman, M., 2008, PoS CONFINEMENT **8**, 014.
Golterman, M., T. Izubuchi, and Y. Shamir, 2005, Phys. Rev. D **71**, 114508.
Golterman, M., Y. Shamir, and B. Svetitsky, 2006, Phys. Rev. D **74**, 071501.
Golterman, M. F. L., 1986a, Nucl. Phys. B **278**, 417.
Golterman, M. F. L., 1986b, Nucl. Phys. B **273**, 663.
Golterman, M. F. L., and J. Smit, 1984, Nucl. Phys. B **245**, 61.
Golterman, M. F. L., and J. Smit, 1985, Nucl. Phys. B **255**, 328.
Gottlieb, S., H. Na, and K. Nagata, 2008, Phys. Rev. D **77**, 017505.
Gottlieb, S., *et al.*, 2006a, PoS LAT **2005**, 203.
Gottlieb, S. A., W. Liu, D. Toussaint, R. L. Renken, and R. L. Sugar, 1987, Phys. Rev. D **35**, 2531.
Gottlieb, S. A., and S. Tamhankar, 2003, Nucl. Phys. B, Proc. Suppl. **119**, 644.
Gottlieb, S. A., *et al.* (Fermilab Lattice and MILC), 2006b, PoS LAT **2006**, 175.
Gray, A., *et al.* (HPQCD), 2003, Nucl. Phys. B, Proc. Suppl. **119**, 592.
Gray, A., *et al.*, 2005, Phys. Rev. D **72**, 094507.
Gregory, E. B., A. C. Irving, C. C. McNeile, S. Miller, and Z. Sroczynski, 2006, PoS LAT **2005**, 027.
Gregory, E. B., A. C. Irving, C. M. Richards, and C. McNeile, 2008, Phys. Rev. D **77**, 065019.
Gregory, E. B., A. Irving, C. M. Richards, C. McNeile, and A. Hart, 2007, PoS LAT **2007**, 099.
Gregory, E. B., C. McNeile, A. C. Irving, and C. Richards (UKQCD), 2009, PoS LAT **2008**, 286.
Gupta, R., G. Guralnik, G. W. Kilcup, and S. R. Sharpe, 1991, Phys. Rev. D **43**, 2003.
Hägler, P., 2007, PoS LAT **2007**, 013.
Hägler, P., *et al.* (LHPC), 2008, Phys. Rev. D **77**, 094502.
Hao, Z., G. M. von Hippel, R. R. Horgan, Q. J. Mason, and H. D. Trottier, 2007, Phys. Rev. D **76**, 034507.
Harada, J., S. Hashimoto, A. S. Kronfeld, and T. Onogi, 2002, Phys. Rev. D **65**, 094514.
Harada, J., *et al.*, 2002, Phys. Rev. D **65**, 094513; **71**, 019903(E) (2005).
Hart, A., G. M. von Hippel, and R. R. Horgan, 2009a, PoS LAT **2008**, 046.
Hart, A., G. M. von Hippel, and R. R. Horgan (HPQCD), 2009b, Phys. Rev. D **79**, 074008.
Hasenbusch, M., 2001, Phys. Lett. B **519**, 177.
Hasenbusch, M., and K. Jansen, 2003, Nucl. Phys. B **659**, 299.
Hasenfratz, A., R. Hoffmann, and S. Schaefer, 2007, J. High Energy Phys. **05**, 029.
Hasenfratz, A., and F. Knechtli, 2001, Phys. Rev. D **64**, 034504.
Hasenfratz, P., 1998, Nucl. Phys. B, Proc. Suppl. **63**, 53.
Hasenfratz, P., V. Laliena, and F. Niedermayer, 1998, Phys. Lett. B **427**, 125.
Hashimoto, S., A. S. Kronfeld, P. B. Mackenzie, S. M. Ryan,

and J. N. Simone, 2002, Phys. Rev. D **66**, 014503.
Hashimoto, S., *et al.*, 1999, Phys. Rev. D **61**, 014502.
Heller, U. M., F. Karsch, and B. Sturm, 1999, Phys. Rev. D **60**, 114502.
Isgur, N., and M. B. Wise, 1992, *B Decays* (World Scientific, Singapore), p. 489.
Ishizuka, N., M. Fukugita, H. Mino, M. Okawa, and A. Ukawa, 1994, Nucl. Phys. B **411**, 875.
Jegerlehner, B., 1996, e-print arXiv:hep-lat/9612014.
Jegerlehner, B., 1998, Nucl. Phys. B, Proc. Suppl. **63**, 958.
Jegerlehner, F., 2007, Acta Phys. Pol. B **38**, 3021.
Jegerlehner, F., 2008, *The Anomalous Magnetic Moment of the Muon*, Springer Tracts in Modern Physics, Vol. 226 (Springer, Berlin).
Jenkins, E. E., 1992, Nucl. Phys. B **368**, 190.
Kaplan, D. B., 1992, Phys. Lett. B **288**, 342.
Karsten, L. H., and J. Smit, 1981, Nucl. Phys. B **183**, 103.
Kawamoto, N., and J. Smit, 1981, Nucl. Phys. B **192**, 100.
Kennedy, A. D., and B. J. Pendleton, 1985, Phys. Lett. B **156**, 393.
Kikukawa, Y., and T. Noguchi, 1999, e-print arXiv:hep-lat/9902022.
Kilcup, G. W., and S. R. Sharpe, 1987, Nucl. Phys. B **283**, 493.
Kluberg-Stern, H., A. Morel, O. Napoly, and B. Petersson, 1981, Nucl. Phys. B **190**, 504.
Kluberg-Stern, H., A. Morel, O. Napoly, and B. Petersson, 1983, Nucl. Phys. B **220**, 447.
Kluberg-Stern, H., A. Morel, and B. Petersson, 1983, Nucl. Phys. B **215**, 527.
Kogut, J. B., and L. Susskind, 1975, Phys. Rev. D **11**, 395.
Kronfeld, A. S., 2000, Phys. Rev. D **62**, 014505.
Kronfeld, A. S., 2004, Nucl. Phys. B, Proc. Suppl. **129**, 46.
Kronfeld, A. S. (Fermilab Lattice), 2006, J. Phys.: Conf. Ser. **46**, 147.
Kronfeld, A. S., 2007, PoS LAT **2007**, 016.
Kühn, J. H., and M. Steinhauser, 2001, Nucl. Phys. B **619**, 588; **640**, 415(E) (2002).
Kühn, J. H., M. Steinhauser, and C. Sturm, 2007, Nucl. Phys. B **778**, 192.
Kuramashi, Y., M. Fukugita, H. Mino, M. Okawa, and A. Ukawa, 1994, Phys. Rev. Lett. **72**, 3448.
Lagae, J. F., and D. K. Sinclair, 1999, Phys. Rev. D **59**, 014511.
Laiho, J., and R. S. Van de Water, 2006, Phys. Rev. D **73**, 054501.
Lange, B. O., M. Neubert, and G. Paz, 2005, Phys. Rev. D **72**, 073006.
Lee, W.-J., and S. R. Sharpe, 1999, Phys. Rev. D **60**, 114503.
Lellouch, L., 1996, Nucl. Phys. B **479**, 353.
Lenz, A., and U. Nierste, 2007, J. High Energy Phys. **06**, 072.
Lepage, G. P., 1990, in *From Actions to Answers*, edited by T. DeGrand and D. Toussaint, Proceedings of the 1989 Theoretical Advanced Study Institute in Elementary Particle Physics (World Scientific, Singapore), p. 197.
Lepage, G. P., 1999, Phys. Rev. D **59**, 074502.
Lepage, G. P., and P. B. Mackenzie, 1993, Phys. Rev. D **48**, 2250.
Lepage, G. P., L. Magnea, C. Nakhleh, U. Magnea, and K. Hornbostel, 1992, Phys. Rev. D **46**, 4052.
Lepage, G. P., *et al.*, 2002, Nucl. Phys. B, Proc. Suppl. **106**, 12.
Lepage, P., 1998, Nucl. Phys. B, Proc. Suppl. **60**, 267.
Leutwyler, H., 1994, Ann. Phys. **235**, 165.
Leutwyler, H., 2006, in *Chiral Dynamics 2006*, edited by M. Ahmed *et al.* (World Scientific, Singapore), p. 17.
Leutwyler, H., and A. V. Smilga, 1992, Phys. Rev. D **46**, 5607.
Levkova, L., and C. DeTar (Fermilab Lattice and MILC), 2009, PoS LAT **2008**, 133.
Lewis, R., N. Mathur, and R. M. Woloshyn, 2001, Phys. Rev. D **64**, 094509.
Lewis, R., and R. M. Woloshyn, 2009, Phys. Rev. D **79**, 014502.
Luke, M. E., 1990, Phys. Lett. B **252**, 447.
Luo, Y.-B., 1997, Phys. Rev. D **55**, 353.
Lüscher, M., 1998, Phys. Lett. B **428**, 342.
Lüscher, M., S. Sint, R. Sommer, and P. Weisz, 1996, Nucl. Phys. B **478**, 365.
Lüscher, M., S. Sint, R. Sommer, P. Weisz, and U. Wolff, 1997, Nucl. Phys. B **491**, 323.
Lüscher, M., and P. Weisz, 1985a, Phys. Lett. B **158**, 250.
Lüscher, M., and P. Weisz, 1985b, Commun. Math. Phys. **97**, 59.
Lüscher, M., and P. Weisz, 1996, Nucl. Phys. B **479**, 429.
Maltman, K., D. Leinweber, P. Moran, and A. Sternbeck, 2008, Phys. Rev. D **78**, 114504.
Manohar, A. V., and M. B. Wise, 2000, Cambridge Monogr. Part. Phys., Nucl. Phys., Cosmol. **10**, 1, and references therein.
Marciano, W. J., 2004, Phys. Rev. Lett. **93**, 231803.
Marinari, E., G. Parisi, and C. Rebbi, 1981a, Phys. Rev. Lett. **47**, 1795.
Marinari, E., G. Parisi, and C. Rebbi, 1981b, Nucl. Phys. B **190**, 734.
Martinelli, G., C. Pittori, C. T. Sachrajda, M. Testa, and A. Vladikas, 1995, Nucl. Phys. B **445**, 81.
Mason, Q., H. D. Trottier, R. Horgan, C. T. H. Davies, and G. P. Lepage (HPQCD), 2006, Phys. Rev. D **73**, 114501.
Mason, Q., *et al.* (HPQCD), 2005, Phys. Rev. Lett. **95**, 052002.
Mason, Q. J., 2004, Ph.D. thesis (Cornell University).
Mathur, N., and S.-J. Dong, 2003, Nucl. Phys. B, Proc. Suppl. **119**, 401.
McNeile, C., and C. Michael (UKQCD), 2001, Phys. Rev. D **63**, 114503.
Metropolis, N., A. W. Rosenbluth, M. N. Rosenbluth, A. H. Teller, and E. Teller, 1953, J. Chem. Phys. **21**, 1087.
Michael, C., 1994, Phys. Rev. D **49**, 2616.
Mitra, P., and P. Weisz, 1983, Phys. Lett. B **126**, 355.
Morningstar, C., and M. J. Peardon, 2004, Phys. Rev. D **69**, 054501.
Morningstar, C. J., and J. Shigemitsu, 1998, Phys. Rev. D **57**, 6741.
Na, H., and S. Gottlieb, 2006, PoS LAT **2006**, 191.
Na, H., and S. A. Gottlieb, 2007, PoS LAT **2007**, 124.
Na, H., and S. Gottlieb, 2009, PoS LAT **2008**, 119.
Naik, S., 1989, Nucl. Phys. B **316**, 238.
Narayanan, R., and H. Neuberger, 1995, Nucl. Phys. B **443**, 305.
Neuberger, H., 1998a, Phys. Rev. Lett. **81**, 4060.
Neuberger, H., 1998b, Phys. Lett. B **417**, 141.
Neuberger, H., 1998c, Phys. Rev. D **57**, 5417.
Neubert, M., 1994, Phys. Rep. **245**, 259.
Nielsen, H. B., and M. Ninomiya, 1981, Phys. Lett. B **105**, 219.
Okamoto, M., 2006, PoS LAT **2005**, 013.
Oktay, M. B., and A. S. Kronfeld, 2008, Phys. Rev. D **78**, 014504.
Omelyan, I. P., I. M. Mryglod, and R. Folk, 2002a, Phys. Rev. E **66**, 026701.
Omelyan, I. P., I. M. Mryglod, and R. Folk, 2002b, Phys. Rev. E **65**, 056706.
Omelyan, I. P., I. M. Mryglod, and R. Folk, 2003, Comput.

Phys. Commun. **151**, 272.
Orginos, K., 2006, PoS LAT **2006**, 018.
Orginos, K., R. Sugar, and D. Toussaint, 2000, Nucl. Phys. B, Proc. Suppl. **83**, 878.
Orginos, K., and D. Toussaint (MILC), 1999, Phys. Rev. D **59**, 014501.
Orginos, K., D. Toussaint, and R. L. Sugar (MILC), 1999, Phys. Rev. D **60**, 054503.
Orginos, K., and A. Walker-Loud, 2008, Phys. Rev. D **77**, 094505.
Parappilly, M. B., *et al.*, 2006, Phys. Rev. D **73**, 054504.
Prelovsek, S., 2006a, PoS LAT **2005**, 085.
Prelovsek, S., 2006b, Phys. Rev. D **73**, 014506.
Renner, D. B., *et al.* (LHP), 2005, Nucl. Phys. B, Proc. Suppl. **140**, 255.
Renner, D. B., *et al.* (LHPC), 2007, PoS LAT **2007**, 160.
Roberts, C. D., 2008, Prog. Part. Nucl. Phys. **61**, 50.
Schaefer, S., A. Hasenfratz, and R. Hoffmann, 2007, PoS LAT **2007**, 132.
Sexton, J. C., and D. H. Weingarten, 1992, Nucl. Phys. B **380**, 665.
Shamir, Y., 1993, Nucl. Phys. B **406**, 90.
Shamir, Y., 2005, Phys. Rev. D **71**, 034509.
Shamir, Y., 2007, Phys. Rev. D **75**, 054503.
Sharatchandra, H. S., H. J. Thun, and P. Weisz, 1981, Nucl. Phys. B **192**, 205.
Sharpe, S. R., 1990, Nucl. Phys. B, Proc. Suppl. **17**, 146.
Sharpe, S. R., 1992, Phys. Rev. D **46**, 3146.
Sharpe, S. R., 2006a, e-print arXiv:hep-lat/0607016.
Sharpe, S. R., 2006b, PoS LAT **2006**, 022.
Sharpe, S. R., and A. Patel, 1994, Nucl. Phys. B **417**, 307.
Sharpe, S. R., and N. Shoresh, 2001, Phys. Rev. D **64**, 114510.
Sharpe, S. R., and R. S. Van de Water, 2005, Phys. Rev. D **71**, 114505.
Sheikholeslami, B., and R. Wohlert, 1985, Nucl. Phys. B **259**, 572.
Silvestrini, L., 2008, preliminary result presented at Lattice 2008, http://www.utfit.org/.
Sirlin, A., 1982, Nucl. Phys. B **196**, 83.
Smit, J., and J. C. Vink, 1987, Nucl. Phys. B **286**, 485.
Sommer, R., 1994, Nucl. Phys. B **411**, 839.
Struckmann, T., *et al.* (TXL), 2001, Phys. Rev. D **63**, 074503.
Susskind, L., 1977, Phys. Rev. D **16**, 3031.
Symanzik, K., 1980, in *Recent Developments in Gauge Theories*, edited by G. 't Hooft *et al.* (Plenum, New York), p. 313.
Symanzik, K., 1983, Nucl. Phys. B **226**, 187.
Takaishi, T., and P. de Forcrand, 2006, Phys. Rev. E **73**, 036706.
Tamhankar, S. S., Ph.D. thesis (Indiana University).
Thacker, B. A., and G. P. Lepage, 1991, Phys. Rev. D **43**, 196.
Toussaint, D., and C. T. H. Davies, 2005, Nucl. Phys. B, Proc. Suppl. **140**, 234.
Toussaint, D., and W. Freeman, 2008, e-print arXiv:0808.2211.
Towner, I. S., and J. C. Hardy, 2008, Phys. Rev. C **77**, 025501
Ukita, N., *et al.* (PACS-CS), 2007, PoS LAT **2007**, 138.
Ukita, N., *et al.* (PACS-CS), 2009, PoS LAT **2008**, 097.
van den Doel, C., and J. Smit, 1983, Nucl. Phys. B **228**, 122.
van den Eshof, J., A. Frommer, T. Lippert, K. Schilling, and H. A. van der Vorst, 2002, Comput. Phys. Commun. **146**, 203.
Van de Water, R. S., and S. R. Sharpe, 2006, Phys. Rev. D **73**, 014003.
Veneziano, G., 1979, Nucl. Phys. B **159**, 213.
Venkataraman, L., and G. Kilcup, 1997, e-print arXiv:hep-lat/9711006.
Venkataraman, L., and G. Kilcup, 1998, Nucl. Phys. B, Proc. Suppl. **63**, 826.
Walker-Loud, A., *et al.*, 2009, Phys. Rev. D **79**, 054502.
Weinberg, S., 1979, Physica A **96**, 327.
Wilcox, W., 1999, e-print arXiv:hep-lat/9911013.
Wilson, K. G., 1974, Phys. Rev. D **10**, 2445.
Wilson, K. G., 1975, in *New Phenomena In Subnuclear Physics*, edited by A. Zichichi (Plenum, New York), pp. 13–32.
Wingate, M., C. T. H. Davies, A. Gray, G. P. Lepage, and J. Shigemitsu, 2004, Phys. Rev. Lett. **92**, 162001.
Wingate, M., J. Shigemitsu, C. T. Davies, G. P. Lepage, and H. D. Trottier, 2003, Phys. Rev. D **67**, 054505.
Witten, E., 1979, Nucl. Phys. B **156**, 269.
Witten, E., 1980, Ann. Phys. **128**, 363.
Wohlert, R., 1987, unpublished.
Yamada, N., T. Blum, M. Hayakawa, and T. Izubuchi (RBC), 2006, PoS LAT **2005**, 092.
Zanotti, J. M., 2009, PoS LAT **2008**, 007.
Zanotti, J. M., *et al.* (CSSM Lattice), 2002, Phys. Rev. D **65**, 074507.